AN ABSTRACT OF THE THESIS OF

RICHARD ALAN SPAULDING for the MASTER OF SCIENCE
(Name) (Degree)

in ELECTRICAL AND ELECTRONICS ENGINEERING presented on August 16, 1968
(Major) (Date)

Title: FIELD-EFFECT TRANSISTOR NOISE AT LOW TEMPERATURES

Abstract approved: Redacted for privacy
Professor James C. Looney

Low temperature noise measurements on junction field-effect transistors tend to substantiate a theory of low frequency field-effect transistor noise based on the presence of generation centers in the gate-channel depletion region. Measurements of device noise voltage versus temperature reveal pronounced maxima and minima over the temperature range of 300° K to 77° K. Analysis of the maxima can yield information on time constants, capture cross-sections and energy levels of generation centers in the depletion region.

The pertinent theories of junction FET noise are reviewed with regard to temperature-dependent phenomena. Contributions due to thermal noise, shot noise, induced gate noise, surface leakage and generation centers are considered.

Techniques for measuring the temperature dependence of FET noise are discussed, and a practical approach is described.

Measurements are made in a typical circuit configuration in order that the results may be directly related to device applications.

Measured data on the temperature dependence of noise in the 300° K to 77° K range is presented for 14 n- and p-channel FET's. Salient features of the data are analyzed and correlated with theoretical predictions.

Field-Effect Transistor Noise at Low Temperatures

by

Richard Alan Spaulding

A THESIS

submitted to

Oregon State University

in partial fulfillment of
the requirements for the
degree of

Master of Science

June 1969

APPROVED:

Redacted for privacy

Professor of Electrical and Electronics Engineering

in charge of major

Redacted for privacy

Head of Department of Electrical and Electronics Engineering

Redacted for privacy

Dean of Graduate School

Date thesis is presented Aug. 16, 1968

Typed by Clover Redfern for Richard Alan Spaulding

TABLE OF CONTENTS

LIST OF FIGURES

FIELD-EFFECT TRANSISTOR NOISE AT LOW TEMPERATURES

I. INTRODUCTION

Recent interest has been expressed in the use of junction field-effect transistors for low temperature applications. Since they are majority carrier devices, silicon junction field-effect transistors (FET's) operate at temperatures as low as 77° K (-196° C). The low noise and high input impedance properties of these devices make them well suited for use with cooled infrared and nuclear radiation detectors (21, 22). Their ability to operate at cryogenic temperatures enables them to be located near the high impedance detectors, thereby reducing stray input capacitances.

In considering FET's for cryogenic applications, it is often assumed that since noise is fundamentally of thermal origin, reducing the device temperature should reduce the noise. Conversely, FET noise often increases at low temperatures, and has been observed to undergo cyclic variations as the temperature is decreased (7, 12, 13, 33). The cause of this anomalous noise behavior has been attributed to impurity deionization (12).

This research was undertaken to make detailed measurements of these noise variations and provide an explanation for the observed behavior. The information presented is intended to contribute to the

understanding of FET performance in cryogenic applications.

The pertinent theories of junction FET noise are reviewed with regard to temperature dependent phenomena. The thermal noise theory of van der Ziel (39) is found to predict a decrease in noise at low temperatures. Factors of shot noise, induced gate noise and surface noise are considered. It is found that a theory of FET noise based on the presence of Shockley-Read-Hall centers in the depletion region (25) accounts for the observed noise behavior. It is further found that analysis of the temperature dependence of the noise maxima can yield estimates of the time constants, activation energies, capture cross-sections and concentrations of the trapping centers.

Considerations in measuring the temperature dependence of FET noise are discussed, and a practical approach is described. The measurements are made in a typical circuit configuration in order that the results may be directly related to device applications.

Measured data on the temperature dependence of noise in the 300° K to 77° K range is presented for 14 n- and p-channel FET's. Salient features of the data are analyzed and correlated with theoretical predictions.

II. THEORY

FET Noise Sources

Junction field-effect transistors exhibit most of the temperature dependent phenomena associated with any semiconductor device. These include mobility variation with temperature, thermal impurity deionization, variation of junction potential with doping and temperature, trapping at impurity sites and surface effects. Since FET's can be characterized by an equivalent active circuit, they may also exhibit thermal noise and shot noise.

By considering FET circuit properties, bulk effects and surface effects, the various sources of noise may be identified.

In the following sections, the mechanisms that contribute to FET noise at low temperatures are examined. These include thermal noise, shot noise, surface leakage and bulk trapping effects. Factors affecting device noise at high input impedances are given, although measurements of these factors could not be made. In order that device operating characteristics may be better understood, the variations of drain current and transconductance with temperature are also considered.

Thus, the important temperature dependent aspects of FET operation are estimated for comparison with measured data.

Thermal FET Noise

A fundamental limiting noise in FET's is the thermal noise of the channel conductance. Using the model devised by Shockley (31), van der Ziel derived an expression for the noise due to thermal fluctuations in the channel (39). It is valid only for non-saturated operating conditions, but can be extended into saturation on the basis of experimental evidence (8).

Van der Ziel obtains the following expression for an equivalent noise current source at the output terminals of the FET:

$$\overline{i_d^2} = 4kTg_{max}\Delta fQ(W_d, W_s)$$

where $Q(W_d, W_s)$ is a function of the potential distribution of the gate-channel depletion region, and W_d, W_s are the drain and source potentials, respectively. When $W_d = W_s$, $Q(W_d, W_s) = 1.0$ (zero drain bias); $Q(W_d, W_s)$ is usually on the order of 0.60 to 0.75 for typical drain bias conditions. The term g_{max} is the maximum value of transconductance in saturation.

Under the condition of zero drain bias, $Q(W_d, W_s) = 1$ and g_{max} becomes the ac output conductance of the channel, g_{do}. The noise current becomes

$$\overline{i_d^2} = 4kTg_{do}\Delta f.$$

This expression is simply the thermal noise due to a conductance g_{do}. Thus, under zero drain bias conditions, the output noise is exactly the thermal noise of the output conductance.

For purposes of device evaluation, it is convenient to express the noise in terms of a voltage generator at the input. Since the transconductance is defined as

$$g_m = - \left(\frac{\partial I_D}{\partial V_{GS}} \right)_{V_D}$$

we may define an equivalent input noise voltage source $\overline{e_n^2}$ giving $\overline{i_d^2}$ at the output terminals:

$$\overline{e_n^2} = \frac{\overline{i_d^2}}{g_m^2} = \frac{4kT\Delta f Q(W_d, W_s)}{g_m} ,$$

where g_m is the transconductance in saturation.

High-Frequency Gate Noise

Capacitive coupling between the channel and the gate can result in additional gate noise at high frequencies. Van der Ziel (37) has calculated the gate noise due to induced thermal noise of the channel. The resulting expression for a gate noise current generator is given as:

$$\overline{i_g^2} = \overline{i_{go}^2} + 4kTR_n\Delta f\omega^2 C_{gs}^2 H(z).$$

The value $H(z)$ is commonly 0.3 to 0.4, and R_n is on the order of g_m^{-1}, yielding

$$\overline{i_g^2} = \overline{i_{go}^2} + 0.3\left(\frac{4kT\Delta f}{g_m}\right)\omega^2 C_{gs}^2.$$

In this expression, $\overline{i_{go}^2}$ is the shot noise due to the gate current. A similar expression has been derived by Klaassen using a transmission-line approach (15).

It should be noted that the techniques used in the above references should apply to situations where nonthermal noise sources are dominant in device operation at sufficiently high frequencies such that the gate-channel coupling results in a significant correlation between the output and input noise of the FET.

Gate Current Shot Noise

The gate-channel leakage current produces shot noise which modulates the channel of the FET (28, p. 46). This noise may be represented by an equivalent noise generator at the input:

$$\overline{i_n^2} = 2eI_{GSX}\Delta f,$$

where I_{GSX} is the gate current under biased conditions.

This noise may be observed when the gate is open-circuited with an impedance much greater than the input resistance of the FET.

Since FET's are operated with a reverse-biased gate-channel junction, I_{GSX} is usually the reverse saturation current of the junction. This current is proportional to $n_i^2 \propto \exp(\frac{-E_g}{kT})$, where E_g is the bandgap energy. An additional nonsaturable reverse current source exists in the generation of carriers from SRH centers in the depletion region (27). Both of these currents are exponential functions of temperature.

Surface Effects

Recombination-generation mechanisms which contribute to the reverse biased gate leakage current may also be sources of noise. The gate-channel junction may be treated as a reverse biased p-n junction in this case. Sah (23) has outlined the basic mechanisms which contribute to diode voltage-current characteristics. Those factors affecting the reverse-bias leakage current are:

(a) bulk diffusion current due to thermal generation of carriers at the bandgap energy;

(b) bulk generation current in the depletion region, such as that due to trapping centers;

(c) surface generation-recombination; and

(d) surface channel conduction.

Since only low temperatures are being considered here, the thermal generation current may be neglected in comparison with the SRH center generation current. The latter is considered in the next section.

Carrier fluctuations due to surface generation and recombination at the junction edge can be a significant source of noise in FET's. Trapping may occur at a localized charge in the passivating oxide layer, or along a channel in the surface adjacent to the depletion region.

Recently, correlation of surface fluctuation noise to surface state concentration has been shown (26). Since a distribution of time constants is usually associated with such surface states, the noise will have a 1/f power spectrum.

On the basis of trapping by surface states, it has been observed that the noise due to distributed time constant fluctuations is temperature independent from 300° K to 77° K (1).

Cutler and Bath (11) present evidence of temperature-dependent surface channel behavior. Sah (23) indicates that the temperature-dependence of channel current should depend on the size of the channel. Thus, on the basis of surface channel noise alone, one may or may not observe variation with temperature.

In most junction FET's of conventional design, the junction edge is physically removed from the modulating or pinchoff region. The

gate noise current due to surface fluctuations may be represented by a current generator between the gate and the source. Thus, this type of noise will not be observed when the gate is short-circuited.

Generation Noise

It is well known that the behavior of silicon junction diodes is influenced by Shockley-Read-Hall (SRH) centers in the depletion region (27). These traps can also be a source of generation noise in junction FET's. This has been shown to be the case in Si:Au FET's (16, 25). Furthermore, it has been shown (25) that SRH depletion-region noise is dominant over SRH channel, donor channel, thermal and shot noise at low frequencies. Previous FET noise theories (8, 9, 10, 35, 37, 39) have treated these special cases.

With the existence of SRH centers established in silicon p-n junctions, the basic properties of a center are reviewed. This is usually an impurity atom; for example, a two-level trap uniformly distributed in the depletion region. It is characterized by a capture cross-section and an activation energy (24).

Following Shockley and Read (32), we derive the expression for the capture rate of a two-level trap. It is assumed that a uniform trap concentration N_t exists in the region of interest. The traps considered are a simple type involving two states; one being negative and the other being neutral. The capture rate is assumed to be

limited by the availability of free carriers, not by the properties of the traps. For such a trap, four processes are possible, as shown in Figure 1.

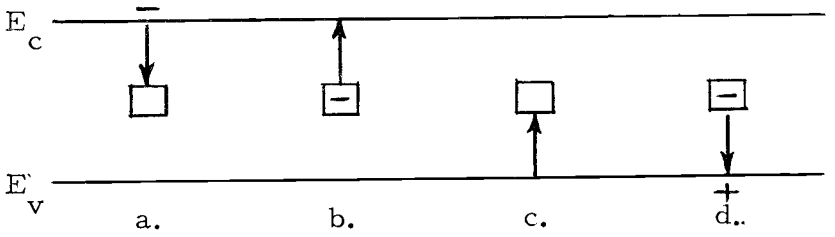

a. electron capture from conduction band
b. electron emission to conduction band
c. hole emission (electron capture from valence band)
d. hole capture (electron emission to valence band)

Figure 1. Basic processes of SRH centers.

For an energy level E, measured from below the valence band, the Fermi factor f and Fermi level F give the occupation probability:

$$f = [\,1 + \exp\,(\frac{E-F}{kT})]^{-1}.$$

The probability that the state is not occupied is defined as

$$f_p = (1-f) = f \exp\,(\frac{E-F}{kT}).$$

Hence, the ratio of filled to empty states is given by

$$\frac{f}{f_p} = [\,\exp\,(\frac{E-F}{kT})]^{-1}.$$

For electrons of energy E, the density of available states in the energy interval dE is $N(E)dE$. Since the occupation probability is $f(E)$, the density of electrons in the interval dE is $f(E)N(E)dE$.

For a single trap, the average probability per unit time of electron capture is given by

$$c_n(E) = <\theta_n \sigma_n>,$$

where θ_n and σ_n are the thermal velocity and capture cross-section for electrons, respectively.

Since the probability that a trap is not occupied is f_{pt}, the density of unoccupied traps is $N_t f_{pt}$.

The rate of electron capture by the traps is given by the product of the capture probability, the density of unoccupied traps, and the density of free electrons:

$$c_n(E) N_t f_{pt} f(E) N(E) dE.$$

By defining an emission probability per unit time, e_n, together with the density of occupied traps and the density of unoccupied electron states, we have the electron emission rate:

$$e_n N_t f_t f_p(E) N(E) dE.$$

The net rate of capture for electrons, U_{cn}, is determined by integrating the difference of the capture and emission rates over the conduction band. The net rate of capture in the energy interval dE is

$$dU_{cn} = [c_n(E)f_{pt}f(E) - e_n f_t f_p(E)]N_t N(E)dE$$

$$= [f_{pt}f(E) - \frac{e_n}{c_n(E)} f_t f_p(E)]c_n(E)N_t N(E)dE.$$

In equilibrium, $dU_{cn} = 0$, so that

$$f_{pt}f(E) = \frac{e_n}{c_n(E)} f_t f_p(E).$$

Using the previously defined ratio f/f_p, and introducing the quasi-Fermi level for electrons, F_n,

$$\frac{e_n}{c_n(E)} = \frac{f_{pt}f(E)}{f_t f_p(E)} = \frac{\exp(\frac{E_t - F_t}{kT})}{\exp(\frac{E - F_n}{kT})}.$$

Since $F_t = F_n$ in thermal equilibrium,

$$\frac{e_n}{c_n(E)} = \exp(\frac{E_t - E}{kT}).$$

Substituting into the nonequilibrium equation for the net rate of capture,

$$dU_{cn} = \left[1 - \exp\left(\frac{E_t - E}{kT}\right) \frac{\exp\left(\frac{E - F_n}{kT}\right)}{\exp\left(\frac{E_t - F_t}{kT}\right)}\right] f_{pt} f(E) c_n(E) N_t N(E) dE$$

$$= \left[1 - \exp\left(\frac{F_t - F_n}{kT}\right)\right] c_n(E) f_{pt} f(E) N_t N(E) dE.$$

Integrating over the conduction band, we obtain the net rate of electron capture:

$$U_{cn} = \left[1 - \exp\left(\frac{F_t - F_n}{kT}\right)\right] f_{pt} N_t \int_{E_c}^{\infty} c_n(E) f(E) N(E) dE .$$

For the application of interest, nondegenerate Fermi statistics can be used. Since the Fermi level is within the bandgap, we can approximate the Fermi function by

$$f(E) \doteq \exp\left(\frac{F - E}{kT}\right).$$

The average value of $c_n(E)$ over the conduction band is calculated as:

$$\langle c_n \rangle = \frac{\int_{E_c}^{\infty} \exp\left(\frac{E_c - E}{kT}\right) c_n(E) N(E) dE}{\int_{E_c}^{\infty} \exp\left(\frac{E_c - E}{kT}\right) N(E) dE} .$$

The denominator in the above expression can be defined as N_c, the

effective density of states in the conduction band.

Also, the electron concentration in the conduction band is

$$n = N_c \exp\left(\frac{F_n - E_c}{kT}\right).$$

Then

$$n\langle c_n \rangle = \exp\left(\frac{F_n - E_c}{kT}\right) \int_{E_c}^{\infty} \exp\left(\frac{E_c - E}{kT}\right) c_n(E)N(E)dE$$

$$= \int_{E_c}^{\infty} \exp\left(\frac{F_n - E}{kT}\right) c_n(E)N(E)dE.$$

Inserting this expression into the equation for U_{cn}, and letting $\langle c_n \rangle = c_n$, the average capture probability rate is

$$U_{cn} = \left[1 - \exp\left(\frac{F_t - F_n}{kT}\right)\right] f_{pt} n N_t c_n.$$

The term $\exp\left(\frac{F_t - F_n}{kT}\right) f_{pt} n$ may be written as

$$\exp\left(\frac{F_t - F_n}{kT}\right) f_t \exp\left(\frac{E_t - F_t}{kT}\right) N_c \exp\left(\frac{F_n - E_c}{kT}\right) = f_t N_c \exp\left(\frac{E_t - E_c}{kT}\right) = f_t n_1,$$

where $n_1 = N_c \exp\left(\frac{E_t - E_c}{kT}\right)$, the number of electrons in the conduction band when the Fermi level is at E_t.

The net rate of electron capture then becomes

$$U_{cn} = N_t c_n (f_{pt} n - f_t n_1).$$

In a similar manner, the net capture rate of holes is derived. The probability rate of hole capture is defined as

$$c_p(E) = <\theta_p \sigma_p>$$

where θ_p and σ_p are the thermal velocity and capture cross-section for holes, respectively. We note that the converse Fermi functions are to be used for holes; a filled electron state is an empty hole state. Similarly, $N(E)$ is now defined as the density of states in the valence band.

For hole capture, the net rate is therefore

$$c_p(E) N_t f_t f_p(E) N(E) dE .$$

For hole emission, the net rate due to the emission probability is

$$e_p N_t f_{pt} f(E) N(E) dE .$$

The net rate of hole capture is

$$dU_{cp} = [c_p(E) f_t f_p(E) - e_p f_{pt} f(E)] N_t N(E) dE .$$

In thermal equilibrium, $dU_{cp} = 0$, and $F_p = F_t$, such that

$$\frac{e_p}{c_p(E)} = \frac{f_t f_p(E)}{f_{pt} f(E)} = \frac{\exp(\frac{E-F_p}{kT})}{\exp(\frac{E_t-F_t}{kT})} = \exp(\frac{E-E_t}{kT}) .$$

Inserting this relation into the general equation for dU_{cp}, we obtain

$$dU_{cp} = \left[1 - \exp\left(\frac{F_p - F_t}{kT}\right)\right] c_p(E) f_t f_p(E) N_t N(E) dE .$$

Integrating over the valence band,

$$U_{cp} = \left[1 - \exp\left(\frac{F_p - F_t}{kT}\right)\right] f_t N_t \int_o^{E_v} c_p(E) f_p(E) N(E) dE .$$

Using nondegenerate Fermi statistics, since $E < F_p$ for holes,

$$f_p = \frac{\exp\left(\frac{E-F_p}{kT}\right)}{1 + \left(\exp\frac{E-F_p}{kT}\right)} \doteq \exp\left(\frac{E-F_p}{kT}\right).$$

The average value of the hole capture probability is then calculated as

$$\langle c_p \rangle = \frac{\int_o^{E_v} \exp\left(\frac{E-E_v}{kT}\right) c_p(E) N(E) dE}{\int_o^{E_v} \exp\left(\frac{E-E_v}{kT}\right) N(E) dE} .$$

The effective density of states in the valence band is defined as

$$N_v = \int_o^{E_v} \exp\left(\frac{E-E_v}{kT}\right) N(E) dE .$$

The density of holes in the conduction band is

$$p = N_v \exp\left(\frac{E_v - F_p}{kT}\right).$$

Then we may write

$$p\langle c_p \rangle = \exp\left(\frac{E_v - F_p}{kT}\right) \int_o^{E_v} \exp\left(\frac{E - E_v}{kT}\right) c_p(E) N(E) dE$$

$$= \int_o^{E_v} \exp\left(\frac{E - F_p}{kT}\right) c_p(E) N(E) dE.$$

To simplify notation, we define $\langle c_p \rangle$ as c_p, the average probability rate of hole capture. Then the net rate of hole capture may be expressed as

$$U_{cp} = \left[1 - \exp\left(\frac{F_p - F_t}{kT}\right)\right] N_t c_p p f_t.$$

Using the fact that $f_t = f_{pt} \exp\left(\frac{F_t - E_t}{kT}\right)$, the term $\exp\left(\frac{F_p - F_t}{kT}\right) p f_t$ may be written as

$$\exp\left(\frac{F_p - F_t}{kT}\right) f_{pt} \exp\left(\frac{F_t - E_t}{kT}\right) N_v \exp\left(\frac{E_v - F_p}{kT}\right)$$

$$= f_{pt} N_v \exp\left(\frac{E_v - E_t}{kT}\right) = f_{pt} p_1$$

where $p_1 = N_v \exp\left(\frac{E_v - E_t}{kT}\right)$.

Thus, we have

$$U_{cp} = N_t c_p (f_t p - f_{pt} p_1).$$

We are now in a position to calculate the fluctuation in electron concentration due to the net rate of capture and emission at the traps (25). The concentration of trapped electrons, n_t, is given by the fraction of filled traps, $N_t f_t$. The fluctuation in trapped electron concentration is the time derivative of this quantity, and this in turn is equal to the difference in capture rates for electrons and holes:

$$\frac{\partial (N_t f_t)}{\partial t} = \frac{\partial n_t}{\partial t} = U_{cn} - U_{cp}$$

$$= N_t [c_n (f_{pt} n - f_t n_1) - c_p (f_t p - f_{pt} p_1)].$$

Since $N_t f_t = n_t$, and $N_t f_{pt} = N_t - N_t f_t = N_t - n_t$, we may write

$$\frac{\partial n_t}{\partial t} = c_n n (N_t - n_t) - c_n n_t n_1 - c_p n_t p + c_p p_1 (N_t - n_t)$$

or

$$\frac{\partial n_t}{\partial t} = - n_t [c_p (p + p_1) + c_n (n + n_1)] + N_t (c_p p_1 + c_n n).$$

The regression of the electron fluctuation is calculated by

expanding the electron and hole concentrations around the steady-state values, such that

$$n = n_o + \delta n, \quad p = p_o + \delta p, \quad \text{and} \quad n_t = n_{to} + \delta n_t .$$

The differential equation may be written

$$\frac{\partial (n_{to} + \delta n_t)}{\partial t} = - (n_{to} + \delta n_t)[c_p (p_o + \delta p + p_1) + c_n (n_o + \delta n + n_1)]$$
$$+ N_t (c_p p_1 + c_n n_o + c_n \delta n).$$

The time-derivative of the fluctuation is given by

$$\frac{\partial (\delta n_t)}{\partial t} = \frac{\partial (n_{to} + \delta n_t)}{\partial t} - \frac{\partial n_{to}}{\partial t}$$
$$= - n_{to}[c_p (p_o + \delta p + p_1) + c_n (n_o + \delta n + n_1)]$$
$$+ N_t (c_p p_1 + c_n N_o + c_n \delta n)$$
$$- \delta n_t [c_p (p_o + \delta p + p_1) + c_n (n_o + \delta n + n_1)]$$
$$+ n_{to}[c_p (p_o + p_1) + c_n (n_o + n_1)] - N_t (c_p p_1 + c_n n_o)$$
$$= - n_{to}[c_p \delta p + c_n \delta n] + N_t c_n \delta n$$
$$- \delta n_t [c_p (p_o + p_1 + \delta p) + c_n (n_o + n_1 + \delta n)]$$
$$= - \delta n_t [c_p (p_o + p_1) + c_n (n_o + n_1)] - c_p \delta n_t \delta p - c_n \delta n_t \delta n$$
$$- n_{to} c_p \delta p + c_n \delta n (N_t - n_{to}) .$$

For small fluctuations, the second-order terms involving $\delta n_t \delta p$ and $\delta n_t \delta n$ are small and may be dropped, yielding

$$\frac{\partial(\delta n_t)}{\partial t} \doteq - \delta n_t [c_p(p_o + p_1) + c_n(n_o + n_1)] - n_{to} c_p \delta p + c_n \delta n (N_t - n_{to}).$$

The complexities of the general solution to this equation can be avoided by considering only the portion in δn_t. The solutions including δp and δn yield much shorter time constants and can be neglected here (25). We must assume that the capture and emission probabilities remain independent of the electric field, since we are concerned with processes within the p-n junction of an FET.

A simple exponential solution is assumed for δn_t:

$$\delta n_t(t) = (\delta n_t)_o \exp(-t/\tau_t)$$

where $(\delta n_t)_o$ is the initial fluctuation and τ_t is the fluctuation time constant. Letting δn and $\delta p = 0$ in the above differential equation, and substituting the above solution, we find that

$$\frac{\partial(\delta n_t)}{\partial t} = -1/\tau_t (\delta n_t)_o \exp(-t/\tau_t) = - (\delta n_t)_o \exp(-t/\tau_t)[c_p(p_o + p_1) + c_n(n_o + n_1)]$$

yielding

$$\tau_t = [c_p(p_o + p_1) + c_n(n_o + n_1)]^{-1}.$$

Since the expression for τ_t is intended to apply in the depletion region of a p-n junction, the electric field will deplete the region of free carriers. Hence, the steady-state hole and electron concentrations, p_o and n_o, may be assumed to be negligible. The resulting maximum time constant, valid for the depletion region, is therefore

$$\tau_t = [c_p p_1 + c_n n_1]^{-1}.$$

The noise spectrum due to the fluctuation in trapped electrons may be calculated from the Wiener-Khintchine Theorem (38, p. 316). The random variable is $\Delta\delta n_t(t)$, the electron fluctuation in an elemental volume Δ.

The correlation coefficient $C(s)$ is

$$C(s) = \frac{<[\Delta\delta n_t(t)][\Delta\delta n_t(t+s)]>}{<[\Delta\delta n_t(t)]^2>}.$$

The random variable corresponds to a stationary process, therefore the ensemble average, and hence the variance, is independent of time (19, p. 149). Therefore the correlation function may be written as

$$<[\Delta\delta n_t(t)][\Delta\delta n_t(t+s)]> = <[\Delta\delta n_t]_o^2> C(s).$$

The spectrum is then

$$S_{\Delta\delta n_t}(f) = 4 \int_o^\infty <[\Delta\delta n_t]_o^2> C(s) \cos \omega s ds.$$

Since $\delta n_t(t)$ has been shown to be an exponential function of time, $C(s)$ is also an exponential function:

$$\frac{\exp(-t/\tau_t) \exp(-\frac{(t+s)}{\tau_t})}{\exp(-2t/\tau_t)} = \exp(-s/\tau_t).$$

The expression for the spectrum then can be written

$$S_{\Delta\delta n_t}(f) = 4 <[\Delta\delta n_t]_o^2> \int_o^\infty \exp(-s/\tau_t) \cos \omega s ds$$

$$= 4 <[\Delta\delta n_t]_o^2> [\frac{\tau_t}{1+\omega^2 \tau_t^2}].$$

The variance may be calculated by differentiation with respect to the Fermi level (17)

$$<[\Delta\delta n_t]_o^2> = kT \left(\frac{\partial(\Delta n_t)}{\partial F_t}\right)_T.$$

We recall that $\Delta n_t = \Delta N_t f_t = \dfrac{\Delta N_t}{1+\exp(\frac{E_t - F_t}{kT})}$

so that

$$\Delta N_t \frac{\partial f_t}{\partial F_t} = \Delta N_t \frac{\partial}{\partial F_t}\left[1+\exp\left(\frac{E_t-F_t}{kT}\right)\right]^{-1}$$

$$= \Delta N_t\left\{-\left[1+\exp\left(\frac{E_t-F_t}{kT}\right)\right]^{-2}\left[-\frac{1}{kT}\exp\left(\frac{E_t-F_t}{kT}\right)\right]\right\}$$

$$= \frac{\Delta N_t}{kT} f_t f_{pt}.$$

Then the variance becomes

$$<[\Delta\delta n_t]_o^2> = \Delta N_t f_t f_{pt}.$$

Dividing both sides of the equation for the variance by Δ^2, we have

$$<[\delta n_t]_o^2> = \frac{N_t f_t f_{tp}}{\Delta}.$$

Thus, the final expression for the generation noise spectrum of the mean-square fluctuation of trapped electrons is

$$S_{\delta n_t}(f) = \frac{4N_t f_t f_{tp}}{\Delta}\left[\frac{\tau_t}{1+\omega^2\tau_t^2}\right].$$

Temperature Dependence of SRH Noise

The general form of the equation for the generation noise spectrum may be related to a variety of simple trapping processes in semiconductors. The frequency dependent term is a consequence of

the single time constant assumed for the trapping mechanism. For example, it may be used to describe majority carrier trapping at ionized impurity sites (35); or minority carrier recombination at SRH centers in a p-n junction (25, 27); or, as in this work, the equation is most useful in describing the noise spectrum due to majority carrier trapping at SRH centers in the depletion region of junction FET's. It has been shown that of the three processes mentioned above, the third dominates at low frequencies (25).

From the previous derivation, it will be shown that τ_t is an exponential function of temperature. Consequently, as the temperature is varied, one would expect to observe variations in S(f).

When the frequency-dependent term $\tau_t(1+\omega^2\tau_t^2)^{-1}$ is differentiated with respect to τ_t, one finds that the term is at a maximum when $\omega^2\tau_t^2 = 1$. Since τ_t is a function of temperature, the noise spectrum S(f) will also be a maximum when $\omega^2\tau_t^2 = 1$.

The previously-derived expression for τ_t, valid in the depletion region is

$$\tau_t = [c_p p_1 + c_n n_1]^{-1}$$

where

$$p_1 = N_v \exp\left(\frac{E_v - E_t}{kT}\right)$$

and

$$n_1 = N_c \exp\left(\frac{E_t - E_c}{kT}\right).$$

We observe that N_c is the effective density of states in the conduction band, and is given by (29, p. 240)

$$N_c = 2\left(\frac{2\pi m_e kT}{h^2}\right)^{3/2} .$$

Similarly,

$$N_v = 2\left(\frac{2\pi m_h kT}{h^2}\right)^{3/2} .$$

In the above equations, m_e and m_h are the effective masses of electrons and holes, respectively.

For only donor traps present in the bandgap, such that p_1 is negligible, the expression for the time constant becomes

$$\tau_{t_n} = (c_n n_1)^{-1} = \left[c_n N_c \exp\left(\frac{E_t - E_c}{kT}\right)\right]^{-1}$$

$$= \frac{T^{-3/2}\exp\left(\frac{E_c - E_t}{kT}\right)}{2\left(\frac{2\pi mk}{h^2}\right)^{3/2}} .$$

For $(E_t - E_c) \gg kT$, the temperature dependence of τ_{t_n} will be dominated by the exponential term. Since most observed trap energies are near the center of the bandgap, τ_{t_n} is nearly an exponential function of temperature.

The function $\tau_{t_n}(1+\omega^2\tau_{t_n}^2)^{-1}$ is plotted versus T in Figure 2a. The maximum is given by $\omega^2\tau_t^2 = 1$, and the leading and

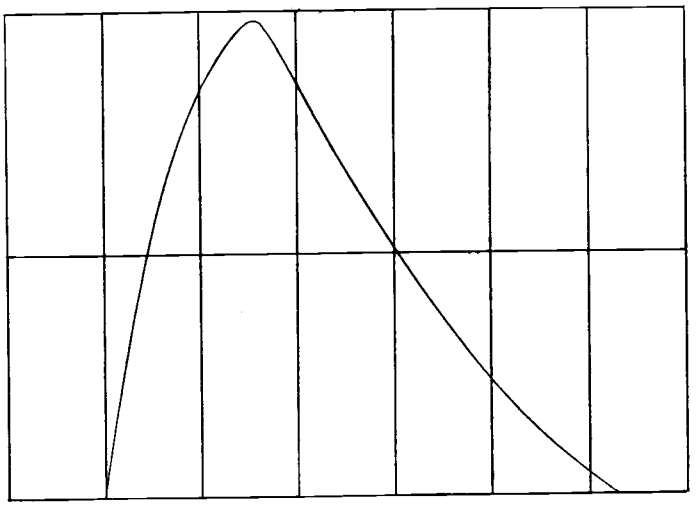

a. LINEAR TEMPERATURE PLOT

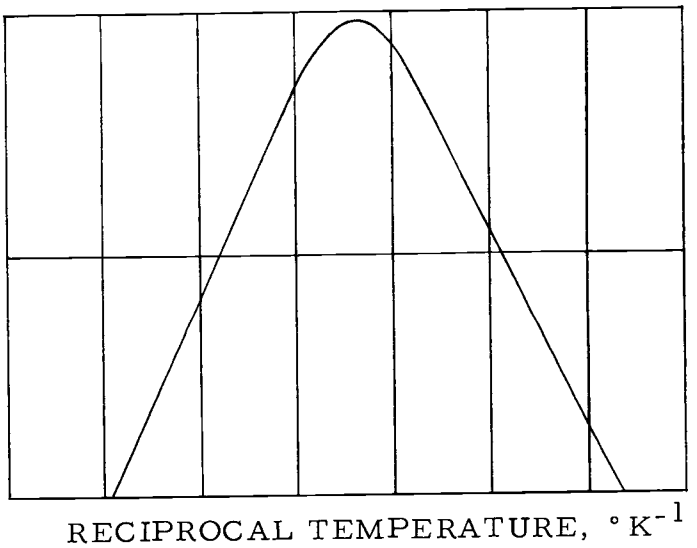

b. RECIPROCAL TEMPERATURE PLOT

Figure 2. $\tau_t(1+\omega^2\tau_t^2)^{-1}$ versus temperature.

trailing edges are exponential functions of T. If this function is replotted versus T^{-1}, as in Figure 2b, the leading and trailing edges have slopes that are proportional to the activation energy of the trap. Furthermore, if the frequencies at which the maximum occurs for various temperatures are known, then the temperature dependence of τ_t can be determined. Again, a plot of τ_{t_n} versus T^{-1} can yield the activation energy of the trap. Methods for relating the activation energy to the slope of the plot are presented in Appendix II.

The above discussion also applies if only acceptor traps are present. In general, both types of traps will be effective. For the special case where the traps are located exactly in the center of the bandgap,

$$E_t = \left(\frac{E_c - E_v}{2}\right) .$$

When the capture cross-sections are equal, τ_t will be inversely proportional to n_i, the intrinsic carrier concentration.

Since

$$n_i^2 = (p_1 n_1) = (N_v N_c) \exp\left(\frac{E_v - E_c}{kT}\right) ,$$

if $N_v = N_c$, then $p_1 = n_1 = n_i$

and

$$\tau_{t_i} = (2c_n n_i)^{-1} \propto T^{-3/2} \exp\left(\frac{E_{go}}{2kT}\right)$$

where $E_{go} = (E_c - E_v)$, the energy gap at $T = 0$.

Noise in the One Dimensional Model

The model used by Shockley (31) is presented in Figure 3 in order to derive the expression for device noise due to fluctuations at SRH centers in the depletion region (25).

The charge distribution also shown in Figure 3 identifies an element of fluctuating charge, δn_t, due to the traps in a small volume $\Delta\Lambda$ at $x = x_1$. This fluctuation modulates the channel width. A voltage generator $V_n(t)$ is connected between the gate and the source, such that variations in the channel width are exactly cancelled by $V_n(t)$. Thus, it is possible to analyze the charge fluctuation for zero drain bias even though no measurable output is available at the drain terminal.

Given the localized charge fluctuation $\delta n_t(x_1, t)$, Poisson's equation is used to calculate the corresponding potential fluctuation. The net charge concentration is the sum of the net free and trapped charge:

$$\rho = q(p - n + N_D - n_t).$$

Then Poisson's equation in one dimension gives

$$\frac{\partial E}{\partial x} = \frac{q}{K\varepsilon_o}(p - n + N_D - n_t).$$

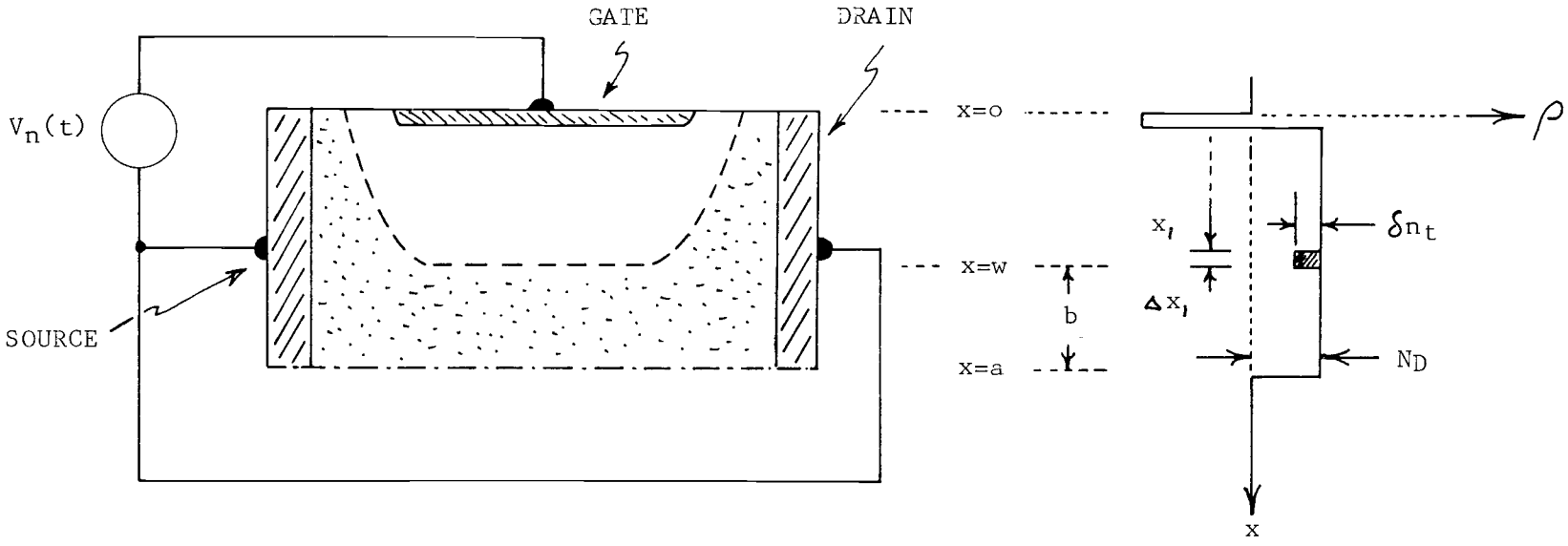

Figure 3. One-dimensional FET model.

Calculating the regression of the charge fluctuation, we find that

$$\frac{\partial(\delta E)}{\partial x} = \frac{\partial(E_o + \delta E)}{\partial x} - \frac{\partial E_o}{\partial x} = \frac{q}{K\varepsilon_o}[\delta p - \delta n - \delta n_t].$$

The quantities δp and δn can be neglected since they represent the high-frequency fluctuations of free carriers.

The fluctuation in the incremental volume is obtained by representing that portion by the Dirac delta function, such that the incremental electron fluctuation is $\delta n_t \Delta x_1 \delta(x-x_1)$. Then Poisson's equation becomes

$$\frac{\partial(\Delta\delta E)}{\partial x} \doteq - \frac{q}{K\varepsilon_o} \delta n_t \Delta x_1 \delta(x-x_1).$$

Solving for $\Delta\delta E$,

$$\Delta(\delta E) = - \frac{q}{K\varepsilon_o} \delta n_t \Delta x_1 \int_{-\infty}^{\infty} \delta(x-x_1)dx$$

$$= - \frac{q}{K\varepsilon_o} \delta n_t \Delta x_1.$$

Then, where $\delta\psi$ is the fluctuation in potential,

$$\Delta(\delta\psi) = - \int_o^{x_1} \Delta(\delta E)dx = \frac{q}{K\varepsilon_o} \delta n_t x_1 \Delta x_1.$$

Since the input source must exactly cancel this potential fluctuation,

$$\Delta V_n(t) = -\frac{q}{K\varepsilon_o}\,\delta n_t x_1 \Delta x_1 .$$

The spectrum of the mean-square voltage fluctuation is obtained by summing the contributions of $\Delta(\delta\psi)$ over the depletion region. The noise voltage becomes

$$(\Delta V_n)^2 = \sum_{\Delta x_1} S_{\Delta(\delta\psi)}(f)\Delta f .$$

The spectrum is obtained in a manner similar to that used for $\Delta\delta n_t$ in the previous section; however, $\Delta(\delta\psi)$ now becomes the random variable. Therefore, we have

$$S_{\Delta(\delta\psi)}(f)\Delta f = 4\Delta f \left(\frac{\tau_t}{1+\omega^2\tau_t^2}\right) \langle (\Delta\delta\psi)_o^2 \rangle .$$

Since

$$\langle (\Delta\delta\psi)_o^2 \rangle = \left(\frac{q}{K\varepsilon_o} x_1 \Delta x_1\right)^2 \langle (\delta n_t)_o^2 \rangle = N_t f_t f_{tp} \Delta\Lambda \left(\frac{q}{K\varepsilon_o} x_1 \Delta x_1\right)^2 ,$$

$$S_{\Delta(\delta\psi)}(f)\Delta f = 4\Delta f \left(\frac{q}{K\varepsilon_o} x_1 \Delta x_1\right)^2 \left(\frac{\tau_t}{1+\omega^2\tau_t^2}\right) N_t f_t f_{tp} \Delta\Lambda .$$

Letting the volume increment $\Delta\Lambda = A\Delta x_1$, and dividing by $(\Delta\Lambda)^2$,

$$V_n^2 = \sum_{\Delta x_1} \frac{4\Delta f}{A} \left(\frac{q}{K\varepsilon_o} x_1\right)^2 \left(\frac{\tau_t}{1+\omega^2\tau_t^2}\right) N_t f_t f_{tp} \Delta x_1 .$$

Allowing the increment Δx_1 to approach dx_1, and replacing the summation with integration from 0 to W,

$$V_n^2 = \frac{4\Delta f N_t}{A} \left(\frac{q}{K\varepsilon_o}\right)^2 \int_o^W \frac{\tau_t}{1+\omega^2\tau_t^2} f_t f_{tp} x_1^2 dx_1 .$$

By assuming that τ_t and $f_t f_{tp}$ are independent of x, as in the case of an ideal depletion region, the integral becomes $W^3/3$. Thus,

$$V_n^2 = \frac{4\Delta f N_t f_t f_{tp} W^3}{3A} \left(\frac{q}{K\varepsilon_o}\right)^2 \frac{\tau_t}{1+\omega^2\tau_t^2} .$$

An analysis of the two-dimensional model by Sah (25) yields the above result for the special case of small drain current and voltage. Other operating conditions yield similar forms, differing in minor geometrical factors. Thus, to an approximation, this equation may be used for the device noise voltage referred to the input.

Temperature Dependence of FET Characteristics

The FET characteristics which determine the operating conditions for noise measurements must be examined for possible variations with temperature. Since the devices studied here are of planar construction, it is useful to review the device geometry of an n-channel FET shown in Figure 4.

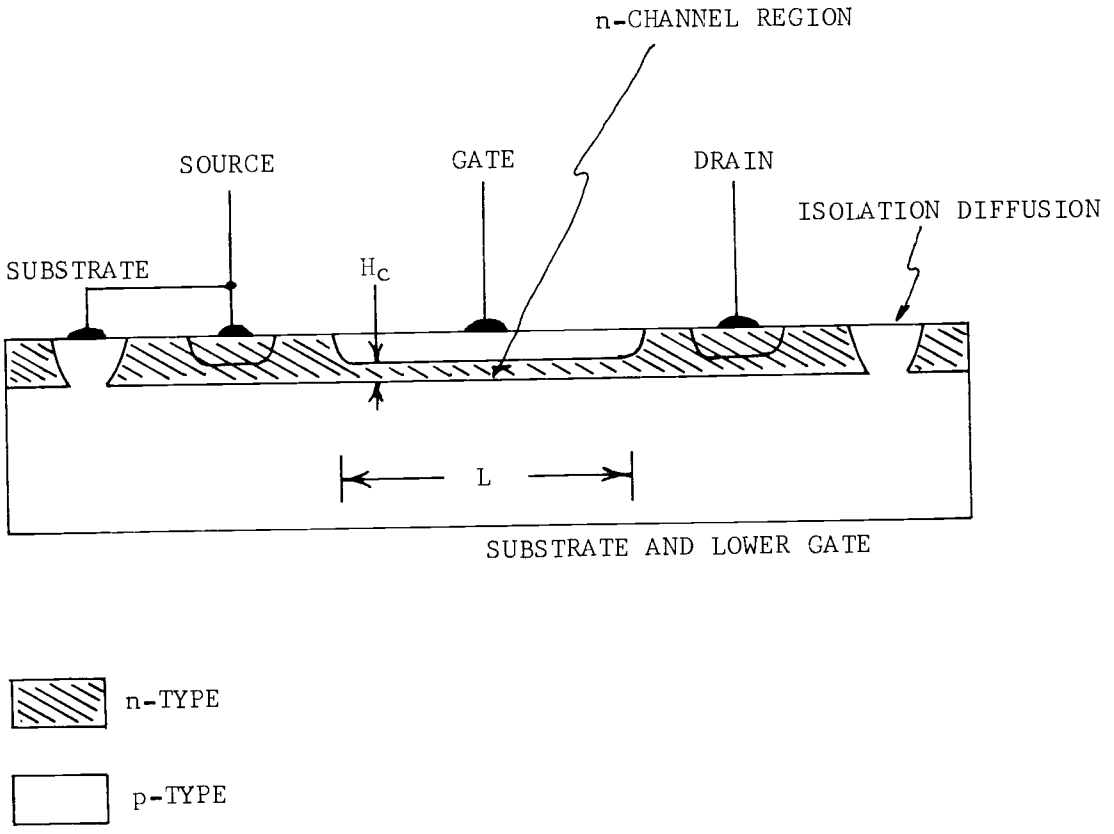

Figure 4. Planar FET construction.

The temperature dependence of device performance may be separated into two temperature regions: (a) above and (b) below the temperature at which the channel carriers begin to become thermally de-ionized. In region (a), the channel carrier concentration may be considered to be constant, and the mobility will vary due to thermal scattering. In region (b), the carrier concentration will exhibit the onset of exponential temperature dependence.

Referring to Figure 4, it is seen that there are two distinct regions in the channel which are affected by the mobility and carrier concentration. The first is the active channel area contiguous to the upper gate region, in which pinchoff occurs. In this region, the channel carrier concentration, mobility, depletion layer width and effective channel height will be functions of temperature. The second channel region which affects device performance are the areas connecting the channel with the source and drain contacts. These areas act as series channel resistances, independent of other characteristics. Both of these channel regions may affect the drain current, transconductance and pinchoff characteristics.

Drain Saturation Current (I_{DSS})

The expression for I_{DSS}, as derived by Sevin (28, p. 22) is

$$I_{DSS} = \frac{qW\mu P_o^2 (H_c/2)^3}{6\varepsilon L}$$

where

q = electronic charge

W = channel width

μ = majority carrier mobility

P_o = channel carrier concentration

H_c = channel height

L = channel length.

In this equation, μ, P_o and H_c are functions of temperature.

Mobility, μ. When the majority carriers are fully ionized, above 200° K, the mobility will vary as $T^{-3/2}$ due to thermal scattering (29, p. 287). In practice, slightly larger values of exponent, between $-3/2$ and -2, are observed due to dependence upon impurity concentration.

Carrier Concentration, P_o. Below 200° K, when the channel impurities begin to become deionized, P_o will vary exponentially with temperature. Assuming that the channel is highly doped and that some residual acceptors are present, the Fermi level will approach E_D at zero temperature (29, p. 360). Thus P_o will vary as $\exp(-E_D/kT)$.

Channel Height, H_c. The height of the channel is established by the edges of the depletion region bounded by the upper and lower gates. The depletion region boundary will vary with carrier

concentration and hence with temperature. Assuming that the channel and gates have the same impurity concentration, the depth of this depletion region is (20, p. 21)

$$d_p = \left(\frac{2\varepsilon \varepsilon_o V_t}{qP_o} \right)^{1/2}$$

where V_t = the applied voltage plus junction potential. For temperatures below 200° K, the carrier concentration will decrease. Assuming the exponential temperature dependence of P_o,

$$H_c \propto d_p \propto P_o^{-1/2} \propto \exp (E_D/2kT).$$

Transconductance

The transconductance may be expressed as (28, p. 42)

$$g_m \doteq \frac{4qW}{\varepsilon L} \mu V_p = \frac{2I_{DSS}}{V_p} .$$

At temperatures above 200° K, all terms except μ and V_p are constant, since the channel carrier concentration is constant. Furthermore, if V_p is independent of temperature, g_m would be proportional to μ, which is in turn proportional to $T^{-3/2}$. As shown below, V_p exhibits a behavior proportional to temperature at sufficiently high temperatures.

Pinchoff Voltage, V_p

The pinchoff voltage is given as (28, p. 7)

$$V_p = \frac{qP_o H_c^2}{8\varepsilon} - \phi,$$

where ϕ is the junction potential, given by

$$\phi = \frac{kT}{q} \ln \left(\frac{N_A N_D}{n_i^2} \right).$$

Since n_i^2 may be expressed as (2, p. 127)

$$n_i^2 = 1.5 \times 10^{33} T^3 \exp \left(\frac{-1.4 \times 10^4}{T} \right),$$

ϕ becomes

$$\phi = \frac{k}{q} \left[1.4 \times 10^4 - T \ln \left(\frac{1.5 \times 10^{33} T}{N_A N_D} \right) \right].$$

Then the expression for the pinchoff voltage may be written as

$$V_p = \frac{k}{q} \left[\frac{q^2 P_o H_c^2}{8k\varepsilon} + T \ln \left(\frac{1.5 \times 10^{33} T}{N_A N_D} \right) - 1.4 \times 10^4 \right].$$

At low temperatures the middle term is small so that V_p is independent of temperature. At higher temperatures, this term is effective and V_p tends to increase with T. The exact temperature

dependence is determined by the relative values of the above terms, and hence varies with the channel and gate doping levels.

Summary

At temperatures above approximately 200° K, the channel carrier concentration is constant, being equal to the impurity concentration. From the expression for I_{DSS}, only μ will be temperature-dependent. Thus, a $T^{-3/2}$ behavior of I_{DSS} should be observed in this region.

Below 200° K, thermal deionization of the channel carriers will occur, resulting in an exponential decrease in carrier concentration. Substituting the low-temperature exponential behavior for P_o and H_c into the expression for I_{DSS},

$$I_{DSS} \propto \mu P_o^2 P_o^{-3/2} = \mu P_o^{1/2} \propto \mu \exp(-E_D/2kT).$$

Thus, at low temperatures only, this expression should describe the behavior of I_{DSS}.

In general, the precise behavior below 200° K is difficult to identify since many factors are present. Variations in mobility, concentration gradients and series resistances all contribute to the observed behavior. The effects of these factors will depend upon the geometry of the device under consideration.

III. MEASUREMENT OBJECTIVES

General Considerations

In order to implement the required measurements, some standardization and hence compromising was required in order to include a variety of representative devices. Since the primary objective of this study was to provide information relevant to circuit design, it was decided to operate all devices in a standard circuit configuration, with operating parameters similar to those used in low-noise, high-gain voltage amplifiers. The following conditions were established:

1. operation in the common-source configuration;
2. operation in the saturation region, beyond pinchoff, with a drain-source potential of six volts; and
3. operation at zero-volts gate-source voltage.

These are the conditions that provide maximum transconductance, minimum gate leakage and lowest noise.

Parameters to be Measured

In Section II the various temperature dependent components of FET noise were identified. To indicate the significance of the various FET operating parameters, the latter are given with their relation to predicted device performance.

Drain Saturation Current, I_{DSS}

This is approximately the drain current by virtue of the standardized operating conditions. It indicates the point at which thermal deionization of channel carriers begins to take place.

Transconductance, g_m

The theoretical expression for thermal device noise contains g_m in the denominator. The measurement of this parameter enables comparison with theory. Also, a necessary consequence of measuring g_m is the measurement of system voltage gain. This gain is required in order to express noise voltages referred to the input of the device. The majority carrier mobility may also be inferred from the measured value of g_m.

Gate Reverse Leakage Current, I_{GSS}

The shot noise of the device and SRH generation noise are consequences of the mechanisms contributing to the gate leakage current. Also, surface leakage is an inseparable part of this current, and may contribute a surface noise component. In low-noise FET's I_{GSS} is very low, decreasing exponentially with temperature. Thus, low-temperature measurements of this parameter are not practical.

Equivalent Input Noise Voltage, e_n

The theoretical discussion derives the device noise voltage referred to the input. This is the standard method of comparing noise performance of devices under the condition of short-circuited input. This parameter is temperature and frequency-dependent.

Equivalent Input Noise Current, i_n

The device noise under open-circuited input conditions may be represented by a current generator i_n at the input. Since truly open-circuited conditions are difficult to establish at the input of an FET due to stray capacitance and the inherently high input impedance, measurement of i_n is usually not practical. Noise contributions from the gate current shot noise and drain-gate coupling are usually manifested in this parameter.

For purposes of system application, the frequency range of measurements was restricted between 20 Hz and 50 KHz. Most circuits with high input impedance are usually limited to this range by the input capacitance.

Preliminary measurements of silicon FET characteristics indicated that device performance deteriorated excessively below liquid nitrogen temperature (77° K). Since low-temperature operation of these devices is the principal objective of this research, the

temperature range of 300° K to 77° K was chosen.

The specified operating conditions, temperature and frequency ranges enable a variety of FET's to be compared on a common basis for their suitability as low-noise, low-temperature voltage amplifiers. The range of parameters to be measured lies within the capabilities of available instrumentation and measurement techniques.

Device Selection

The selection of FET's was restricted to devices suitable for use in practical, high-gain, low-noise voltage amplifier circuits. The general qualifications were low I_{DSS}, low V_p, high g_m, and low I_{GSS}. Both n- and p-channel devices were selected. In order to obtain possible evidence of process control, FET's from many different manufacturers were selected. Aside from one hetero-epitaxial germanium unit, all FET's were silicon. A total of 14 FET's, many in duplicate, were selected for the measurements. The pertinent characteristics of these devices are shown in Table 1.

Table 1. FET characteristics.

No.	Type	Mfg. * Code	Channel	Characteristics at 300° K			Notes
				I_{DSS}, ma	V_p, v.	g_m, μ℧	
1	2N-3089A	a.	n	1.0	2.8	600	Low-noise at 77° K
2	2N-3089A	a.	n	0.8		550	
3	2N-3821	d.	n	1.6	0.8	4,500	Low-noise at 300° K
4	( )**	c.	n	4.0	5.0	1,250	Epi-diffused, same geometry
5	( )**	c.	n	0.8	2.0	1,000	as 2N-3376
6	2N-3684	e.	n	4.0	2.8	2,700	Noisy at 77° K
7	2N-2608	c.	p	2.0	1.6	2,000	Diffused
8	2N-2608	c.	p	1.2	1.5	1,600	
9	(2N-2608)	e.	p	4.0	2.5	3,000	Epitaxial, same geometry as
10	(2N-2608)	e.	p	2.3	1.8	2,300	2N-2608 (FP-6)
11	2N-3578	c.	p	2.3	2.2	2,300	Low-noise, large geometry
12	2N-3578	c.	p	2.2	2.2	2,300	
13	2N-4382	b.	p	23.0	6.5	3,500	Large geometry
14	TIXM301	d.	p	8.0	1.8	10,000	Heteroepitaxial germanium - silicon

* Manufacturer Code:
a. Crystallonics
b. Fairchild
c. Siliconix
d. Texas Instruments
e. Union Carbide

**Prototype of 2N-4867

( ) = Developmental sample

IV. MEASUREMENT TECHNIQUES

Apparatus

The device parameters to be measured as a function of temperature were discussed previously. Those that could be conveniently measured in the temperature range of interest were I_{DSS}, g_m and e_n. The frequency spectrum of e_n was also measured since the noise spectrum may be due to multiple time constant traps. Also, the measurement instrumentation voltage gain and noise was measured to avoid possible measurement errors. A set of characteristic curves at representative temperatures was necessary to assure proper circuit operation. Thus, the data taken for each FET included:

drain-source characteristic curves at 300° K, 200° K, 77° K;

I_{DSS} versus temperature, 300° K to 77° K;

g_m versus temperature, 300° K to 77° K;

e_n versus temperature, 300° K to 77° K, at 20, 200 and 1000 Hz;

e_n versus frequency at 300° K, 200° K, 77° K;

overall system voltage gain versus frequency and temperature, 20 Hz to 50 KHz; and

measurement system gain and noise versus frequency.

For all temperature dependent measurements, an x-y chart recorder was selected for automatic plotting of the parameters. This enabled unanticipated phenomena to be observed and greatly increased

the effective number of data points that could be taken.

The measurement of device temperature was accomplished by means of a thermocouple attached to a heat sink which was attached to the case of the FET. A great deal of experimentation was required to achieve good temperature control and tracking. Since liquid nitrogen (77° K) was to be the lower temperature limit, this was used as a cold reference with a thermal gradient established to control the device temperature. A preliminary system using an electrical heater around the FET proved to be unstable. The final system consisted of the apparatus sketched in Figure 5.

The copper block attached to the case of the FET served as a cold sink, lengthened the thermal time constant, and provided a common thermal sink for the FET and thermocouple. Since some FET's have the gate connected to the case, the thermocouple must be electrically insulated but thermally connected to the block. This was accomplished by placing a thin layer of mica between the thermocouple and the block. The FET was located at the end of a glass rod and enclosed in a shielded test-tube. The tube was filled with nitrogen gas to avoid moisture condensation. The FET and thermal sink were surrounded with polyurethane foam to further reduce the thermal time constant.

Prior to the measurements, the rod, FET and thermal sink were immersed in liquid nitrogen. It was then withdrawn and placed

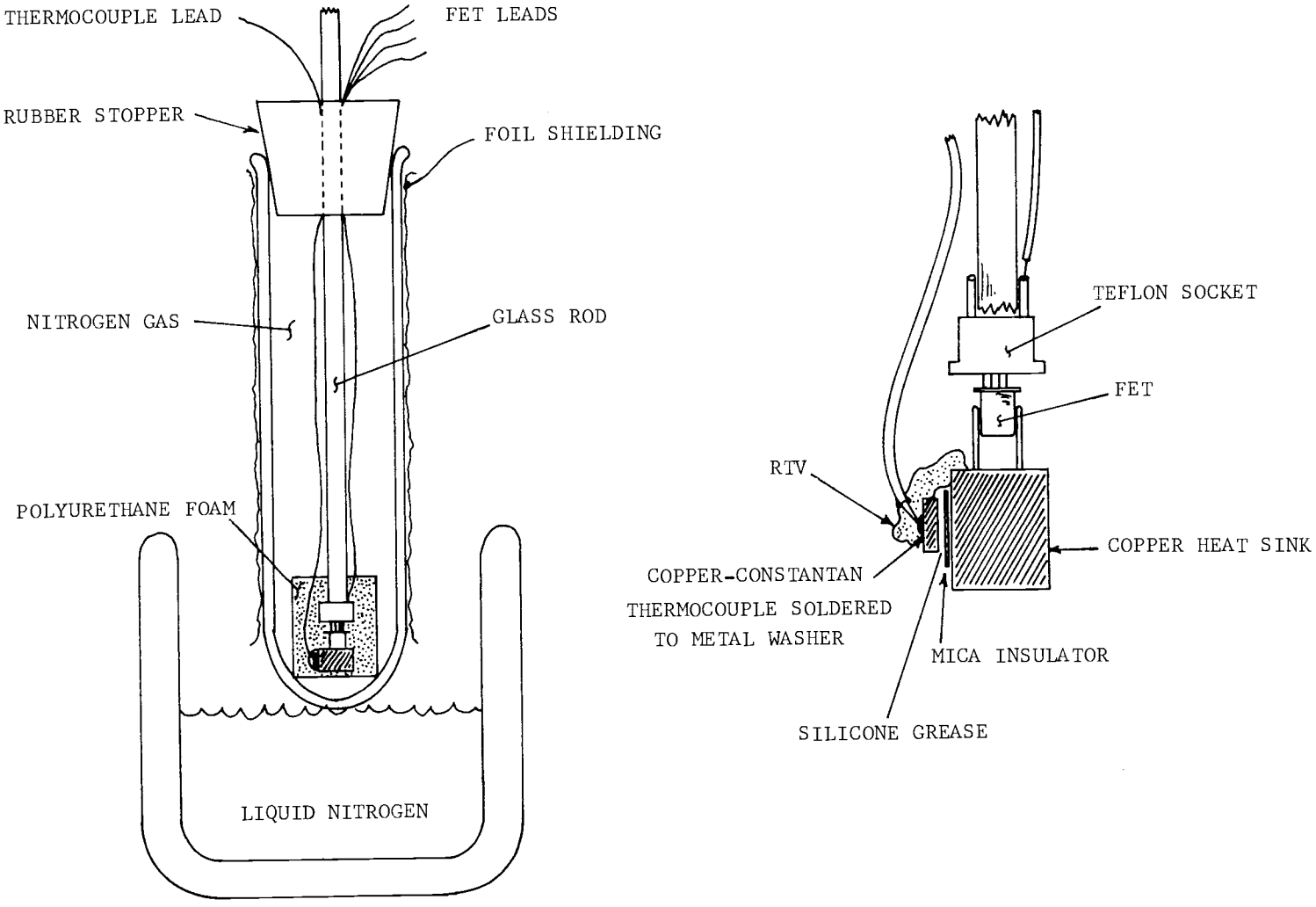

Figure 5. Temperature control apparatus

in the test tube. A sufficient amount of liquid nitrogen was retained in the foam to maintain the FET temperature at 77° during this process. Then, the FET was allowed to warm slowly by the process of thermal conduction in the test tube. The bottom end of the test tube was placed at or near the liquid nitrogen level to achieve some control over the conduction rate. This method provides a scan time of approximately 15 minutes between 77° K and 300° K. This period was required to achieve sufficient accuracy in the noise-averaging process.

The thermocouple voltage, relative to a 0° C reference junction, was plotted on the x-axis of the recorder, and the parameter to be measured was plotted on the y-axis. As a test of the temperature tracking accuracy of the apparatus, a dummy FET was made by installing a second thermocouple in a TO-18 transistor can. Comparison of the two thermocouple voltages on the x-y plotter showed less than 2% tracking error.

Constant temperatures for the noise-frequency spectrum measurements were obtained by the following means:

300° K - water at ambient room temperature;

200° K - mixture of dry ice (CO_2) and acetone;

77° K - liquid nitrogen.

The copper heat sink was partially immersed in the fluid such that the FET was above the liquid level. The FET temperature was

monitored by the thermocouple and the fluid temperature was measured with a bimetallic dial thermometer.

For measurements of I_{DSS} and g_m, the circuits shown in Figure 6 were used. The drain-source potential was maintained at a constant value by a 100-ohm drain load resistor. The voltage-drop across this resistor was used as a measure of the drain current. The signal voltage across this resistor for a fixed gate input voltage was used as a measure of g_m.

Measurements of noise voltage required more elaborate precautions to avoid extraneous noise pickup in the circuitry. The critical apparatus was placed in a shielded enclosure and was carefully connected to avoid ground loops. All critical circuits were battery-operated. Most of the FET's measured had very low noise levels. This required that the input circuit under test have large voltage gain in order that the device noise be greater than the instrumentation noise. Since a low-resistance dc load was simultaneously required, an inductor was used as the drain load. This provided a large drain impedance and maintained the required dc operating point. The input circuit is shown in Figure 7. Switching is included for proper biasing of n- or p-channel units, and for input noise and gain measurements.

To satisfy the requirement that the instrumentation noise be much less than the FET noise, a special preamplifier was designed. Using FET's throughout, the unit had very low noise, wide dynamic

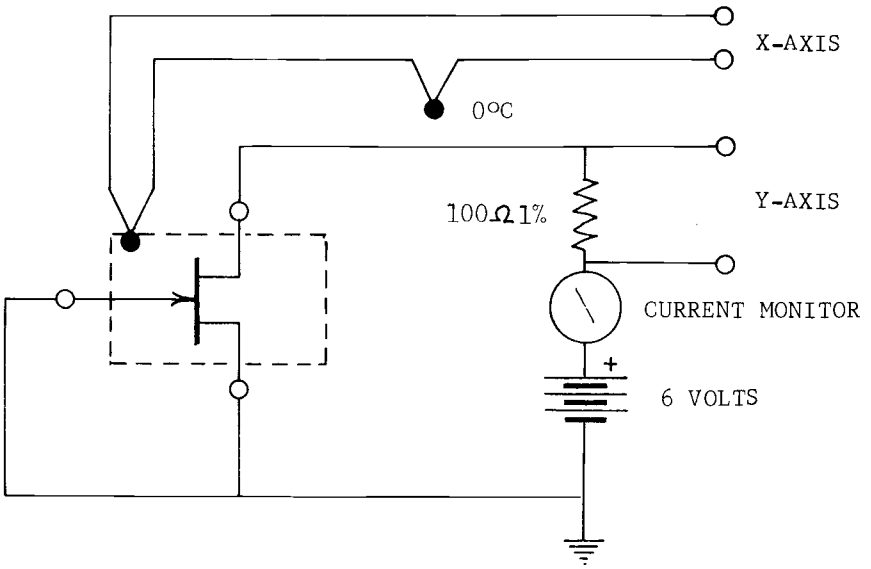

a. MEASUREMENT OF I_{DSS}

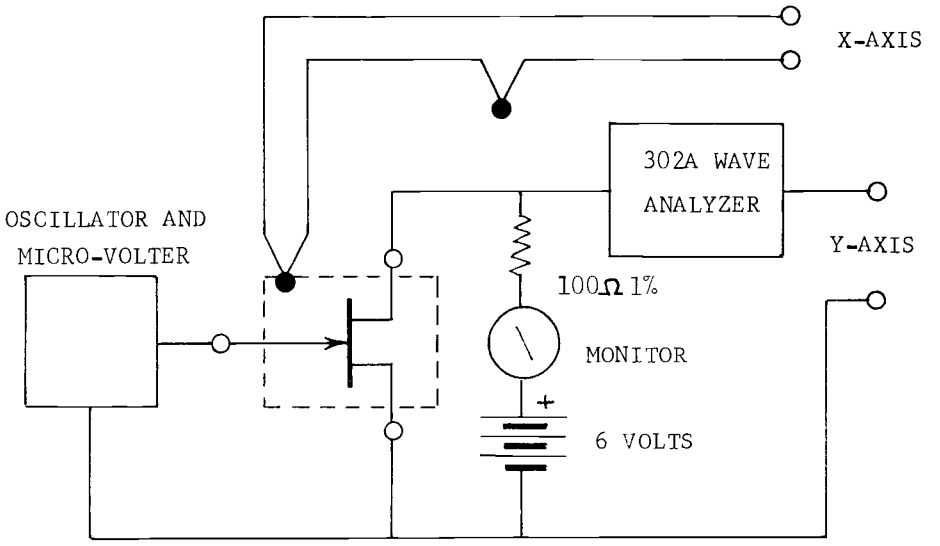

b. MEASUREMENT OF g_m

Figure 6. Parameter measurement

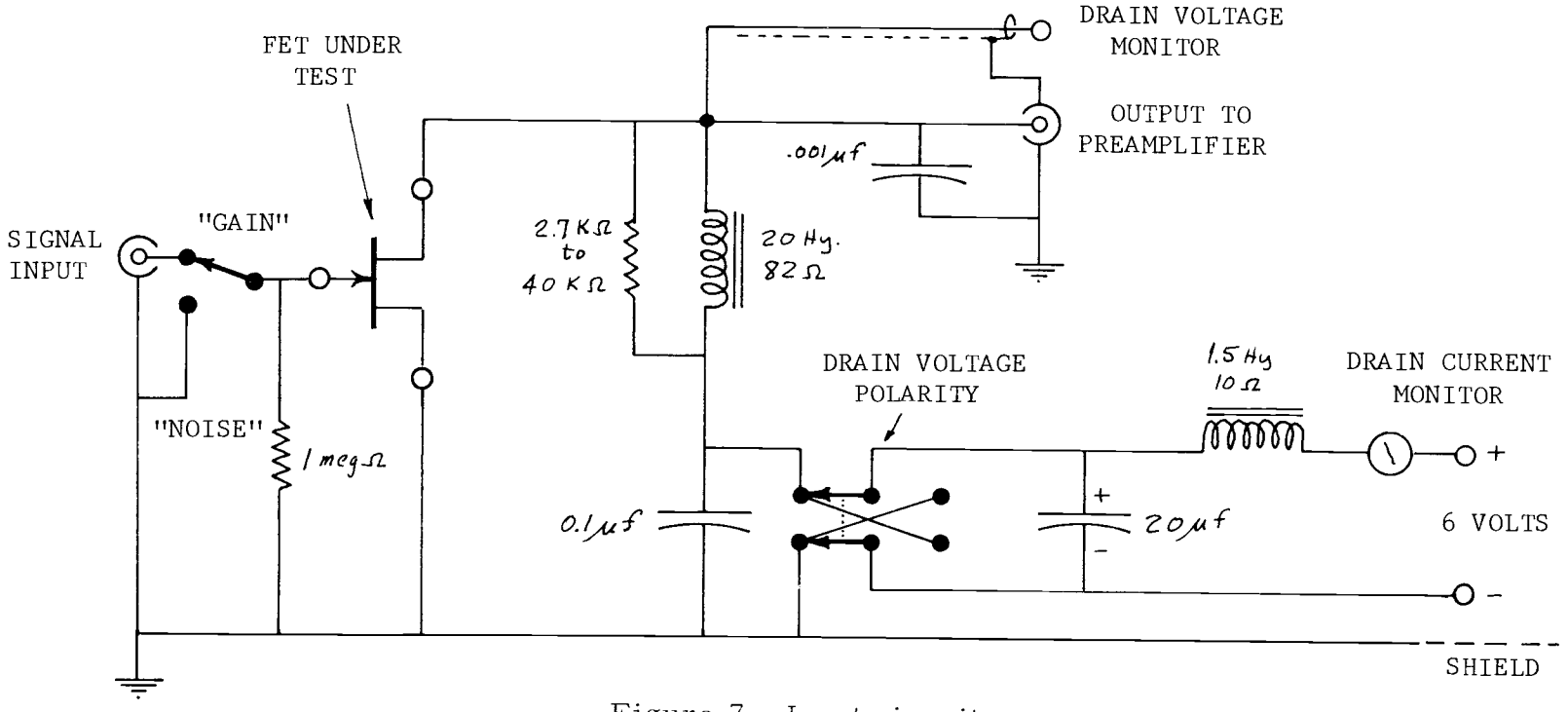

Figure 7. Input circuit.

range, low distortion and low output impedance. An FET selected for low noise from 20 Hz to 50 KHz was used. The wide dynamic range of the preamplifier is necessary when making accurate noise measurements. The performance of this preamplifier was superior to that of any commercially available unit. The circuit diagram is shown in Figure 8, and electrical performance is shown in Figure 9.

The complete measurement system is shown in Figure 10. The same equipment configuration was maintained throughout the series of measurements.

The method of noise measurement involved the use of a Hewlett-Packard 302A wave analyzer. This unit functions as a calibrated, tuned voltmeter with a constant bandwidth 6 Hz filter with a center frequency variable from 20 Hz to 50 KHz. A recitified dc output is available, proportional to the RMS value of the noise voltage in the filter bandwidth.

This rectified output was averaged by a 10-second RC integration network to obtain a stable value, and this noise voltage was then plotted by the x-y recorder. The minimum error attainable is (6, p. 246)

$$E = [2BK]^{-1/2} = [2 \cdot 6 \cdot 10]^{-1/2} = 9.15\%,$$

where B is the filter bandwidth and K is the RC time constant. Since approximately 200C° were scanned in 15 minutes, an average

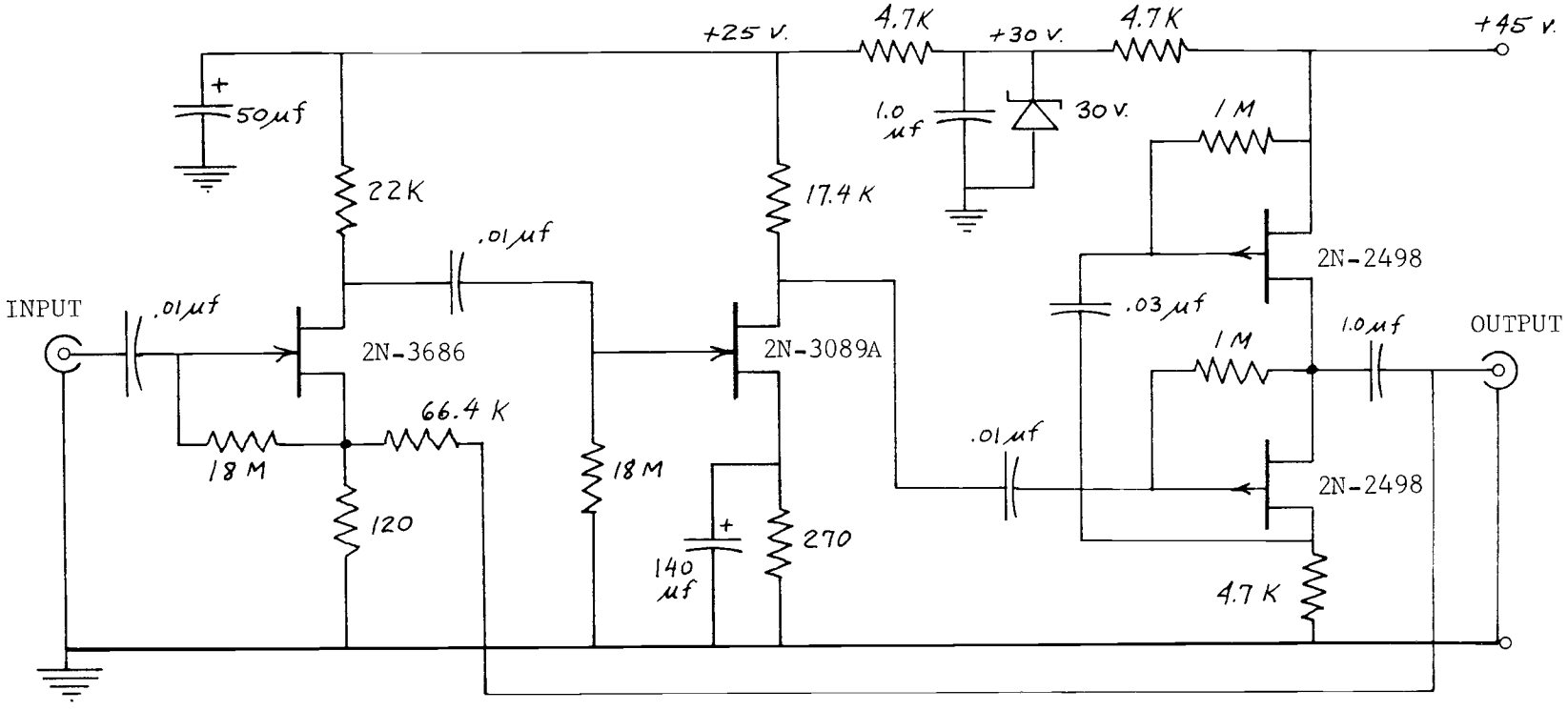

Figure 8. Preamplifier circuit.

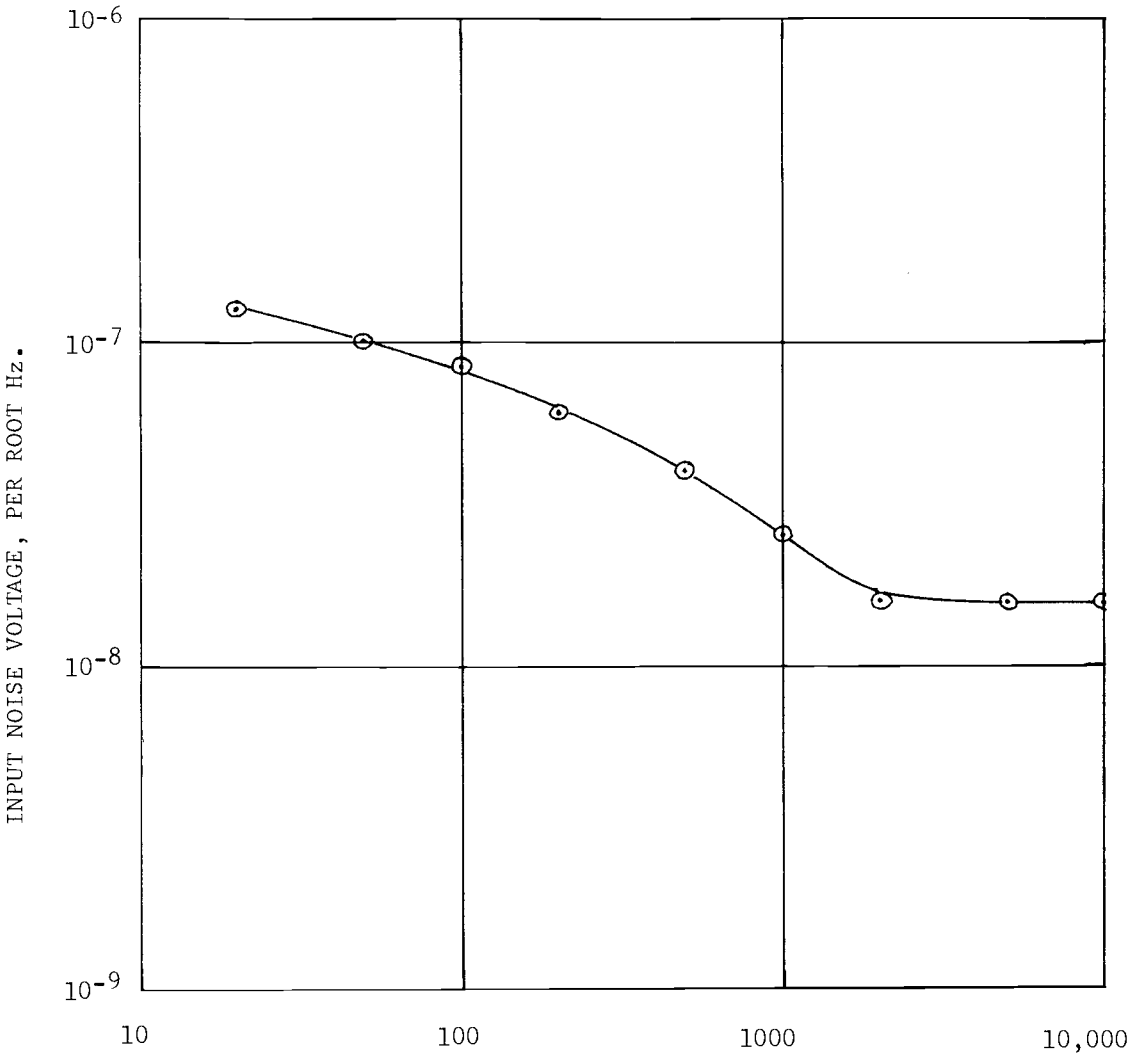

Figure 9. Preamplifier noise characteristic.

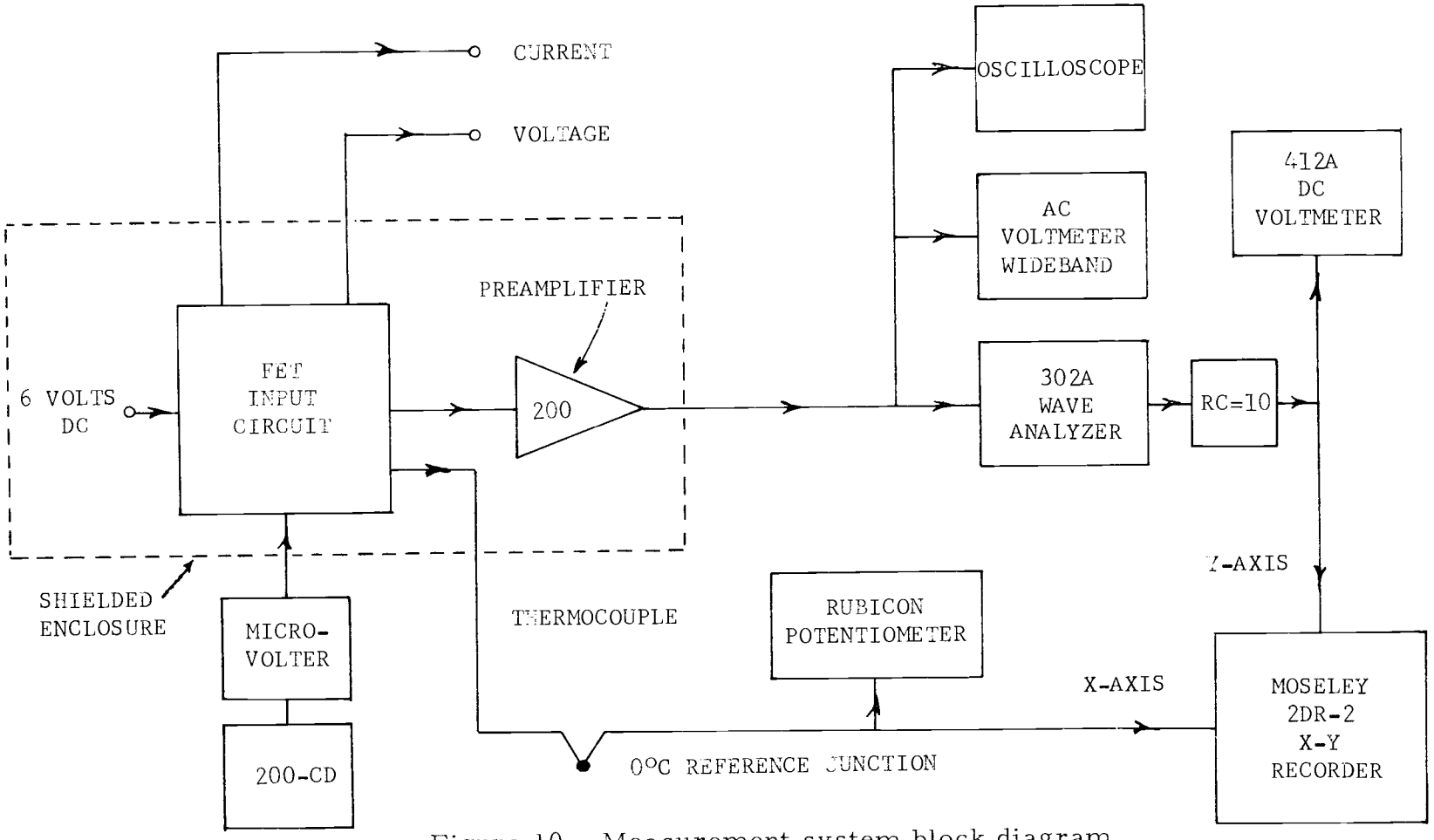

Figure 10. Measurement system block diagram.

scan rate of 0.2C° per second resulted. Since the noise was averaged with a 10-second time constant, a temperature resolution of approximately 2° C was achieved. Actually, since the scan rate was exponential in time, the x-axis temperature resolution was poorer near 77° K and better near 300° K.

Data Reduction

The process by which I_{DSS} and g_m were measured was relatively straightforward in accordance with the definitions of these quantities. Since the 100 ohm drain load resistor was orders of magnitude smaller than the output conductance of the FET's, these measurements were made with an accuracy of 5% or better.

The measurement of noise voltage versus temperature required a careful procedure to assure reasonable accuracy. The voltage gain of the system was measured immediately before the noise voltage was plotted. Both measurements were recorded on the same chart to assure coincidence of temperature scales. As stated previously, the noise voltage was averaged to reduce amplitude fluctuations in the plot. Since the noise plot produced by the x-y recorder still contained random fluctuations, the curve was graphically averaged to obtain data points for the calculations. A sample of the raw data is shown in Figure 11.

At selected intervals of 10C°, the equivalent input noise voltage

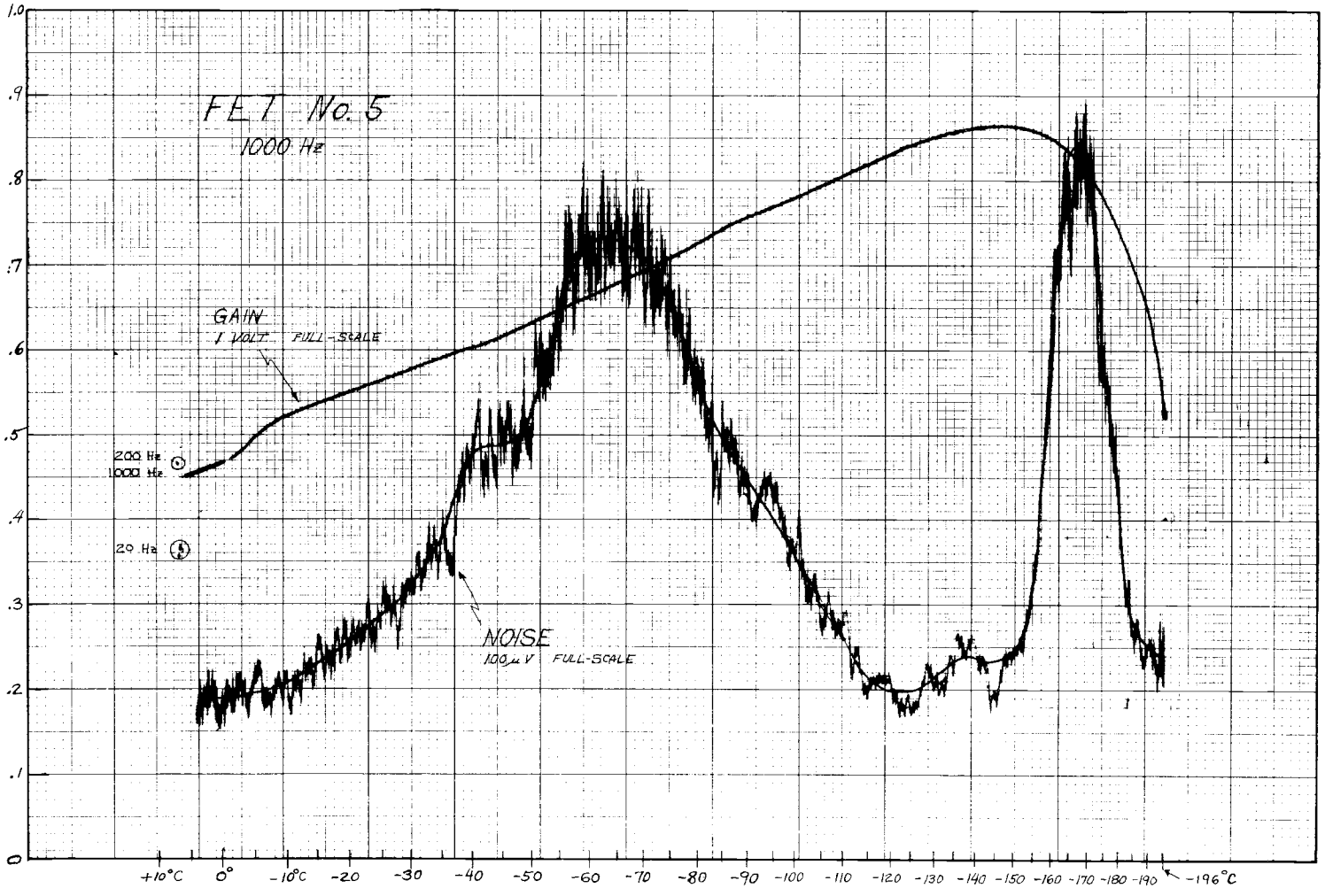

Figure 11. Sample raw data.

was calculated from the relationship

$$e_n(T) = \frac{V_n(T)}{A(T)(\Delta f)^{1/2}} ,$$

where $V_n(T)$ is the measured RMS noise voltage in a narrow bandwidth Δf and $A(T)$ is the overall system voltage gain at the measurement frequency. The voltage gain was measured from the input of the FET under the same conditions as V_n was measured. The resulting values for $e_n(T)$ were then replotted in convenient form. When necessary, points at special temperatures were calculated to preserve the shape of the original curve. From the error analysis presented in Appendix III, it is estimated that the total error in these noise voltage values is 12.8%.

V. DATA ANALYSIS

Measured Data

A complete set of measured noise data for each FET appears in Appendix I. Each set contains measured noise voltage versus temperature and frequency. The noise voltage versus temperature data was measured at frequencies of 20, 200 and 1000 Hz. The theoretical thermal noise calculated from the measured transconductance is also plotted on the same coordinates.

The upper temperature limit was 273° K on most data. This was necessary since melting ice at the electrical contacts caused spurious results above this temperatures.

Many separate comparisons can be made with the existing data. In the sections that follow, the individual aspects of the data are analyzed. The most significant results are derived from analysis of the noise maxima and comparison to the previous theoretical predictions.

Temperature Dependence of I_{DSS} and g_m

The measured variation of I_{DSS} and g_m provide good correlation with the behavior predicted in Section II. Both parameters were observed to change in a similar manner over the temperature range of this work.

Above 200° K, a $T^{-3/2}$ dependence was predicted due to

thermal scattering of the majority carriers. The temperature dependence of I_{DSS} and g_m is plotted in Figure 12 for a representative selection of devices. It is apparent that both parameters exhibit approximately a $T^{-3/2}$ behavior in the range 200° K to 300° K.

At lower temperatures, a turning point and subsequent decrease with temperature is observed. This was attributed to thermal deionization of majority channel impurities. Plots of I_{DSS} and g_m versus reciprocal temperature consistently yielded activation energies of approximately 0. 04 eV. , the energy level of all common dopant impurities in silicon.

Thus, at these temperatures, either the mobility or thermal deionization is the dominant factor affecting I_{DSS} and g_m.

General Noise Features

Distinct similarities in the behavior of similar groups of silicon FET's were evident. All of the FET's exhibited noise levels above thermal noise at low frequencies, and the variation in noise with temperature showed multiple maxima and minima, shifting in a regular manner with frequency. All n-channel units exhibited a sharp noise peak in the -160 to -196° C temperature region.

A composite of 200 Hz noise versus temperature for three different n-channel FET's is presented in Figure 13. Each device was produced by a different manufacturer, and each had dissimilar

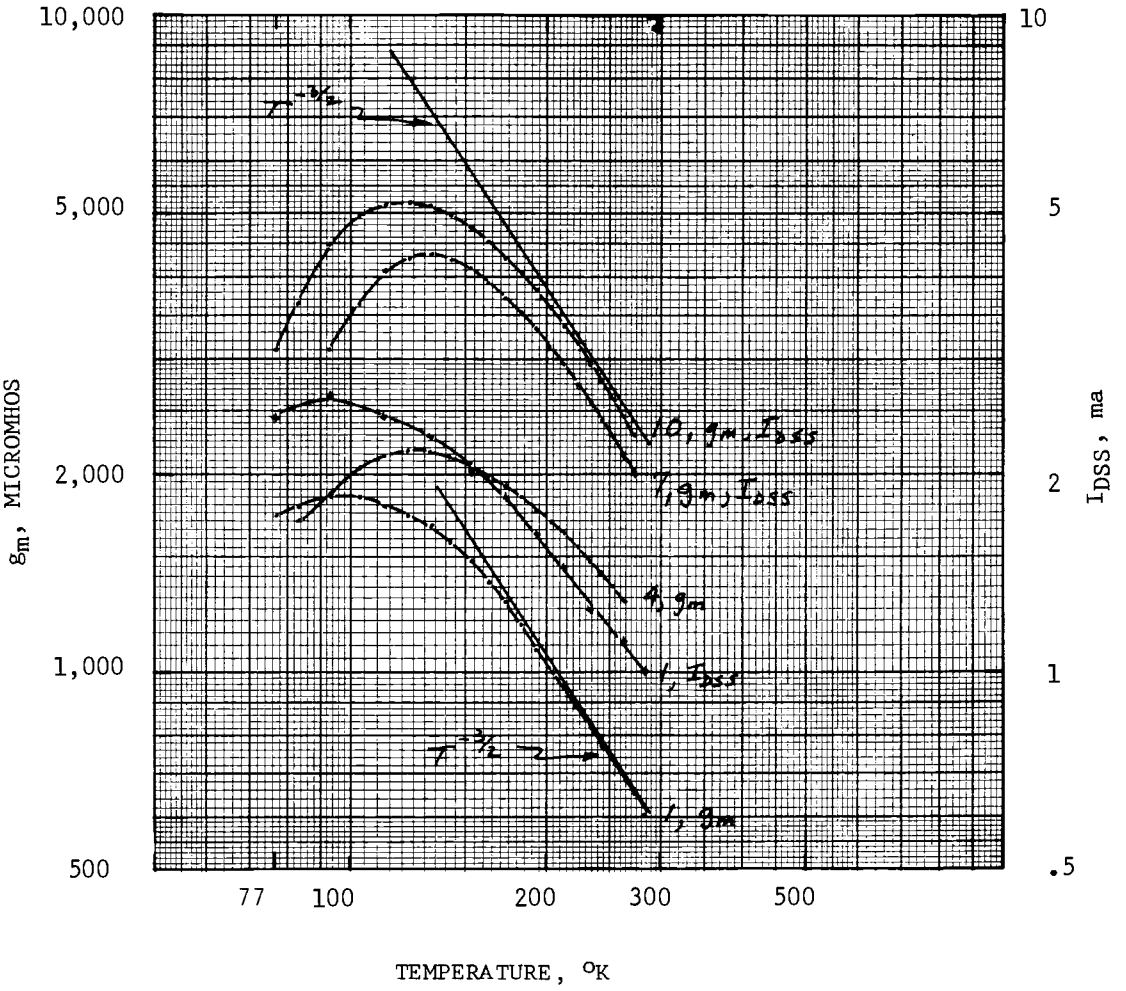

Figure 12. Temperature dependence of g_m and I_{DSS}.

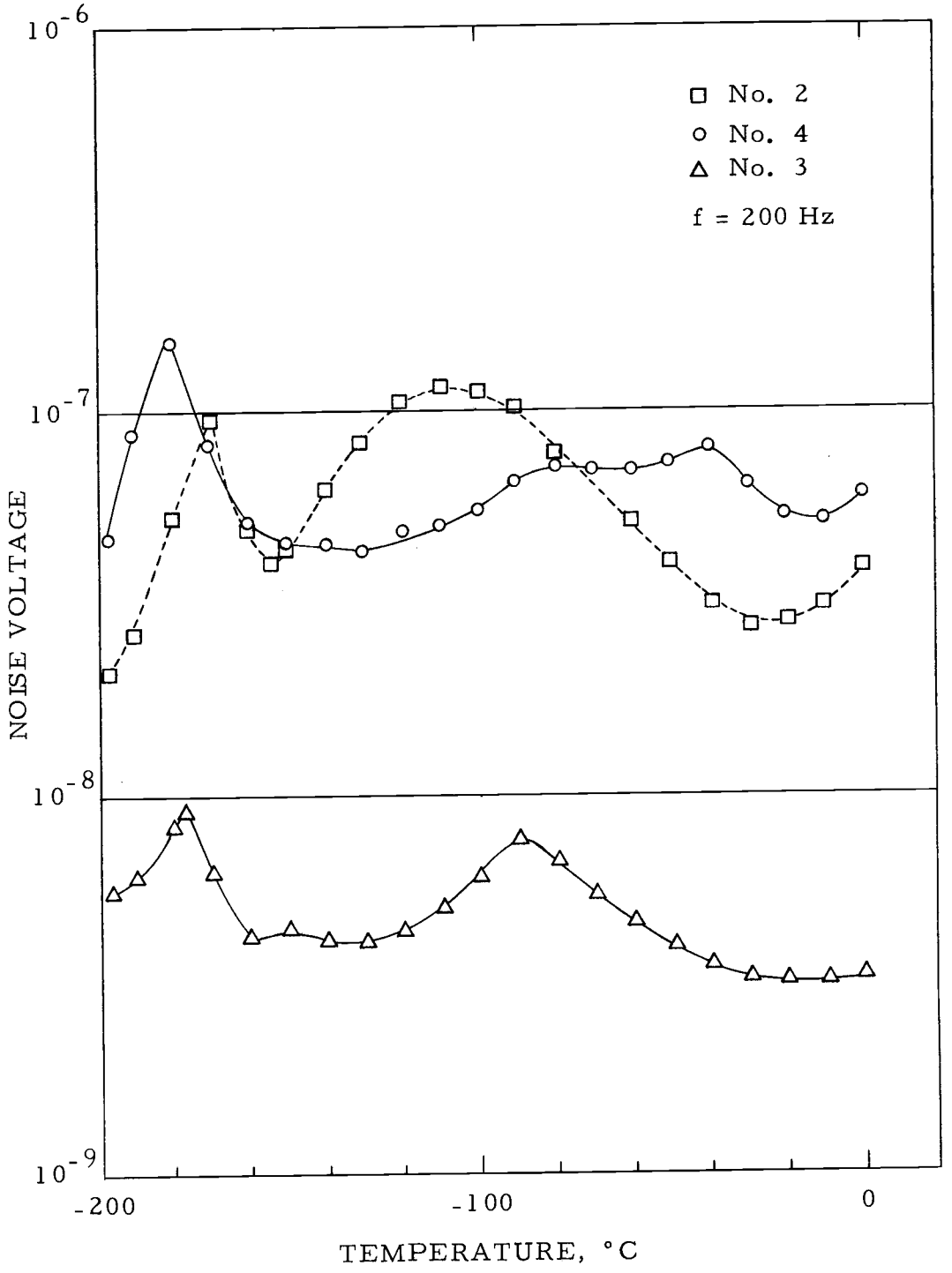

Figure 13. N-channel FET's.

geometry. The common low-temperature noise peak is clearly evident in each curve, even though the higher-temperature peaks bear no distinct similarities.

A corresponding selection of p-channel FET noise data is presented in Figure 14. Units 7 and 9 have the same geometry; units 7 and 11 were produced by the same manufacturer. The low temperature peak of the n-channel units is conspicuously absent, but a higher-temperature peak is consistently present in these p-channel units. The general shape of this noise peak is similar for each unit, although the temperature at which it occurs is different. The high-temperature slope of the curve is concave; the low-temperature slope is convex. This general curve shape is indicative of an exponential temperature-dependence.

In the n-channel data, an average trend of increasing noise magnitudes at low temperatures is indicated, whereas for p-channel units, the trend is toward decreasing noise at lower temperatures.

Some insight to the nature of the noise data presented above can be obtained by examining the noise-frequency spectrum. Consider sample number 5, presented as noise versus temperature in Figure 15. A 200 Hz noise maximum occurs at -75° C (approximately 200° K). Referring to Figure 16, in which the noise spectrum for this device is plotted, we observe that the spectrum at 200° K is flat below 200 Hz, decreasing with increasing frequency above 200 Hz, and is -3 db, or

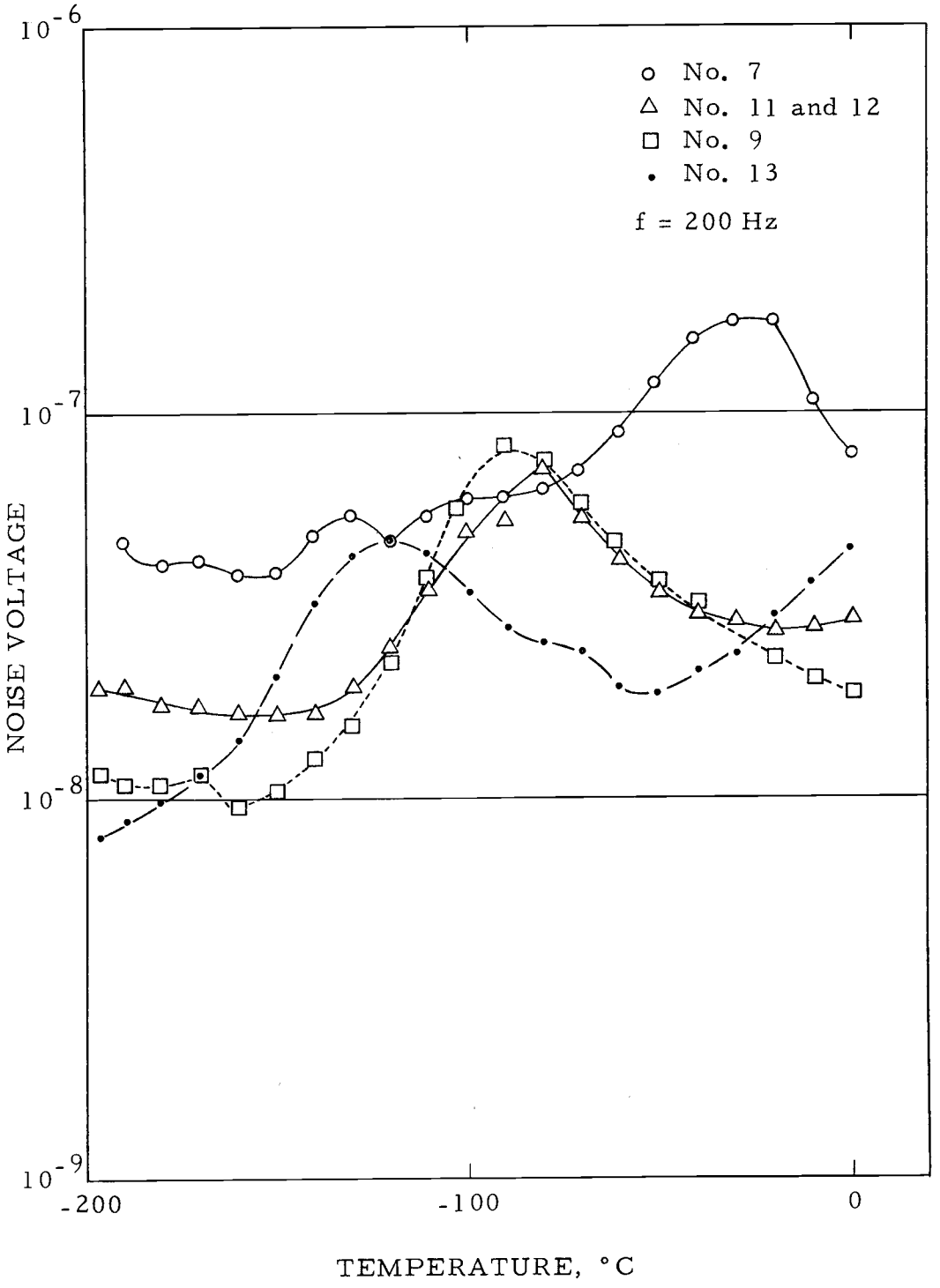

Figure 14. P-channel FET's.

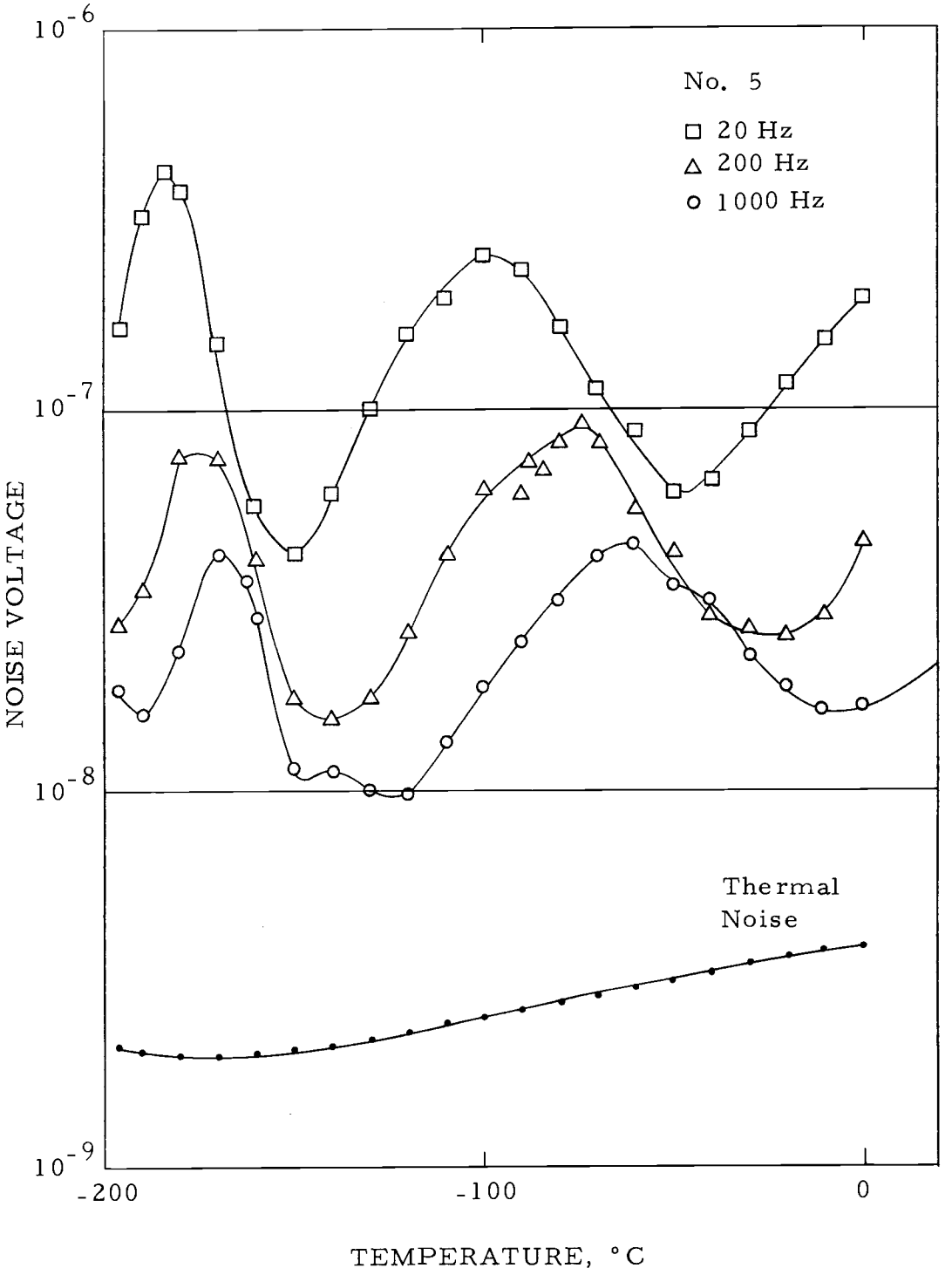

Figure 15. No. 5 noise voltage versus temperature.

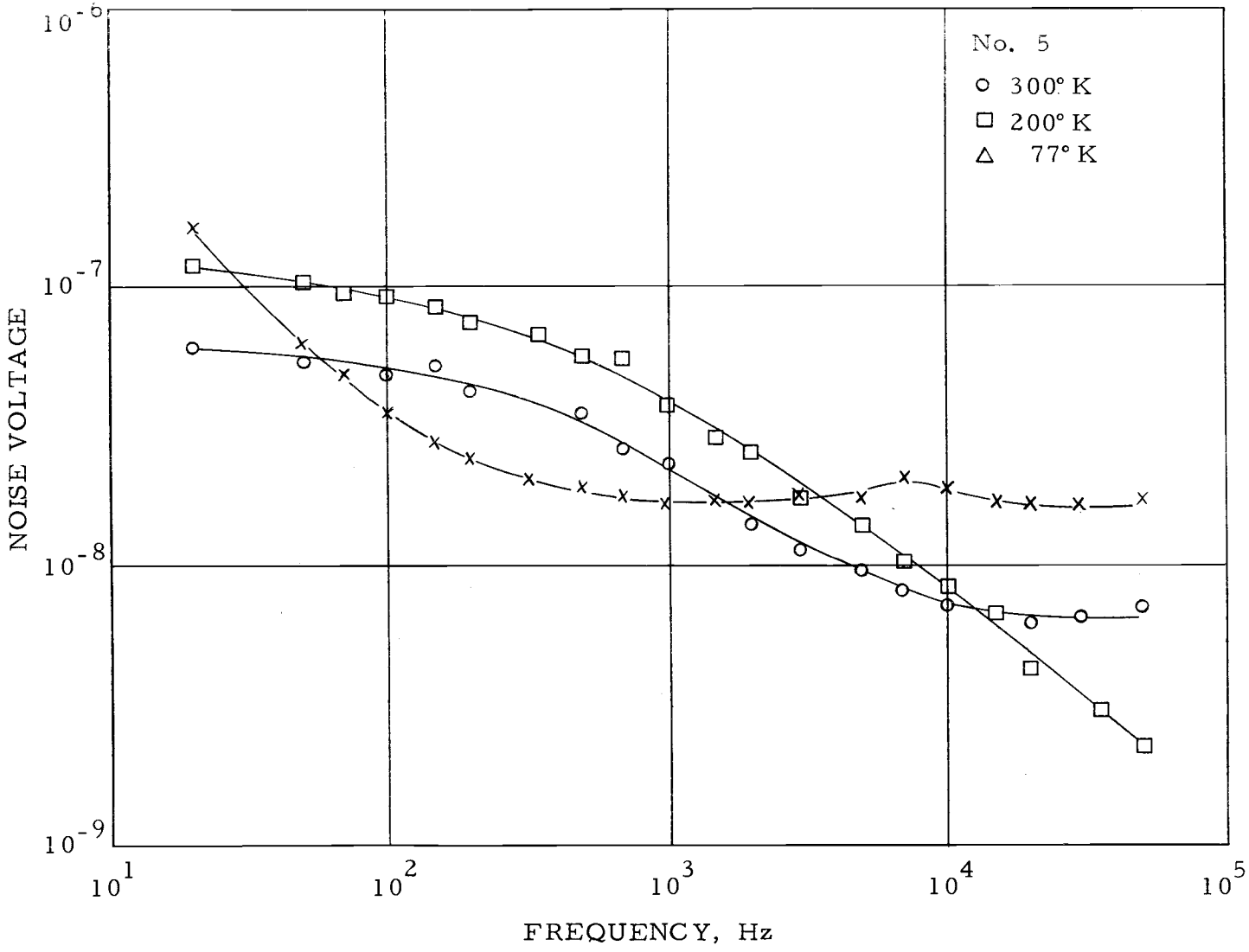

Figure 16. No. 5 noise spectrum.

0.707 of its low-frequency value, at 200 Hz. Thus, the behavior of this noise voltage spectrum at 200° K is similar to that produced by a single fluctuation time-constant. The fact that the exact shape of the noise spectrum is complex, approaching $f^{-1/2}$ in many cases, indicates that multiple time-constants are present at any given temperature.

Thermal Noise

The limiting noise is due to the thermal noise of the transconductance, as discussed in Section II. To compare the measured noise values with this theoretical prediction, the thermal noise was calculated from the expression

$$\overline{e_n^2(T)} = \frac{4kT}{g_m(T)} ,$$

where $g_m(T)$ is the transconductance measured as a function of temperature. With the exception of units 3 and 5, all FET's exhibited measured noise in excess of values calculated from the above equation. Unit number 5 at 200° K, approaches this limiting thermal noise at high frequencies on the order of 50 KHz, as evident in Figure 16. Unit number 3 approaches this noise level for frequencies greater than 1 KHz and temperatures greater than 300° K, as indicated in Figure 17.

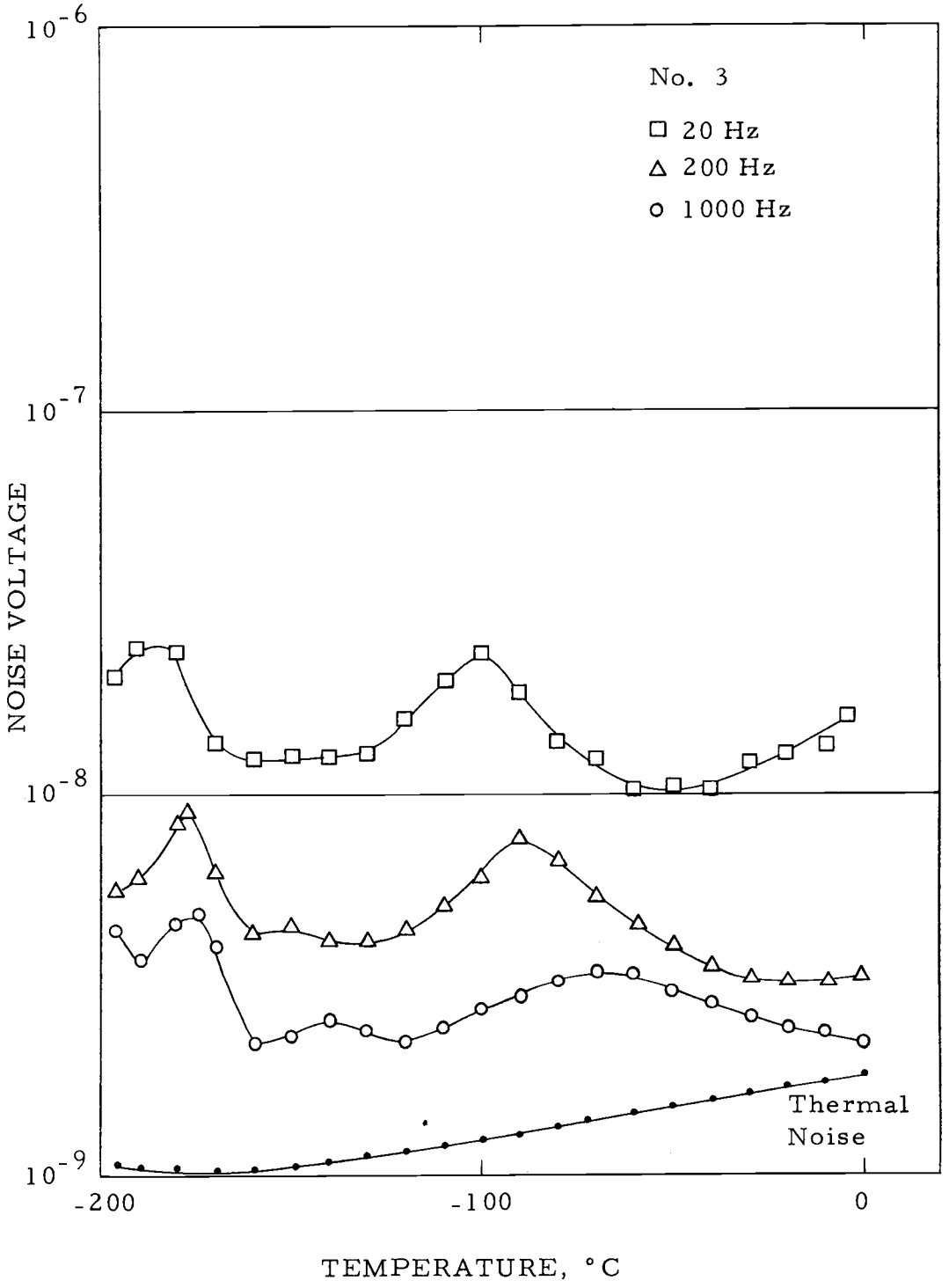

Figure 17. No. 3 noise voltage versus temperature.

Noise Due to Shockley-Read-Hall Centers

In the previous discussion of SRH centers, it was determined that this mechanism could be the dominant source of low frequency FET noise. It was observed that a single fluctuation time constant with an exponential temperature-dependence would yield a maximum noise voltage when $\omega\tau = 1$. Furthermore, the activation energy of the center is related to the slope of the leading and trailing edges of the peak when the noise is plotted versus reciprocal temperature. The activation energy may also be determined from a plot of τ versus reciprocal temperature.

The noise voltage data of sample number 5 is re-plotted versus T^{-1} in Figure 18. The leading and trailing edges of the noise maxima yield linear slopes which can be assigned activation energies. The noise voltage is theoretically proportional to

$$[\tau(1+\omega^2\tau^2)^{-1}]^{1/2}$$

with

$$\tau \propto \exp\left(\frac{E_a}{kT}\right),$$

where E_a is the trap activation energy equal to $-(E_t-E_c)$ for donors and $-(E_v-E_t)$ for acceptors. Therefore, at temperatures on the sides of the noise maximum the noise voltage will be proportional

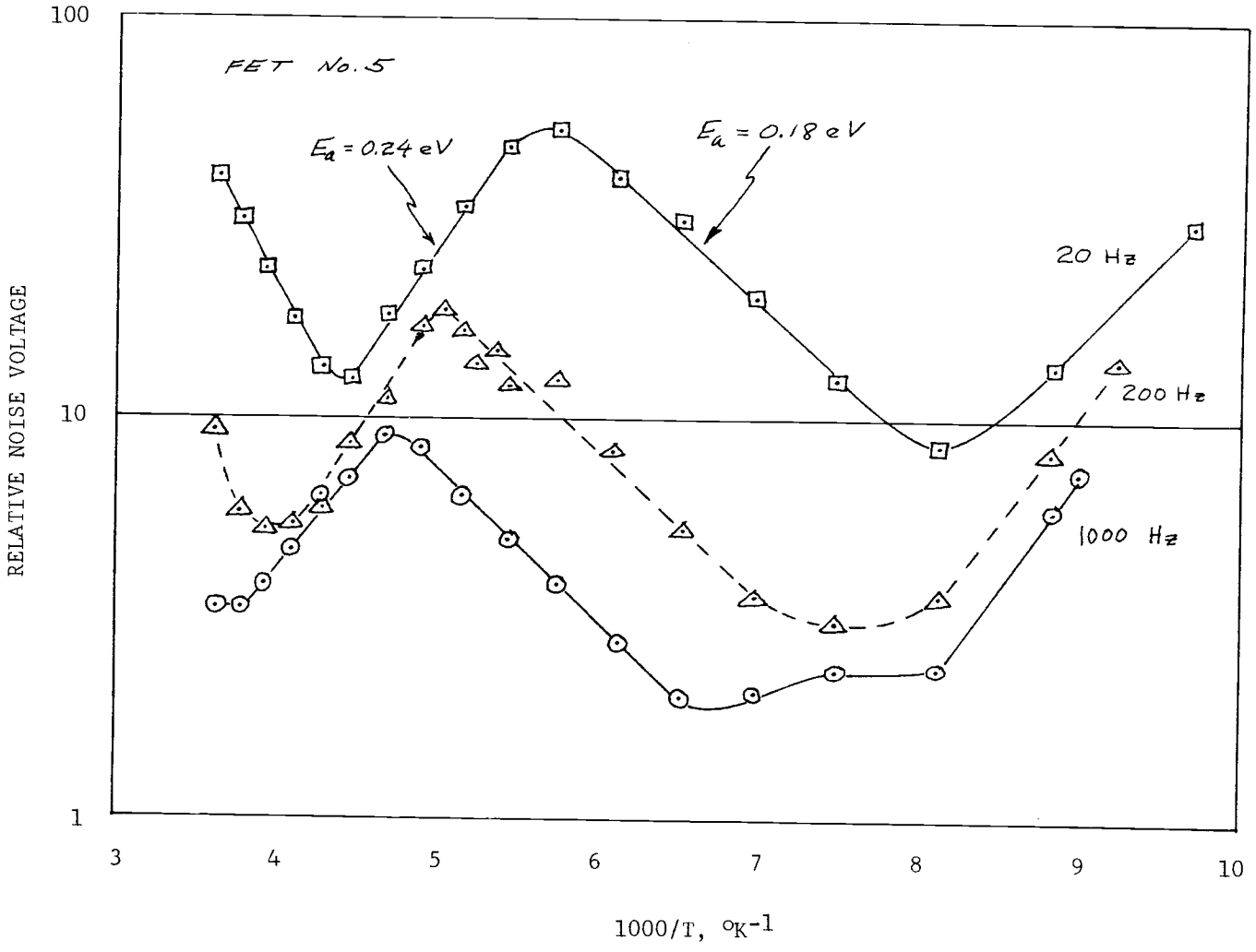

Figure 18. No. 5 noise versus reciprocal temperature.

to

$$\exp\left(\frac{\pm E_a}{2kT}\right).$$

Utilizing the method described in Appendix II, the activation energies in the 200° K region are 0. 28 eV for the leading edge and 0. 16 eV for the trailing edge.

By computing the time constant of this same maximum from $\tau = \omega^{-1}$ and plotting $(\tau T^{3/2})$ versus T^{-1} as in Figure 19, an activation energy of 0. 34 eV is obtained. This method is inherently more accurate since ω is known exactly and the peak of the noise voltage curve may be determined with more certainty than the slope of the same curve.

Sufficient data now exist to estimate the capture cross-section of this SRH center. From the measured data, we found that $\tau = 8 \times 10^{-4}$ seconds at 200° K. An approximate energy level of 0. 3 eV is assumed.

To simplify the procedure, we assume that the SRH center is a donor impurity with a time constant described by

$$\tau_t = (c_n n_1)^{-1}$$

where

$$n_1 = N_c \exp\left(\frac{E_t - E_c}{kT}\right) = N_c \exp\left(\frac{-E_a}{kT}\right)$$

and

$$c_n = \theta_n \sigma_n.$$

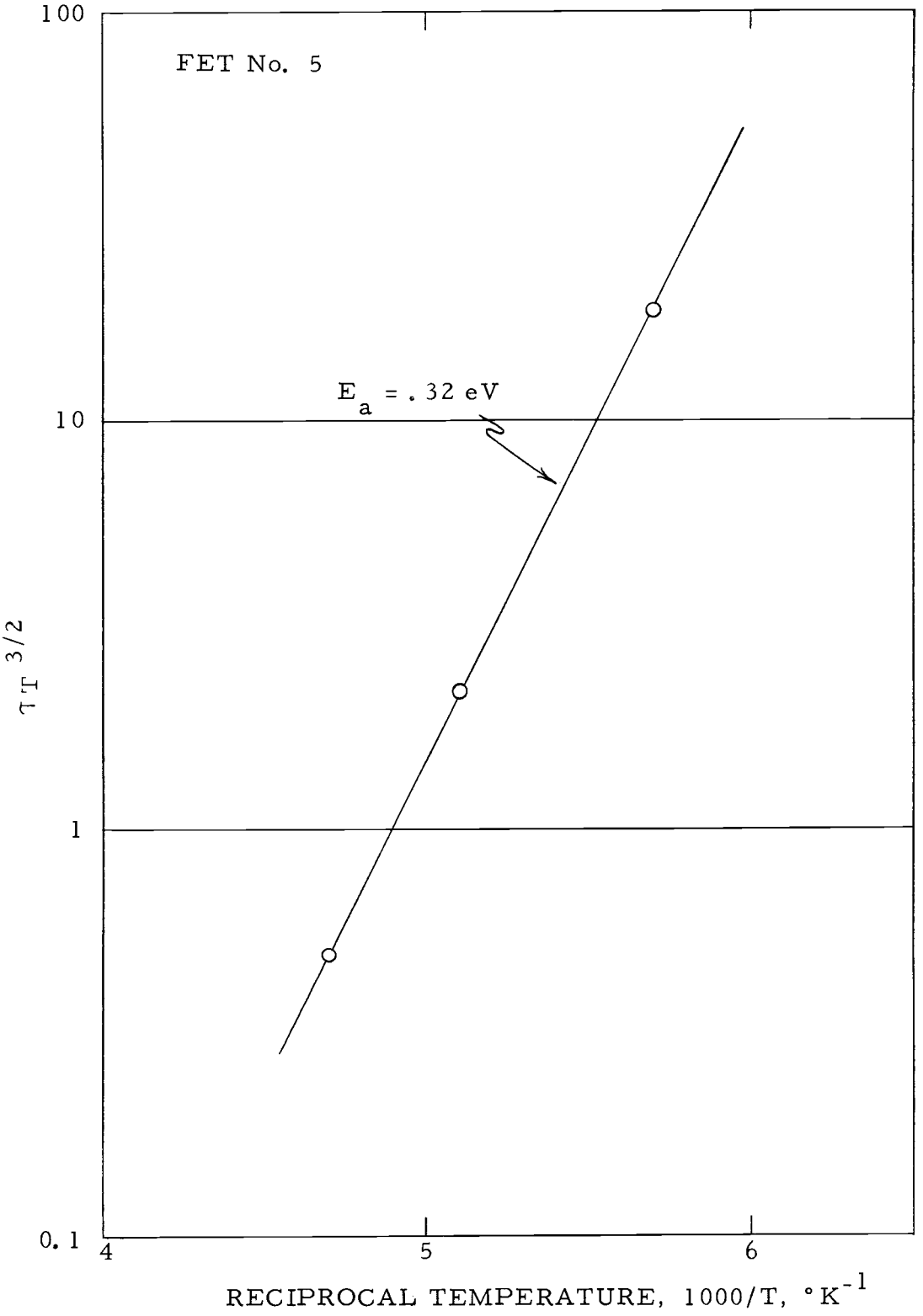

Figure 19. Activation energy near 200° K.

Substituting and solving for σ_n, we find

$$\sigma_n = [\tau_t \theta_n N_c \exp(\frac{E_a}{kT})]^{-1}.$$

The thermal velocity, θ_n, is given by

$$\theta_n = [\frac{2kT}{m}]^{1/2} = 7.85 \times 10^6 \text{ cm s}^{-1},$$

and the remaining values are

$$T = 200^\circ \text{K}$$

$$\tau_t = 8 \times 10^{-4}$$

$$N_c = 4.78 \times 10^{15} T^{3/2} = 1.36 \times 10^{19} \quad \text{at} \quad 200^\circ \text{K}$$

$$E_a = 0.3 \text{ eV}.$$

Inserting these values into the expression for σ_n, we find

$$\sigma_n \doteq 4.7 \times 10^{-16} \text{ cm}^2.$$

The FET under present consideration is an n-channel device. Since the depletion region extends into the channel in pinchoff, it is reasonable to assume that electron trapping in the channel depletion region would be the dominant process. Gold is a common impurity present in silicon. The published value for the electron capture cross-section for Au in n-type silicon is 5×10^{-16} cm^2 (5). Other

recombination-center capture cross-sections are also on the order of 10^{-15} cm^2. The agreement with the calculated cross-section is surprisingly good.

Since SRH centers are known to contribute to the reverse leakage current of silicon diodes, measurement of the gate leakage current versus T^{-1} should yield the activation energy of these centers. With this as the objective, the leakage current of unit number 5 was measured. The data was analyzed in the manner used by Sah, Noyce and Shockley (27), with the result that a 0.586 eV activation energy was measured over the temperature range +10° C to +80° C. Unfortunately, the 10° C gate leakage current of 1 x 10^{-13} ampere at 6 volts was at the lower limit of the measurement instrumentation, so that measurements at -75° C were not possible. Also, noise measurements were not made above 0° C on this sample, so that confirmation of the 0.586 eV level was not possible. Extrapolations from trends of the noise versus temperature data indicate that a 0.6 eV center could be present.

Low Temperature n-Channel Noise Maxima

The behavior of the n-channel samples was examined in closer detail near the low-temperature noise maximum. A composite plot of τ_t versus T^{-1} was made in order to determine the activation energy. As shown in Figure 20, this data yielded an energy of 0.26 eV

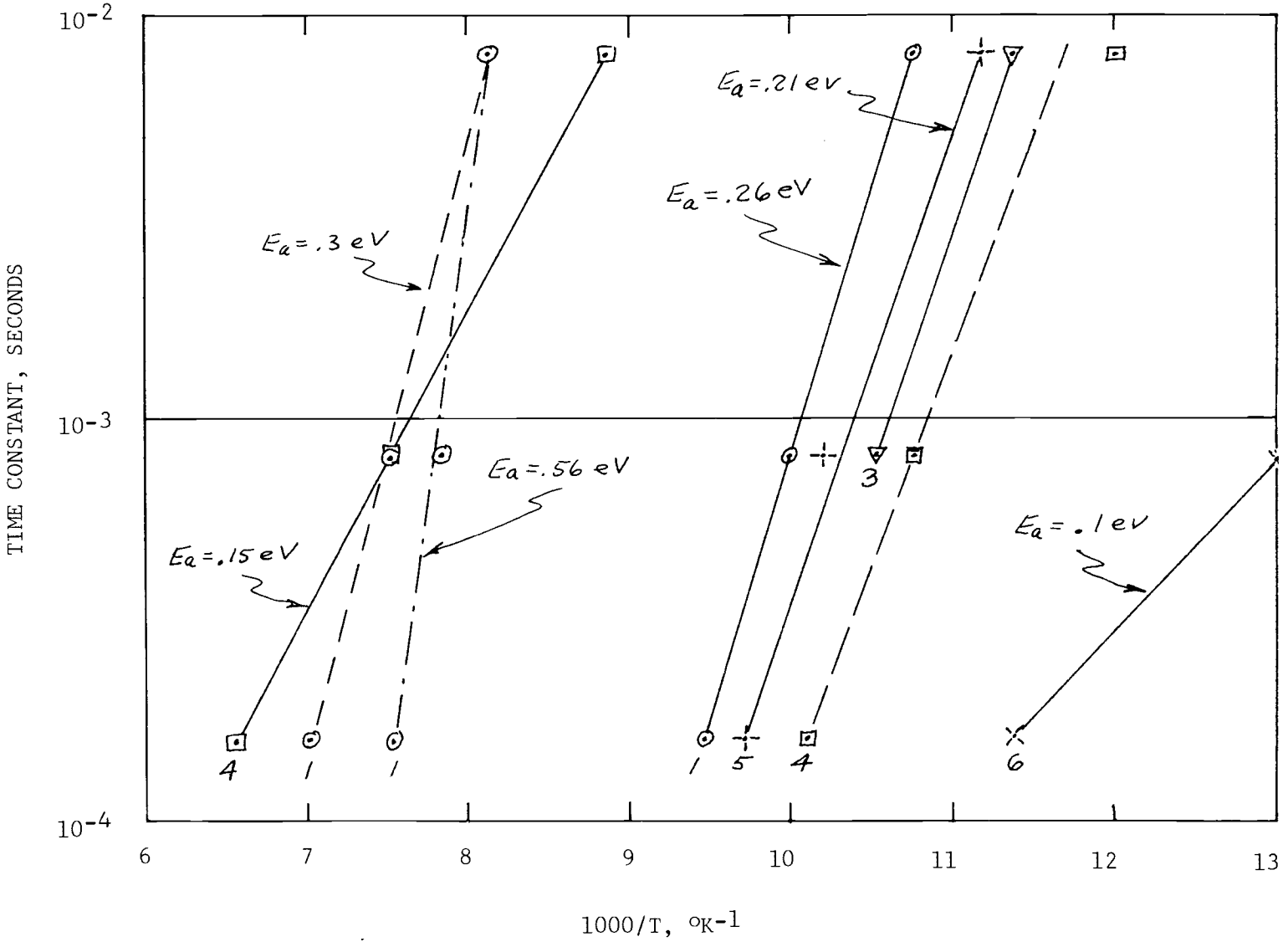

Figure 20. Time constants for n-channel FET's.

for units 1, 2 and 3; and an energy of 0. 22 eV for units 4 and 5.

The temperature dependence of the curve shape of unit 5 was measured in detail and plotted versus T^{-1}, as in Figure 21. The leading edge yields an activation energy of 0. 22 eV, and the trailing edge yields 0. 12 eV. It should be noted that the trailing edge appears to be a composite of slopes.

The agreement of the two methods for unit 5 in yielding a 0. 22 eV energy level suggests that the capture cross-section might be validly calculated.

For the conditions of

$$E_a = 0.22 \text{ eV}$$

$$T = 105^\circ \text{K}$$

$$\tau_t = 1.56 \times 10^{-4}$$

$$N_c = 5.13 \times 10^{18} \text{ at } 105^\circ \text{K}$$

$$\theta_n = 5.67 \times 10^{6} \text{ cm s}^{-1} \text{ at } 105^\circ \text{K}$$

the capture cross-section is calculated as

$$\sigma_n \doteq 8.7 \times 10^{-12} \text{ cm}^2.$$

This value is in excess of most published values for large capture cross-sections, and hence suggests that a more complex trapping process is responsible for the observed low-temperature behavior.

As indicated previously, the energies of the leading and trailing edges do not always correspond to those of the noise maxima; often

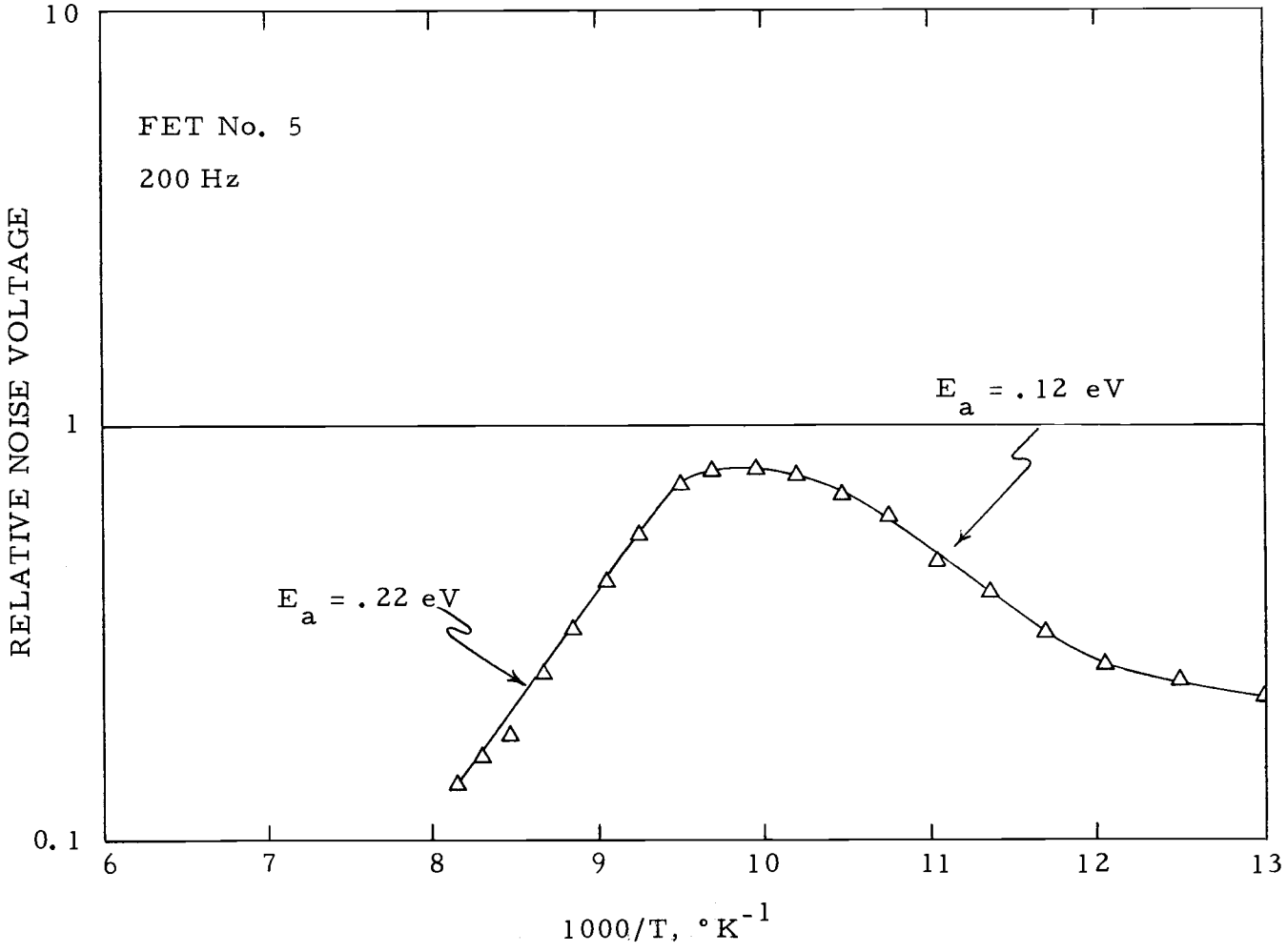

Figure 21. No. 5 low-temperature noise maximum.

the slopes are different on each side of the peak. The noise data was measured with insufficient accuracy to enable resolution of more subtle structures in the slopes. However, the original data for sample number 5 at 200 Hz shows definite double maxima separated by five degrees at 100° K. This fine structure was not evident at other measurement frequencies.

Most of the measured FET's showed low noise at 77° K. Sample number 6, however, exhibited a large increase in noise near this temperature. Examination of the 1000 Hz noise versus temperature data in Figure 22 will indicate that this is a large-magnitude noise peak similar to other n-channel units. The frequency spectrum at 77° K, Figure 23, clearly shows the single-time-constant nature of the noise, yielding $\tau_t = 8 \times 10^{-4}$ seconds at 77° K. The plot of τ_t versus T^{-1} for this unit in Figure 20 yields an activation energy of 0.1 eV. A plot of the noise voltage versus T^{-1} in Figure 24, yields an activation energy of 0.12 eV from the leading edge slope.

Trapping Center Concentration

The density of traps N_t may be calculated from the measured noise versus temperature data by making use of the previously derived expression for noise voltage.

The approximate spot noise voltage magnitude from Section II is

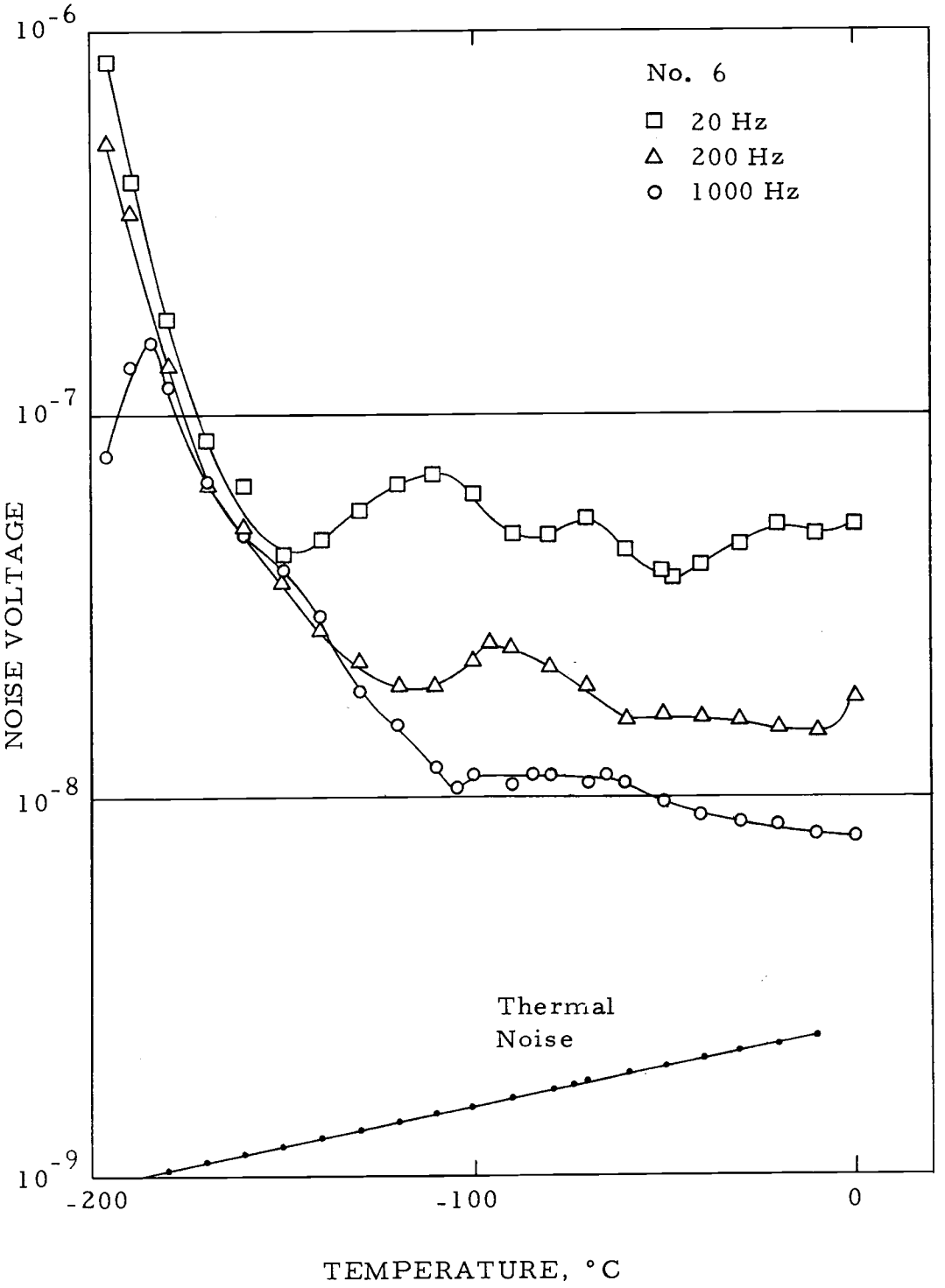

Figure 22. No. 6 noise voltage versus temperature.

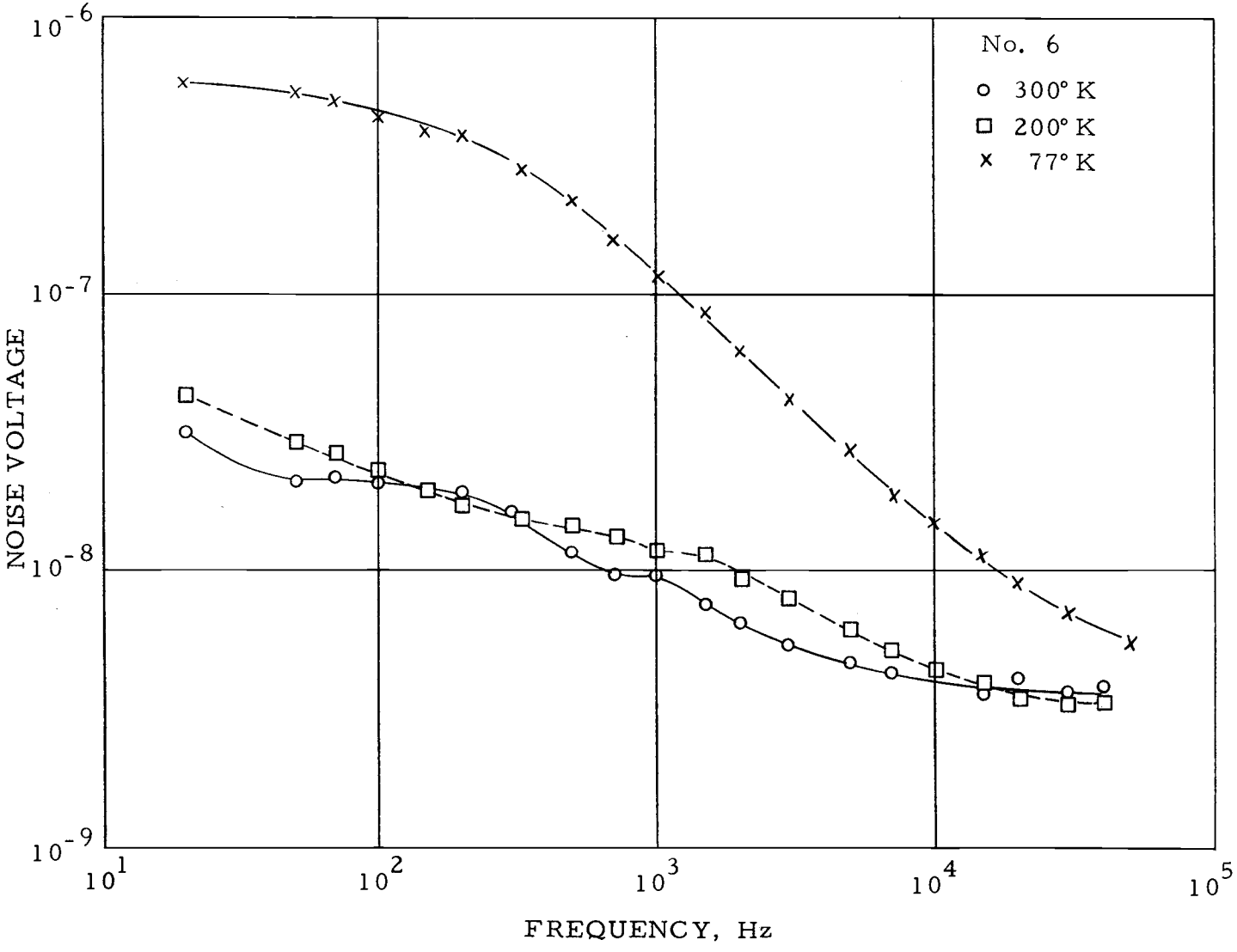

Figure 23. No. 6 noise spectrum.

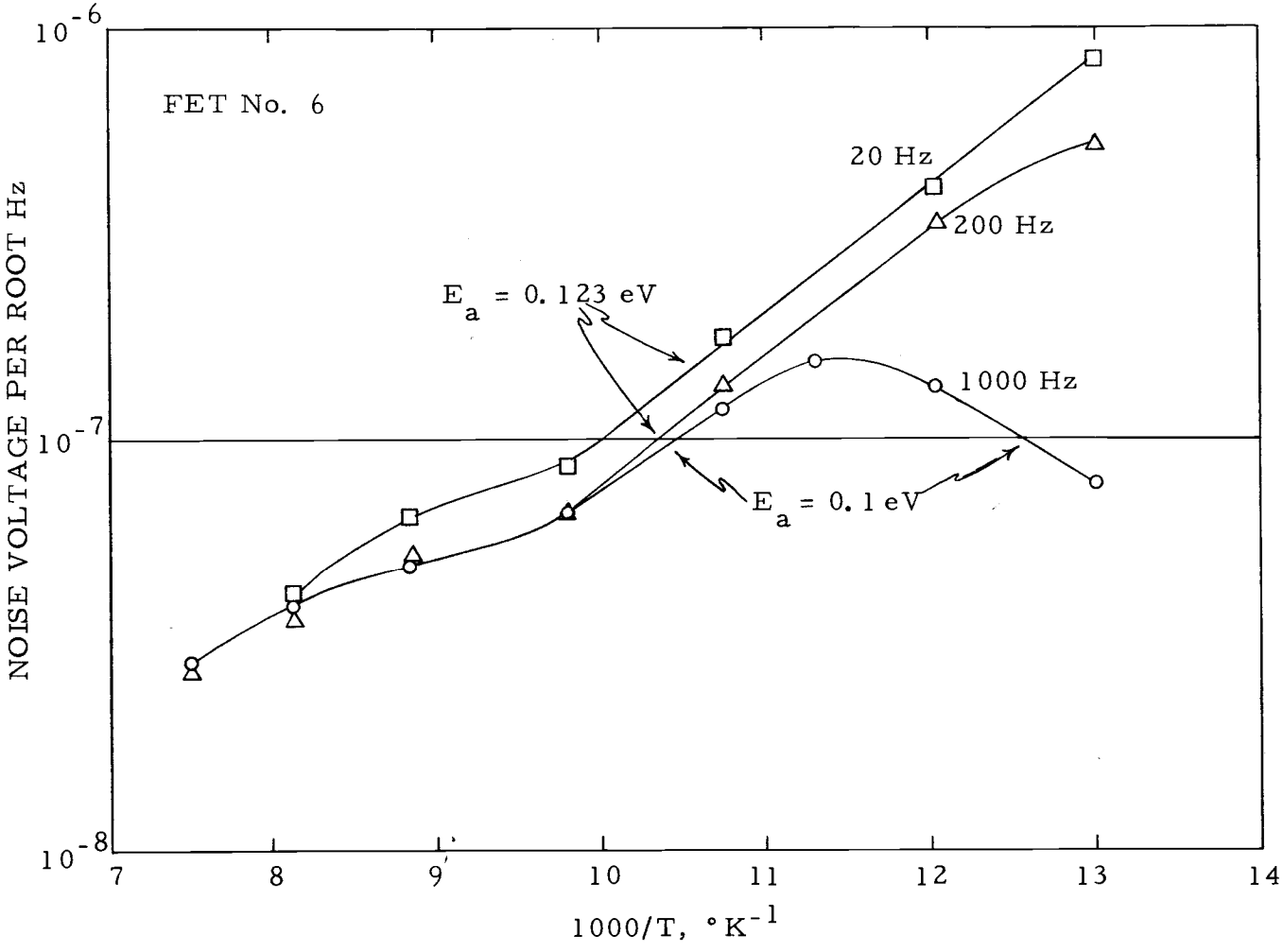

Figure 24. No. 6 low-temperature noise maximum.

$$e_n = \left[\frac{4N_t f_t f_{tp} W^3}{3A} \left(\frac{q}{K\varepsilon_o}\right)^2 \frac{\tau_t}{1+\omega^2\tau^2} \right]^{1/2}$$

where W is the width of the gate-channel depletion region and A is the gate area.

For this calculation p-channel sample number 9 has been selected since it has the known geometry of a 2N-2608. The pertinent dimensions are

$$W = 3 \times 10^{-4} \text{ cm} \quad \text{and} \quad A = 1.56 \times 10^{-4} \text{ cm}^2.$$

We make use of the fact that at $T = 200°\text{K}$, $\tau_t = 1.56 \times 10^{-4}$s, as indicated by the measured noise voltage maximum. This corresponds to the condition $\omega\tau = 1$. The expression for the noise voltage at 200°K becomes

$$e_n = \left[\frac{4W^3}{3A} \left(\frac{q}{K\varepsilon_o}\right)^2 \frac{\tau_t}{2}\right]^{1/2} [N_t f_t f_{tp}]^{1/2}$$

$$= (6.68 \times 10^{-13})[N_t f_t f_{tp}]^{1/2}.$$

The noise voltage measured at the 200°K maximum for unit 9 is 3×10^{-8} volts in a unit bandwidth. Assuming that $f_t = f_{tp} = 0.5$, we calculate that

$$N_t = \frac{1}{0.25} \left(\frac{3 \times 10^{-8}}{6.68 \times 10^{-13}} \right)^2 = 8.1 \times 10^9 \text{ cm}^{-3}.$$

This is an interesting result, since it indicates that small trap concentrations may be measured in the presence of the usual donor or acceptor impurities.

The trap concentration calculated here is a reasonable value for the measured noise voltage. Since Lauritzen (16) measured 4×10^{-6} volts equivalent input noise voltage for a gold-doped FET with $N_t = 10^{14}$ cm^{-3}, and since the noise voltage varies with $(N_t)^{1/2}$, the measured value of noise voltage for sample number 9 at 200° K should correspond to a trap concentration on the order of 6×10^{9} cm^{-3}.

A similar calculation may be carried out for sample number 5, an n-channel unit. Using the known values

$$W = 2\mu = 2 \times 10^{-4} \text{ cm}$$

$$A = 0.1 \text{ mil} \times 22.0 \text{ mil} = 1.37 \times 10^{-5} \text{ cm}^2$$

$$\tau_t = 1.56 \times 10^{-4} \text{ seconds at } 200^\circ \text{K},$$

we calculate e_n as

$$e_n = (1.21 \times 10^{-12})[N_t f_t f_{tp}]^{1/2}.$$

The measured value for e_n at the 1KHz, 200° K noise maximum is 4.5×10^{-8} volts. Assuming that $f_t = f_{tp} = 0.5$, N_t is calculated as

$$N_t = \left(\frac{1}{0.25}\right)\left[\frac{4.5 \times 10^{-8}}{1.21 \times 10^{-12}}\right]^2 = 5.5 \times 10^{9} \text{ cm}^{-3}.$$

The similar values of N_t in this n-channel unit and in the above

p-channel unit further suggest that the trap concentration may be a basic property of the starting silicon material.

Frequency Dependence of Noise Maxima

From the measured noise data presented, a regular change in the magnitude of the noise maxima is evident at different frequencies. From the theory presented earlier, the condition for a noise voltage maximum was $\omega\tau = 1$. The noise voltage was proportional to $[\tau(1+\omega^2\tau^2)^{-1}]^{1/2}$. Substituting $\omega = \tau^{-1}$, one finds that the magnitude of the noise voltage maxima is proportional to $\omega^{-1/2}$:

$$V_{n(max)} \propto [\omega^{-1}(1+1)^{-1}]^{1/2} = (2\omega)^{-1/2}.$$

The values of the noise voltage maxima at 20, 200, and 1000 Hz are plotted in Figure 25a and for n-channel FET's, and in Figure 25b for p-channel units. The trend of the measured data is definitely that of $\omega^{-1/2}$. This result may be interpreted as evidence that noise produced by a distribution of time constants does indeed exhibit an $\omega^{-1/2}$ voltage spectrum.

Summary of Trap Energy Levels

The trap activation energy levels have been determined for all distinct maxima in the measured FET noise data. These energy

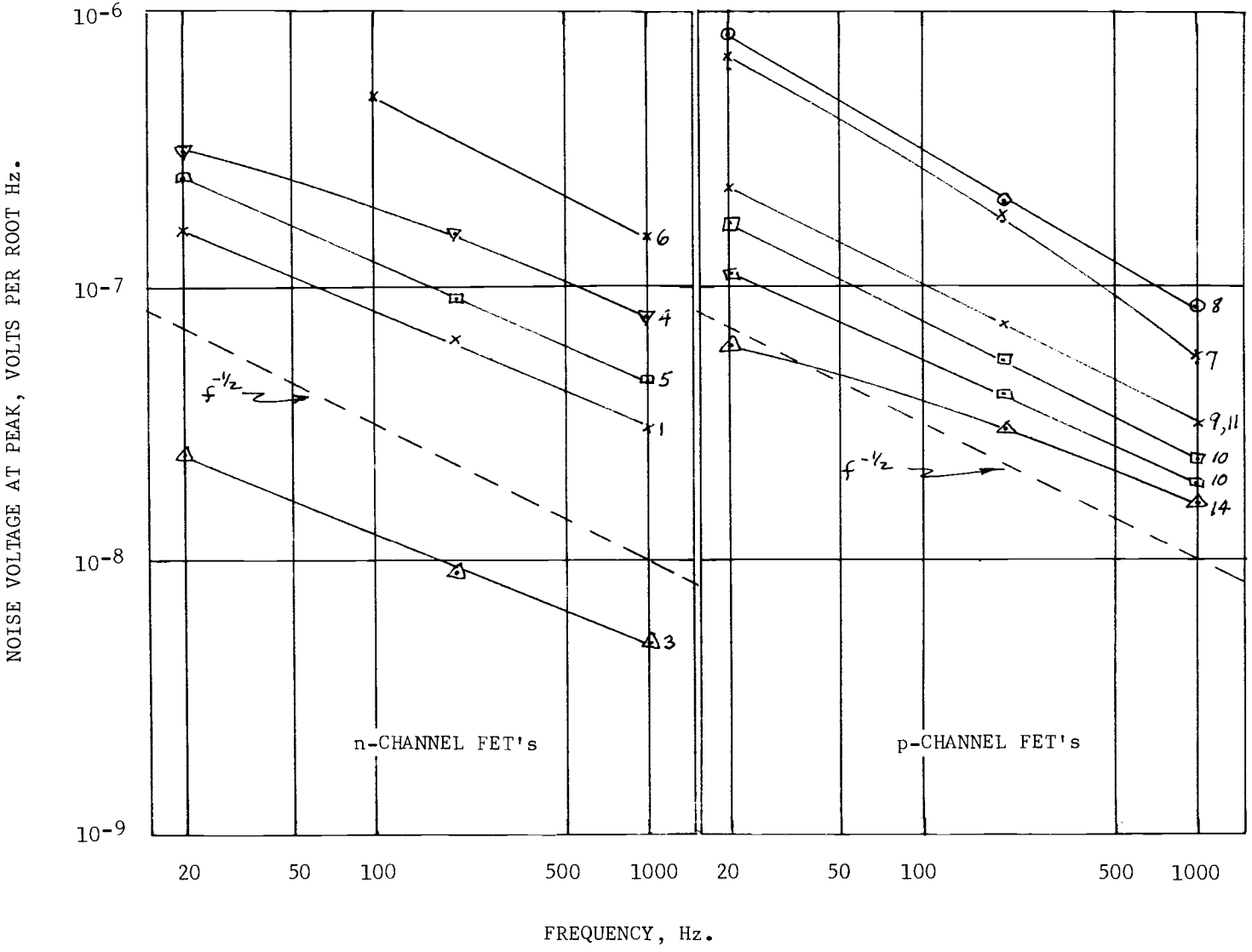

Figure 25. Noise voltage maxima as a function of frequency.

levels, calculated from the temperature dependence of time constants, are summarized in Figure 26 for each FET. Most silicon units of the same channel type possess similar levels. For example, all n-type units except number 6 have a 0.32 eV level. Units 1, 2 and 3 have a 0.26 eV level in common; units 4 and 5 have a 0.22 eV level in common. P-channel types have levels at 0.36 and 0.51 eV in most cases. The estimated error in these activation energies is 6%.

It is significant that identical units made by the same manufacturer have similar trap levels. Thus, only the material type and manufacturing process appear to determine the types of traps present.

Germanium FET

Sample number 14 was the only germanium FET tested. The noise versus temperature and noise spectra, Figures 27 and 28, bear similar characteristics to the silicon units tested, indicating that the dominant noise mechanism is similar to the Shockley-Read-Hall mechanism used for silicon FET's. In Figure 27, a noise structure is evident, superimposed on a slowly-changing structure. The measurement temperature range was insufficient to observe peaks in the latter. However, if the fine-structure peaks are assumed to follow the SRH theory, the energy level structure shown in Figure 26, device number 14, results. One level is located in the center of the bandgap; the others are within about 0.1 eV of the band-edges.

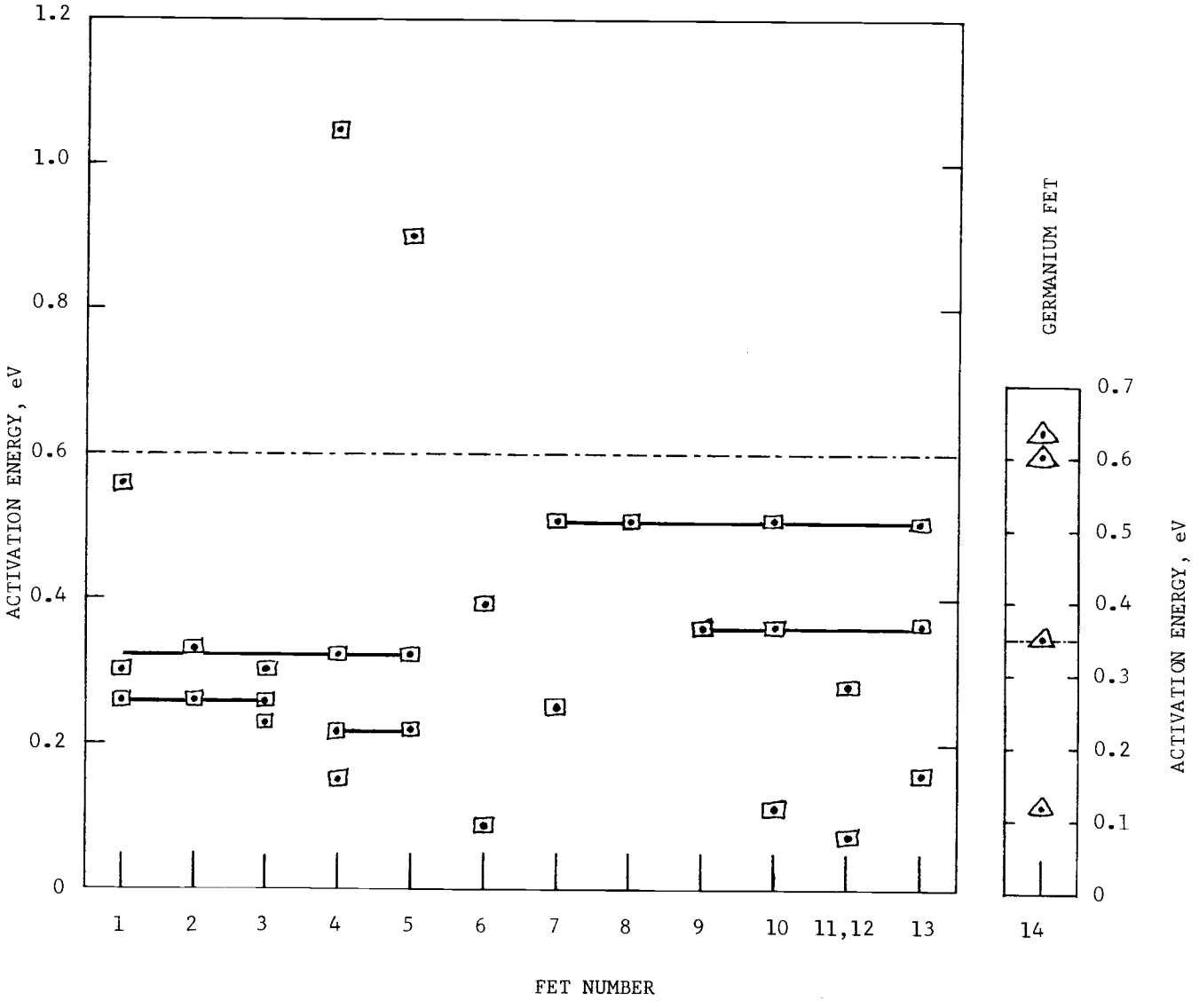

Figure 26. Activation energy level summary.

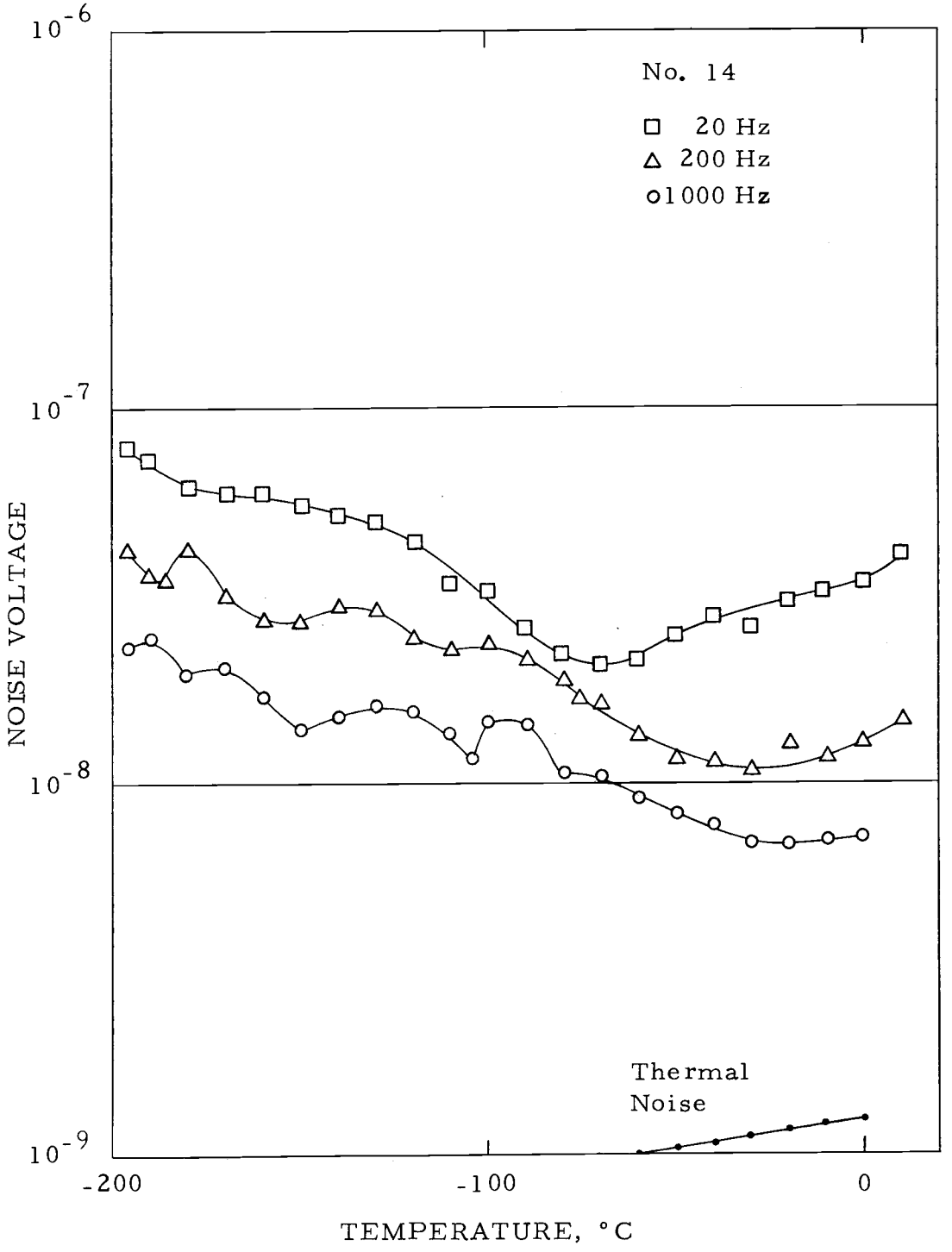

Figure 27. No. 14 noise voltage versus temperature.

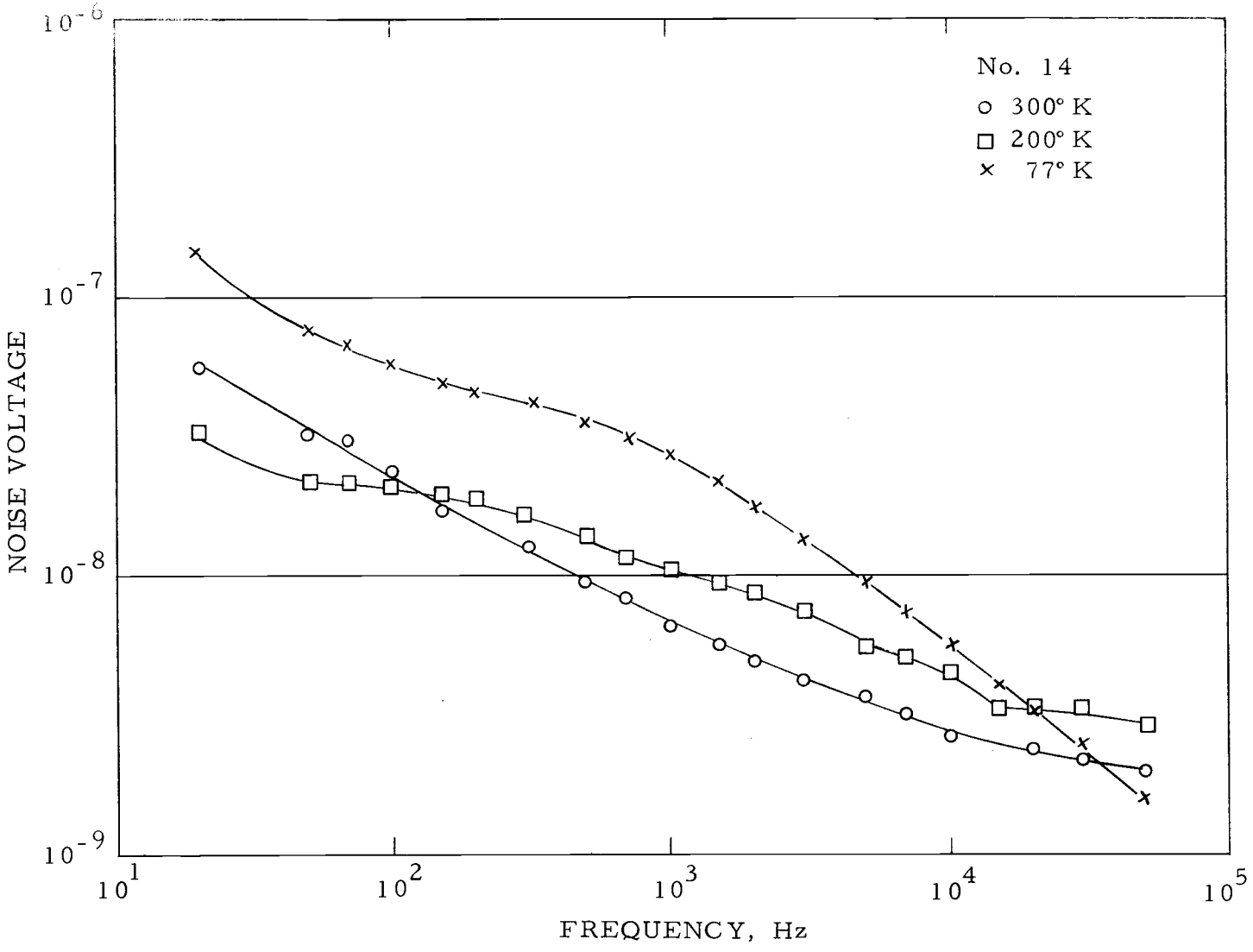

Figure 28. No. 14 noise spectrum.

Similarities in Noise Data

In addition to similar characteristics between FET's of similar channel type, some interesting comparisons can be made between similar units.

Consider the noise data of units 4 and 5, shown in Figure 29. These are units of identical geometry produced by the same manufacturer. The noise magnitudes are similar, but differ at every other maximum. Thus it seems possible that the distinct maxima of unit 5 resulted from the super-position of two similar noise peaks; whereas in unit 4 these peaks are distributed evenly in temperature. Further validity is given to this possibility by the fact that the leading and trailing slopes of unit 5 have energy values different from those given by the noise maxima.

Units 7 and 9 are of the same 2N-2608 geometry, but are made by two different manufacturers. As is evident from the data in Figure 30, there is no correlation between the different noise behavior, either at 20 Hz or at 1000 Hz. Thus it must be concluded that the manufacturing process, not device geometry, determines the low temperature, low frequency noise behavior.

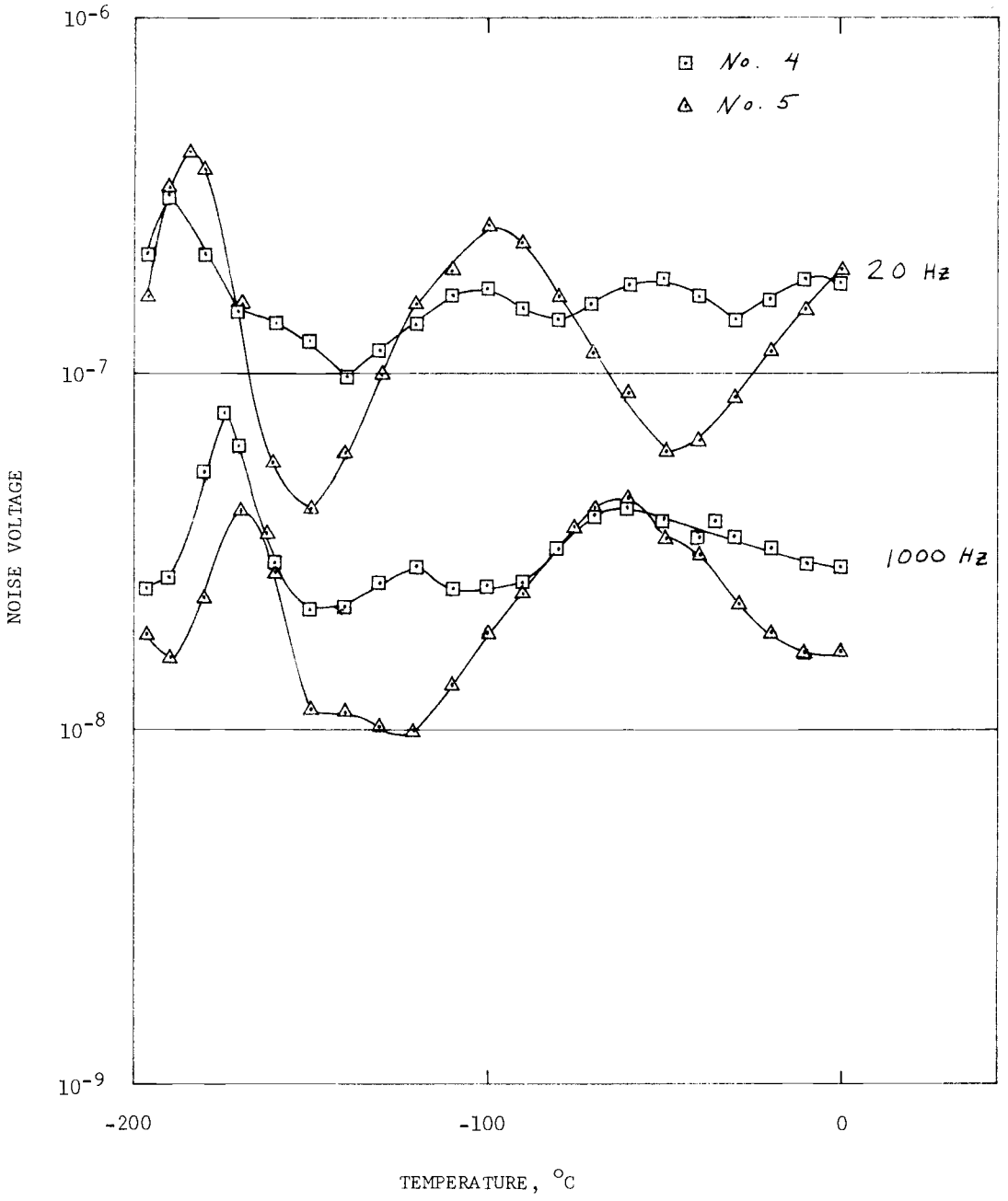

Figure 29. FET's No. 4 and 5.

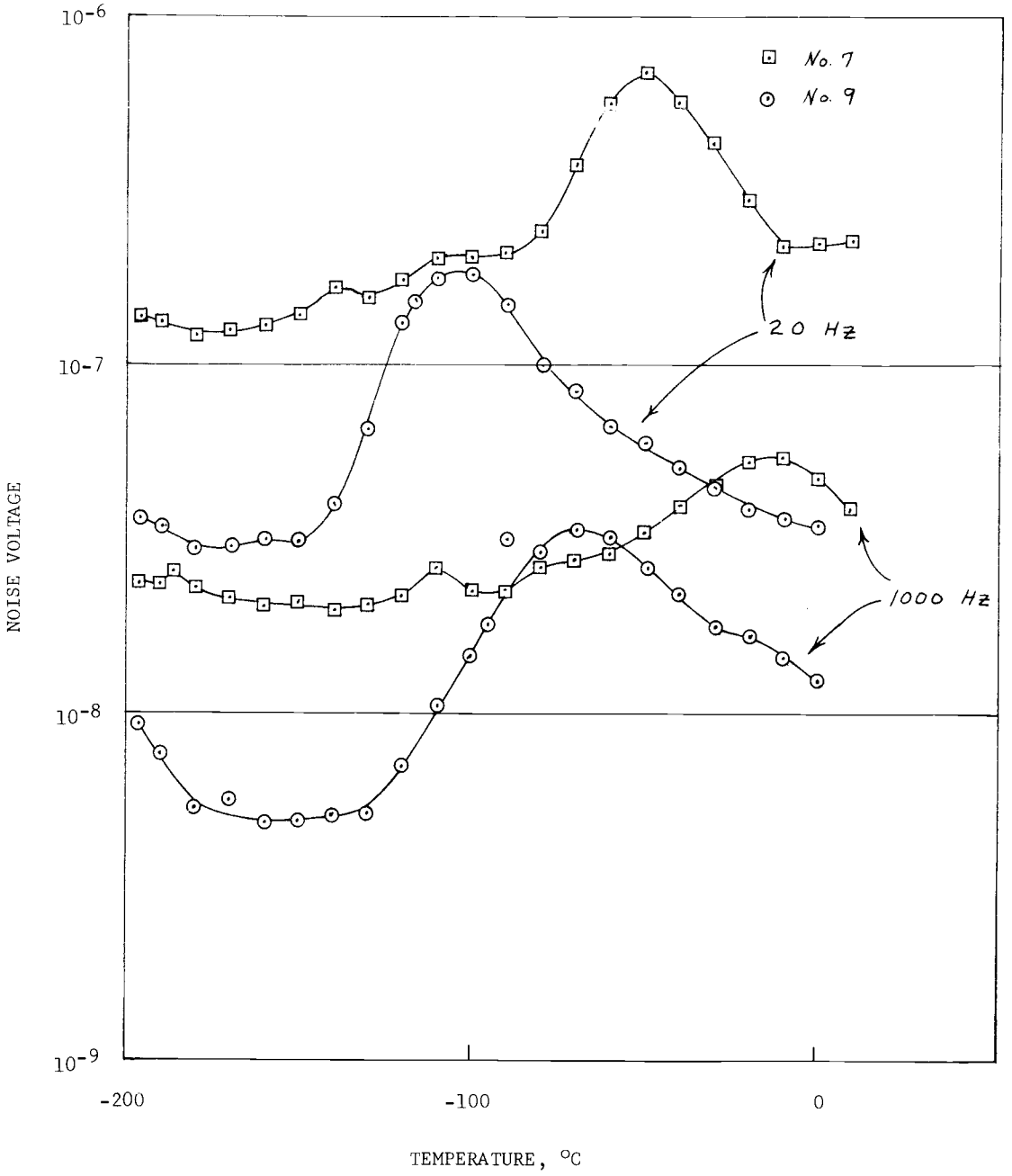

Figure 30. Similar p-channel geometry.

VI. CONCLUSIONS

Measurements of FET noise in the 300 to 77° K region indicate that the noise spectrum is highly temperature dependent. Devices of the same channel type exhibited similar variations with temperature although the noise magnitudes varied with individual FET's. P-channel devices exhibited a greater reduction in noise when cooled below 300° K; some n-channel devices exhibited lower noise at all temperatures. No correlation of noise magnitude with device geometry was evident.

From comparison of theoretical predictions and measured data, it has been shown that low frequency junction FET noise in the 300 to 77° K region can be attributed to the presence of Shockley-Read-Hall centers in the gate-channel depletion region. Estimates of the capture cross-sections, energy levels and concentrations of these centers were made by analysis of the temperature dependence of device noise voltage. Different capture cross-sections for these centers yielded a series of temperature dependent time constants which established the noise spectra. Estimates of SRH center concentrations on the order of 8×10^{9} cm^{-3} were obtained from the data.

It is concluded that variable temperature noise measurements on field-effect transistors can be a useful means of studying deep trapping centers of low concentration.

BIBLIOGRAPHY

1. Abowitz, G., E. Arnold and E. A. Leventhal. Surface states and 1/f noise in MOS transistors. Institute of Electrical and Electronics Engineers Transactions on Electron Devices ED-14: 775-777. 1967.

2. Alder, R. B., A. C. Smith and P. L. Longini. Introduction to semiconductor physics. New York, Wiley, 1964. 247 p.

3. Bartholomew, C. Y. Recombination centers in silicon transistor emitter-base junctions. Institute of Electrical and Electronics Engineers Transactions on Electron Devices ED-14: 452-453. 1967.

4. Beers, Y. Introduction to the theory of error. Reading, Addison-Wesley, 1957. 66 p.

5. Bemski, G. Recombination in semiconductors. Proceedings of the Institute of Radio Engineers 46:990-1004. 1958.

6. Bendat, J. S. and A. G. Piersol. Measurement and analysis of random data. New York, Wiley, 1966. 390 p.

7. Blalock, T. V. A low noise charge-sensitive preamplifier with an FET in the input stage. Institute of Electrical and Electronics Engineers Transactions on Nuclear Science NS-11:365-370. 1964.

8. Bruncke, W. C. Noise measurements in field-effect transistors. Proceedings of the Institute of Electrical and Electronics Engineers 51:378-379. 1963.

9. Bruncke, W. C. and H. E. Halladay. Excess noise in field-effect transistors. Proceedings of the Institute of Electrical and Electronics Engineers 51:1671. 1963.

10. Bruncke, W. C. and A. van der Ziel. Thermal noise in junction-gate field-effect transistors. Institute of Electrical and Electronics Engineers Transactions on Electron Devices ED-13: 323-329. 1966.

11. Cutler, M. and H. M. Bath. Surface leakage current in silicon fused junction diodes. Proceedings of the Institute of Radio Engineers 45:39-43. 1957.

12. Evans, L.A., Engineer, Siliconix Incorporated. Personal communication. Sunnyvale, California. June 16, 1966.

13. Gfeller, J. FET parameter variations over a wide temperature range. Mountain View, Calif., 1965. 4 p. (Union Carbide Corporation. Technical Note no. 1)

14. Kittel, C. Introduction to solid-state physics. New York, Wiley, 1963. 616 p.

15. Klaassen, F.M. High-frequency noise of the junction field-effect transistor. Institute of Electrical and Electronics Engineers Transactions on Electron Devices ED-14:368-378. 1967.

16. Lauritzen, P.O. Low-frequency generation noise in junction field-effect transistors. Solid-State Electronics 8:41-58. 1965.

17. Lax, M. Fluctuations from the nonequilibrium steady state. Reviews of Modern Physics 32:25-64. 1960.

18. Lax, M. Giant traps. Journal of the Physics and Chemistry of Solids 8:66-73. 1959.

19. Lee, Y.W. Statistical theory of communication. New York, Wiley, 1964. 509 p.

20. Lindmayer, J. and C.Y. Wrigley. Fundamentals of semiconductor devices. Princeton, Van Nostrand, 1965. 486 p.

21. Nybakken, T.W. and V. Vali. A hybrid preamplifier for cooled lithium ion-drifted semiconductor detectors. Nuclear Instruments and Methods 32:121-124. 1965.

22. Radeka, V. The field-effect transistor, its characteristics and applications. Institute of Electrical and Electronics Engineers Transactions on Nuclear Science NS-11:358-364. 1964.

23. Sah, C.T. Effect of surface recombination and channel on p-n junctions and transistor characteristics. Institute of Radio Engineers Transactions on Electron Devices ED-9:94-108. 1962.

24. Sah, C.T. The equivalent circuit model in solid-state electronics. Part I. The single energy level defect center. Proceedings of the Institute of Electrical and Electronics Engineers 55: 603-736. 1967.

25. Sah, C. T. Theory of low-frequency generation noise in junction-gate field-effect transistors. Proceedings of the Institute of Electrical and Electronics Engineers 52:795-814. 1964.

26. Sah, C. T. and F. H. Hielscher. Evidence of the surface origin of the 1/f noise. Physical Review Letters 17:956-958. 1966.

27. Sah, C. T., R. N. Noyce and W. Shockley. Carrier generation and recombination in p-n junctions and p-n junction characteristics. Proceedings of the Institute of Radio Engineers 45:1228-1243. 1957.

28. Sevin, L. J. Field-effect transistors. New York, McGraw-Hill, 1965. 130 p.

29. Shockley, W. Electrons and holes in semiconductors. Princeton, Van Nostrand, 1950. 554 p.

30. Shockley, W. Electrons, holes and traps. Proceedings of the Institute of Radio Engineers 46:973-990. 1958.

31. Shockley, W. A unipolar "field-effect" transistor. Proceedings of the Institute of Radio Engineers 40:1365-1376. 1952.

32. Shockley, W. and W. T. Read, Jr. Statistics of the recombinations of holes and electrons. Physical Review 87:835-842. 1952.

33. Spaulding, R. A. Field-effect transistor noise at low temperatures. Proceedings of the Institute of Electrical and Electronics Engineers 56:886-887. 1968.

34. Storm, H. F. Field-effect transistor (FET) bibliography. Institute of Electrical and Electronics Engineers Transactions on Electron Devices ED-14:710-717. 1967.

35. van der Ziel, A. Carrier density fluctuation noise in field-effect transistors. Proceedings of the Institute of Electrical and Electronics Engineers 51:1671-1672. 1963.

36. van der Ziel, A. Fluctuation phenomena in semi-conductors. New York, Academic, 1959. 168 p.

37. van der Ziel, A. Gate noise in field-effect transistors at moderately high frequencies. Proceedings of the Institute of Electrical and Electronics Engineers 51:461-467. 1963.

38. van der Ziel, A. Noise. New York, Prentice-Hall, 1954. 450 p.

39. van der Ziel, A. Thermal noise in field-effect transistors. Proceedings of the Institute of Radio Engineers 50:1808-1812. 1962.

APPENDICES

APPENDIX I

Measured Data

The measured noise data for the FET's used in this research are presented. The first group contains noise voltage versus temperature at 20, 200 and 1000 Hz, and theoretical noise calculated from measured values of g_m. The second group contains noise voltage spectra at 300, 200 and 77° K.

In several instances, the measured data for an FET is presented in the main body of the text. These data are omitted from this appendix and are as follows.

Noise voltage versus temperature:

No. 3, Figure 17

No. 5, Figure 15

No. 6, Figure 22

No. 14, Figure 27

Noise voltage versus frequency:

No. 5, Figure 16

No. 6, Figure 23

No. 14, Figure 28

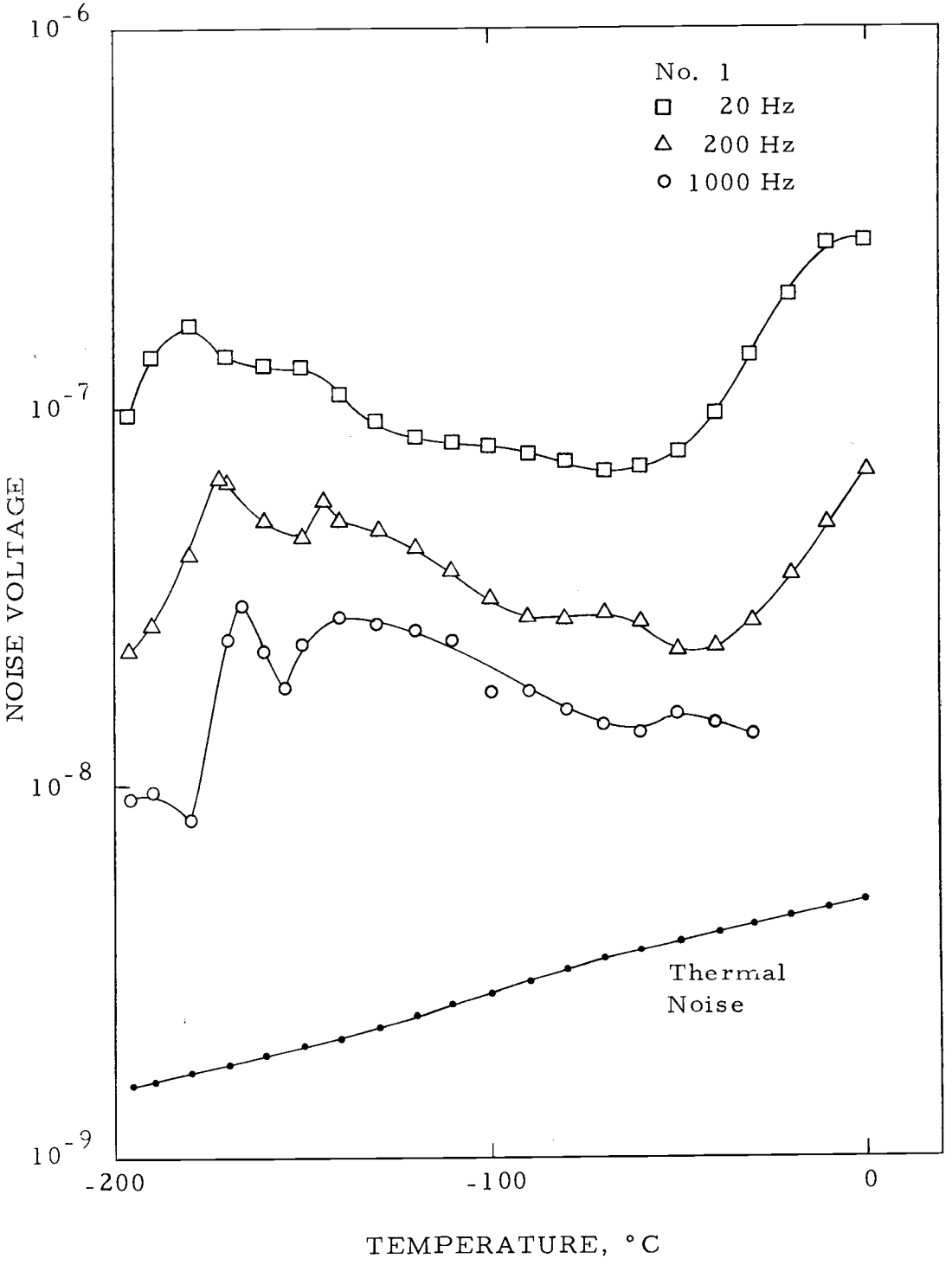
No. 1
20 Hz
200 Hz
1000 Hz
Thermal Noise
NOISE VOLTAGE
10^{-6}
10^{-7}
10^{-8}
10^{-9}
-200
-100
0
TEMPERATURE, °C

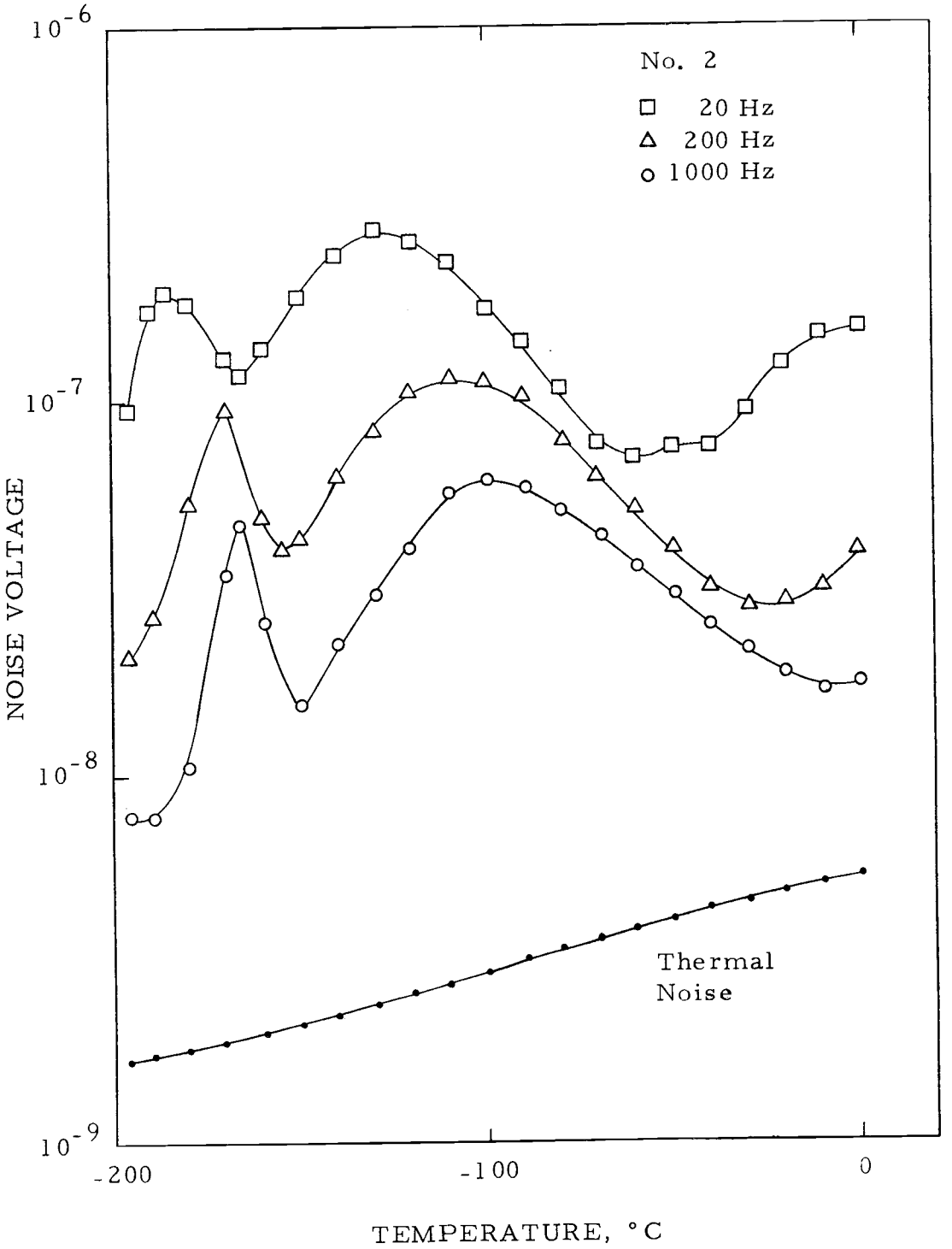
No. 2
20 Hz
200 Hz
1000 Hz
Thermal
Noise
NOISE VOLTAGE
10^{-6}
10^{-7}
10^{-8}
10^{-9}
-200
-100
0
TEMPERATURE, °C

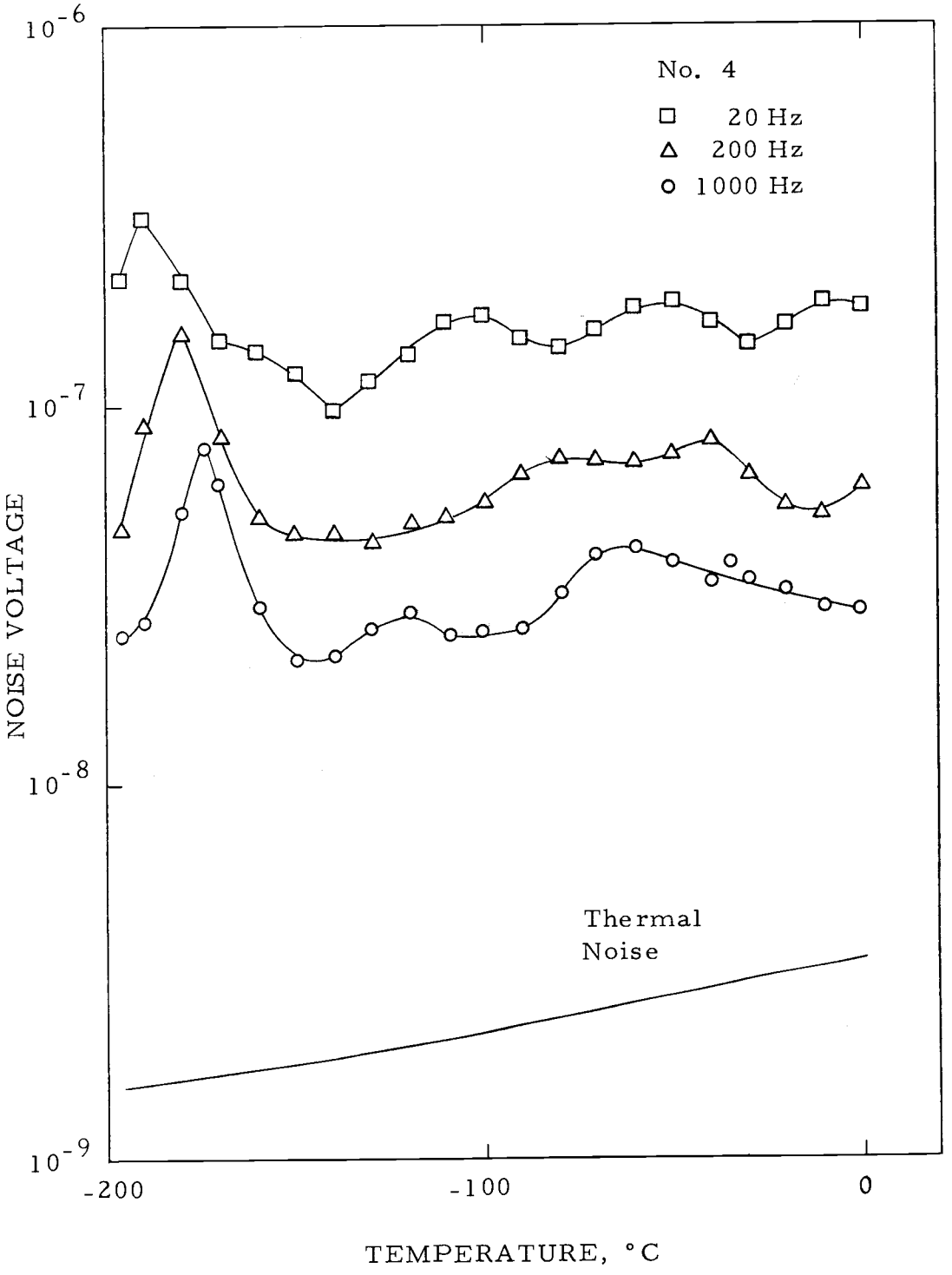
No. 4
20 Hz
200 Hz
1000 Hz
Thermal
Noise
NOISE VOLTAGE
10^{-6}
10^{-7}
10^{-8}
10^{-9}
-200
-100
0
TEMPERATURE, °C

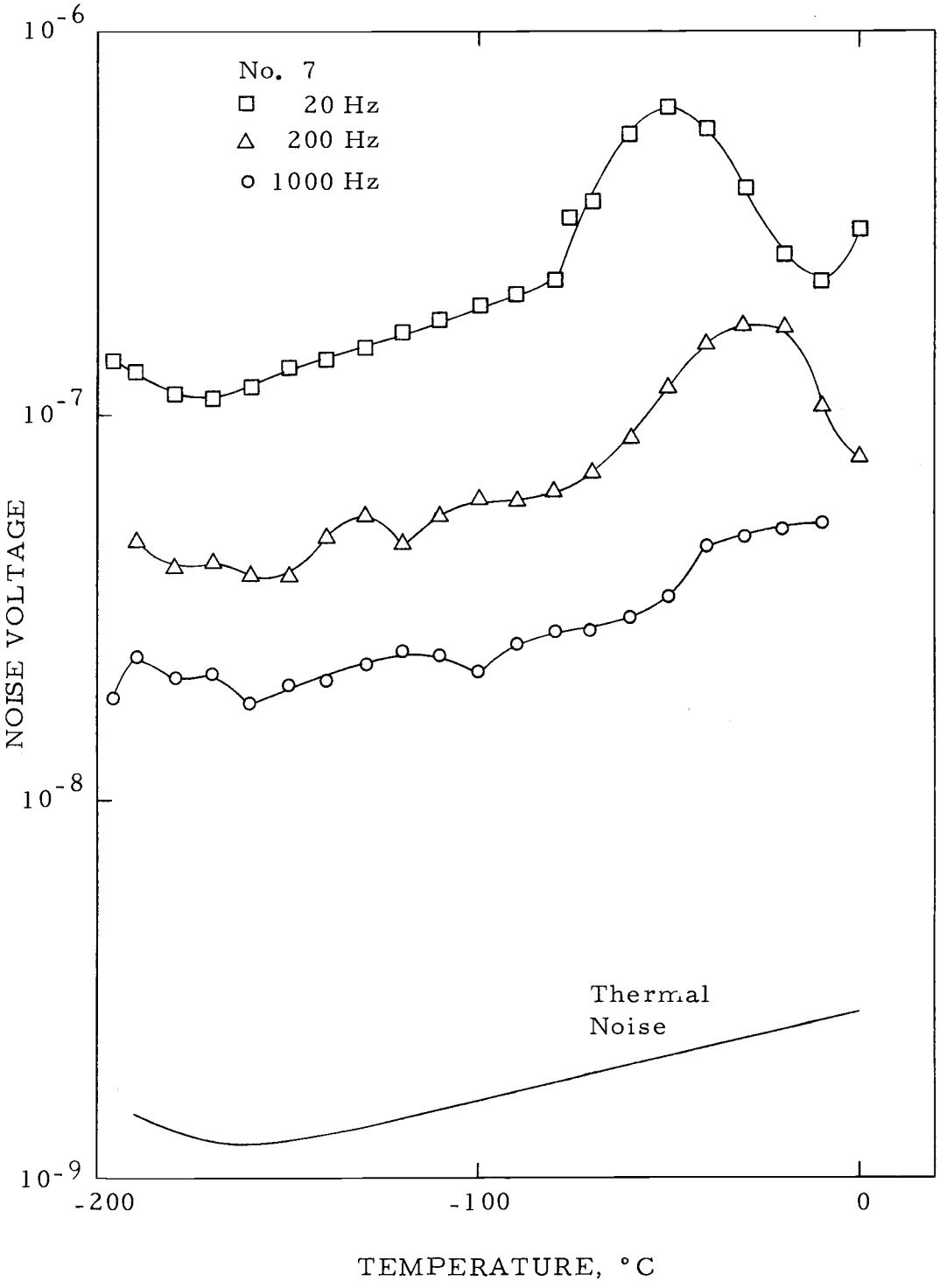
No. 7
20 Hz
200 Hz
1000 Hz
Thermal
Noise
NOISE VOLTAGE
10^{-6}
10^{-7}
10^{-8}
10^{-9}
-200
-100
0
TEMPERATURE, °C

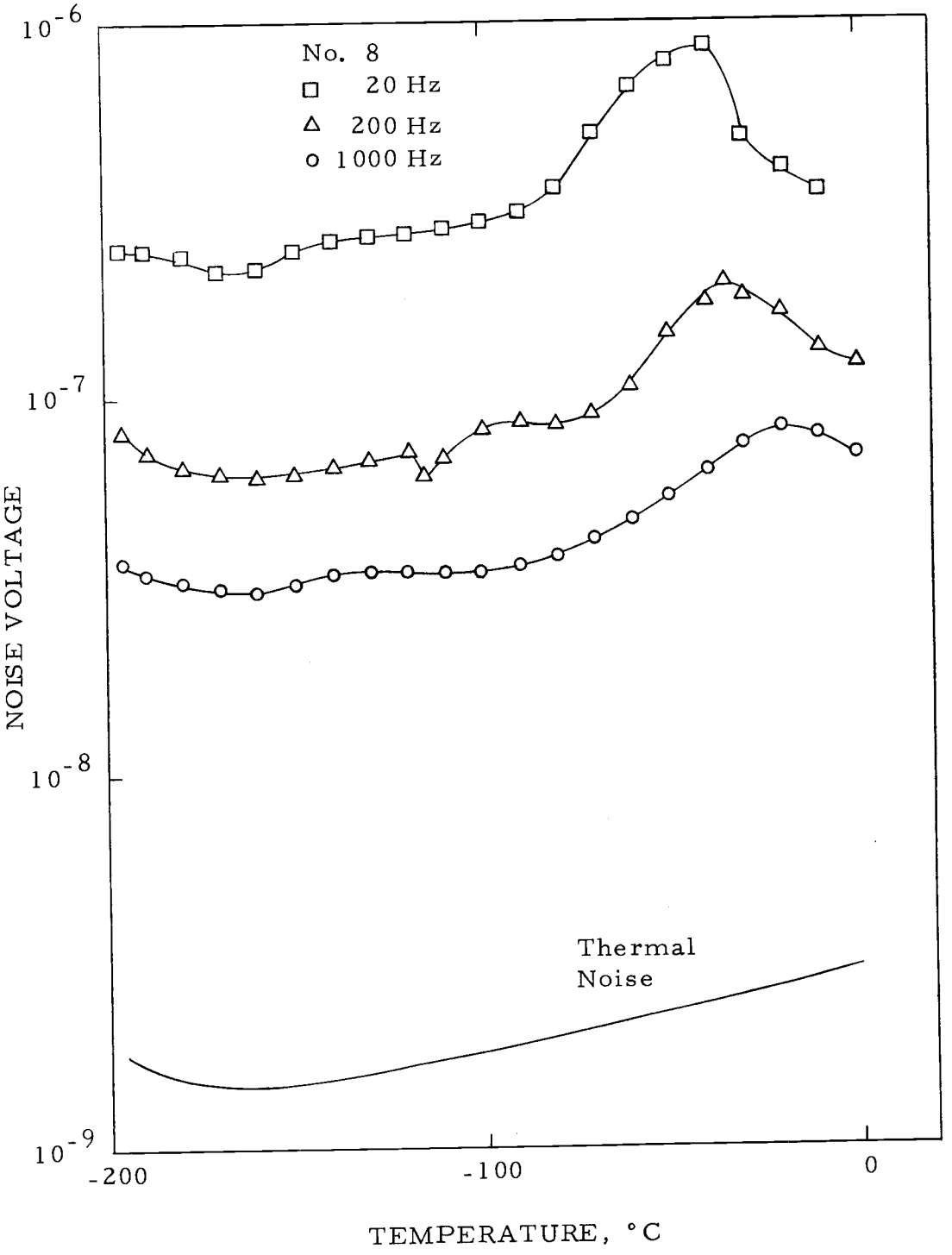
No. 8
20 Hz
200 Hz
1000 Hz
10^{-6}
10^{-7}
10^{-8}
10^{-9}
NOISE VOLTAGE
Thermal
Noise
-200
-100
0
TEMPERATURE, °C

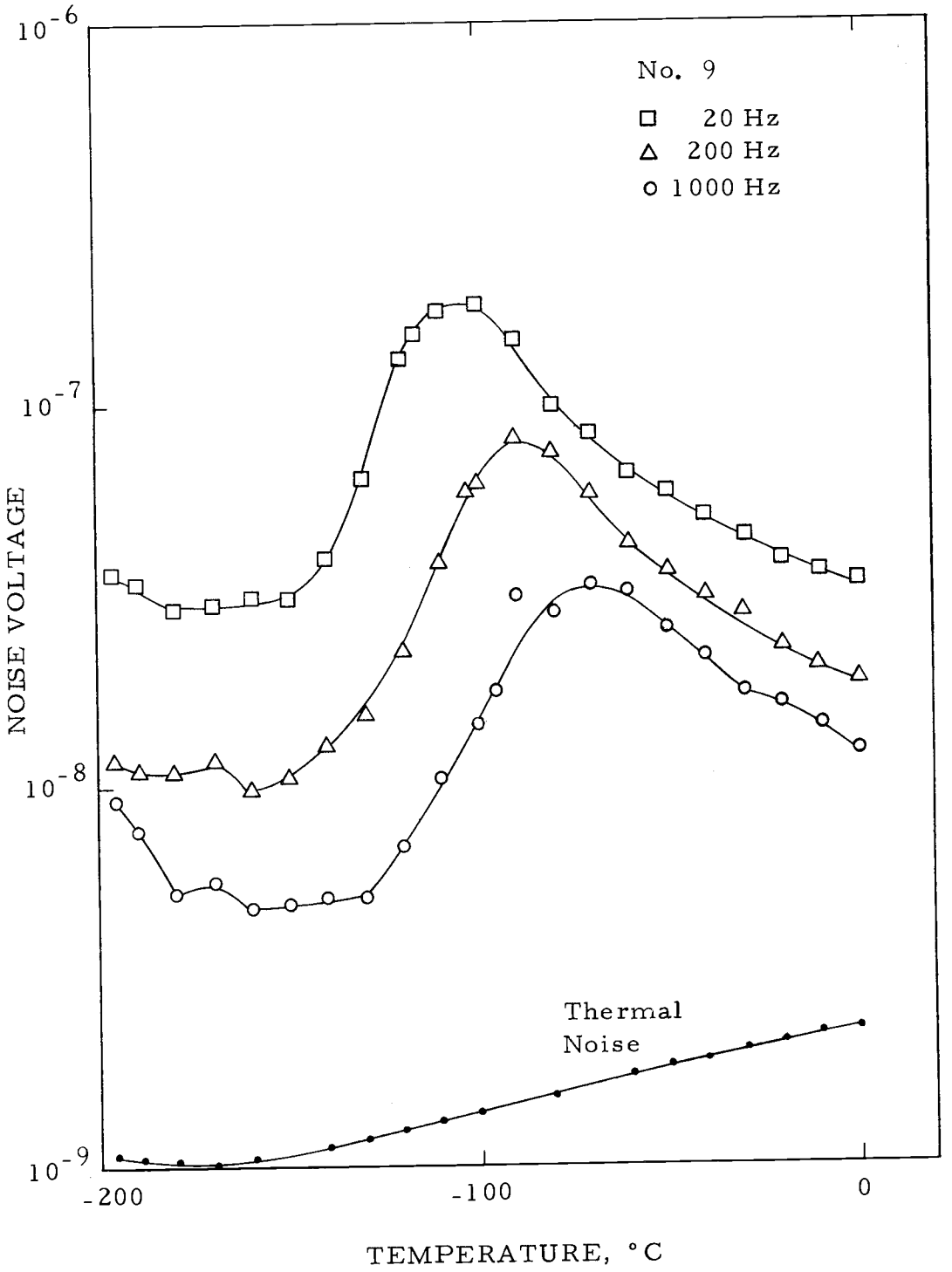
No. 9
20 Hz
200 Hz
1000 Hz
Thermal
Noise
NOISE VOLTAGE
10^{-6}
10^{-7}
10^{-8}
10^{-9}
-200
-100
0
TEMPERATURE, °C

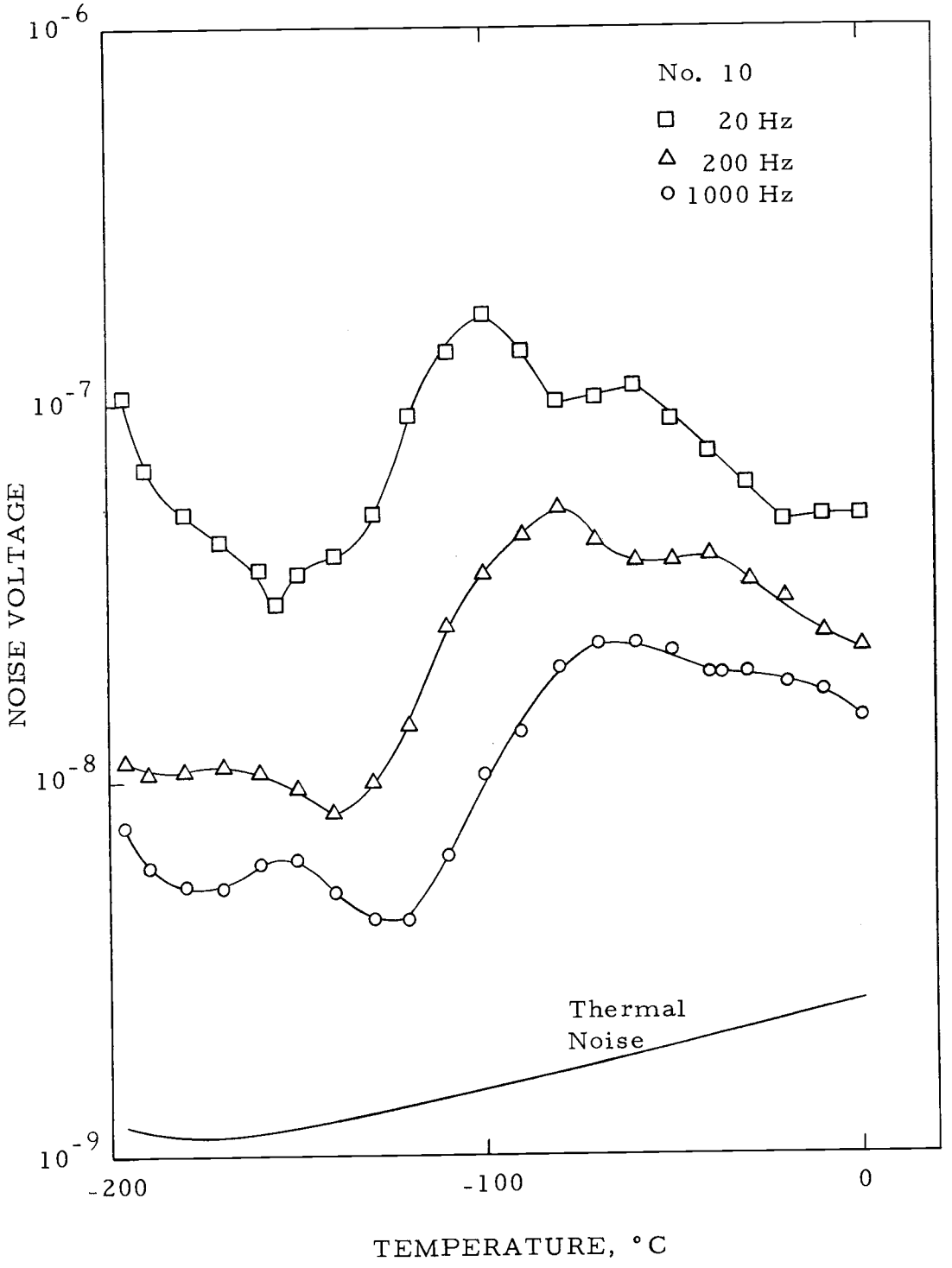
No. 10
20 Hz
200 Hz
1000 Hz
Thermal
Noise
NOISE VOLTAGE
TEMPERATURE, °C
10-6
10-7
10-8
10-9
-200
-100
0

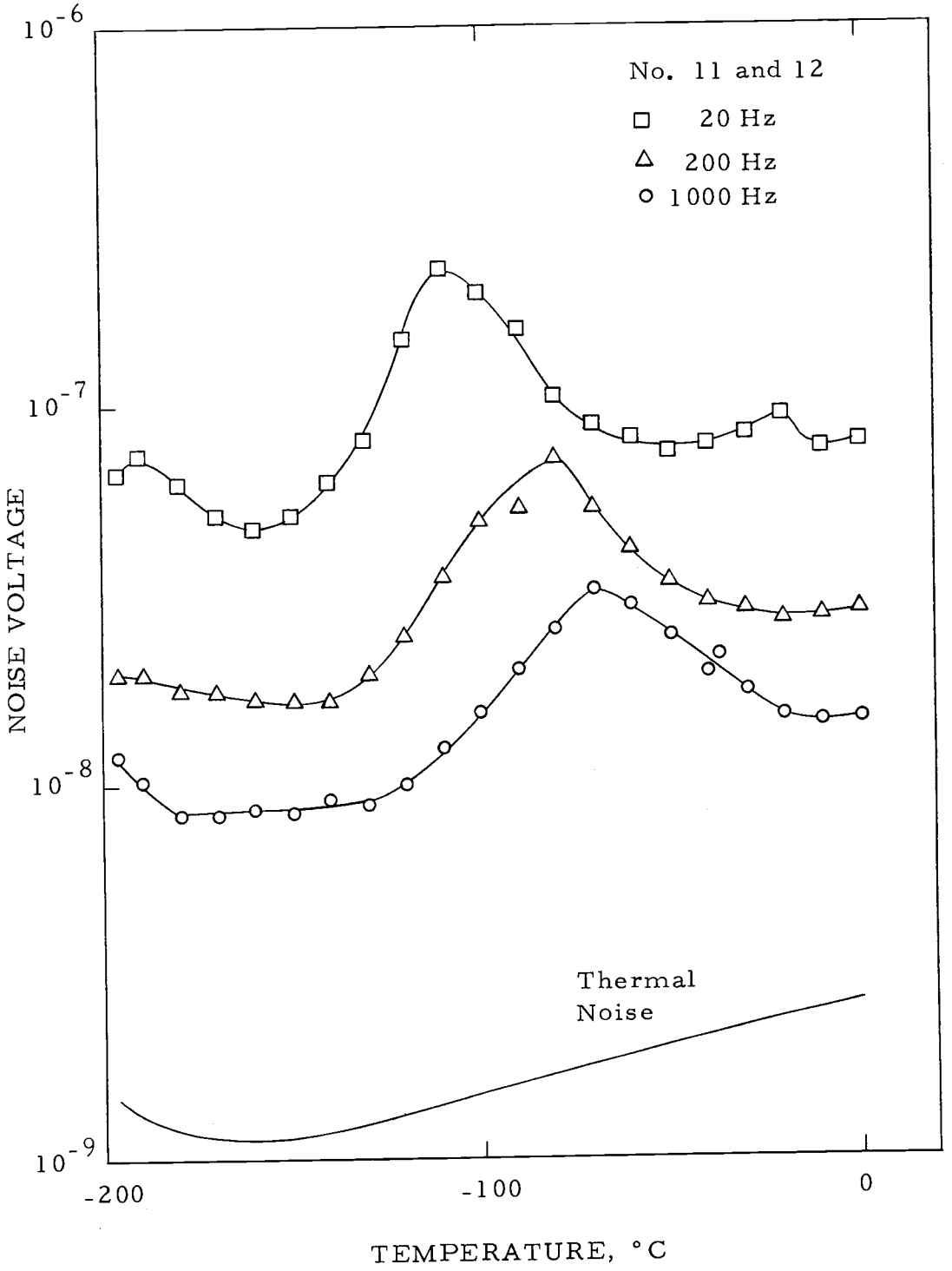
No. 11 and 12
20 Hz
200 Hz
1000 Hz
10^{-6}
10^{-7}
10^{-8}
10^{-9}
NOISE VOLTAGE
Thermal
Noise
-200
-100
0
TEMPERATURE, °C

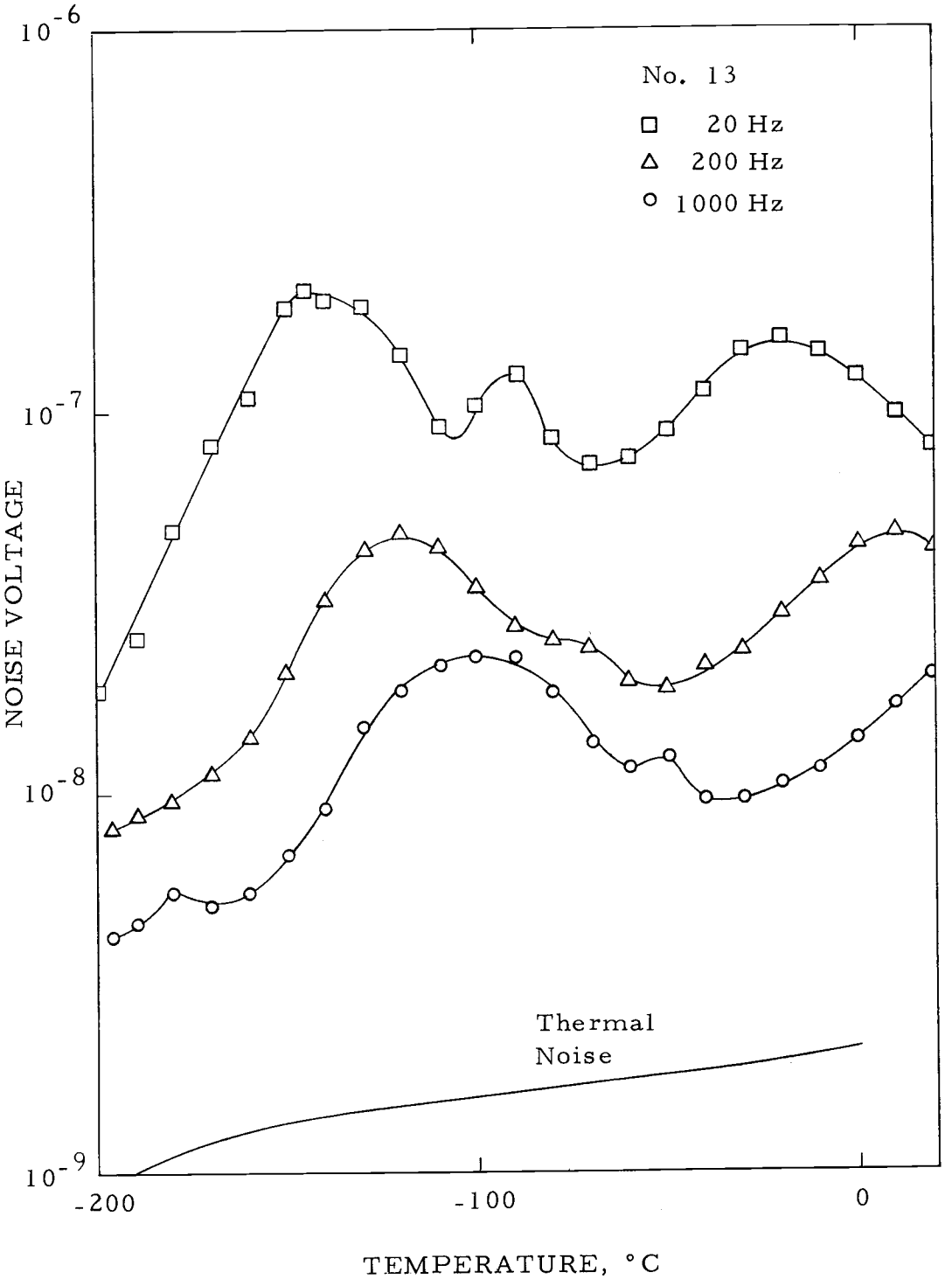
No. 13
20 Hz
200 Hz
1000 Hz
Thermal
Noise
NOISE VOLTAGE
10^{-6}
10^{-7}
10^{-8}
10^{-9}
-200
-100
0
TEMPERATURE, °C

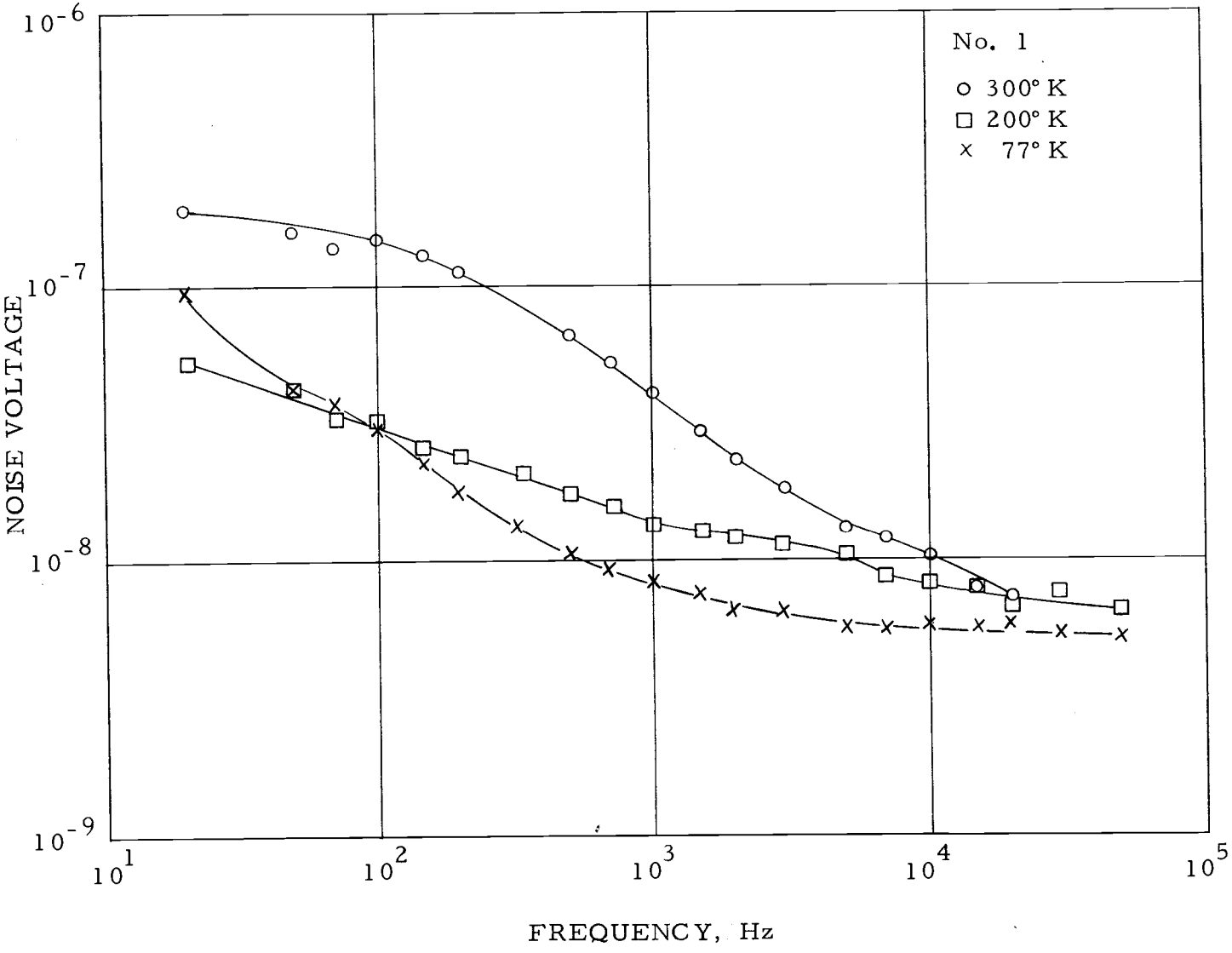
No. 1
o 300° K
□ 200° K
x 77° K
NOISE VOLTAGE
10-6
10-7
10-8
10-9
10¹
10²
10³
10⁴
10⁵
FREQUENCY, Hz

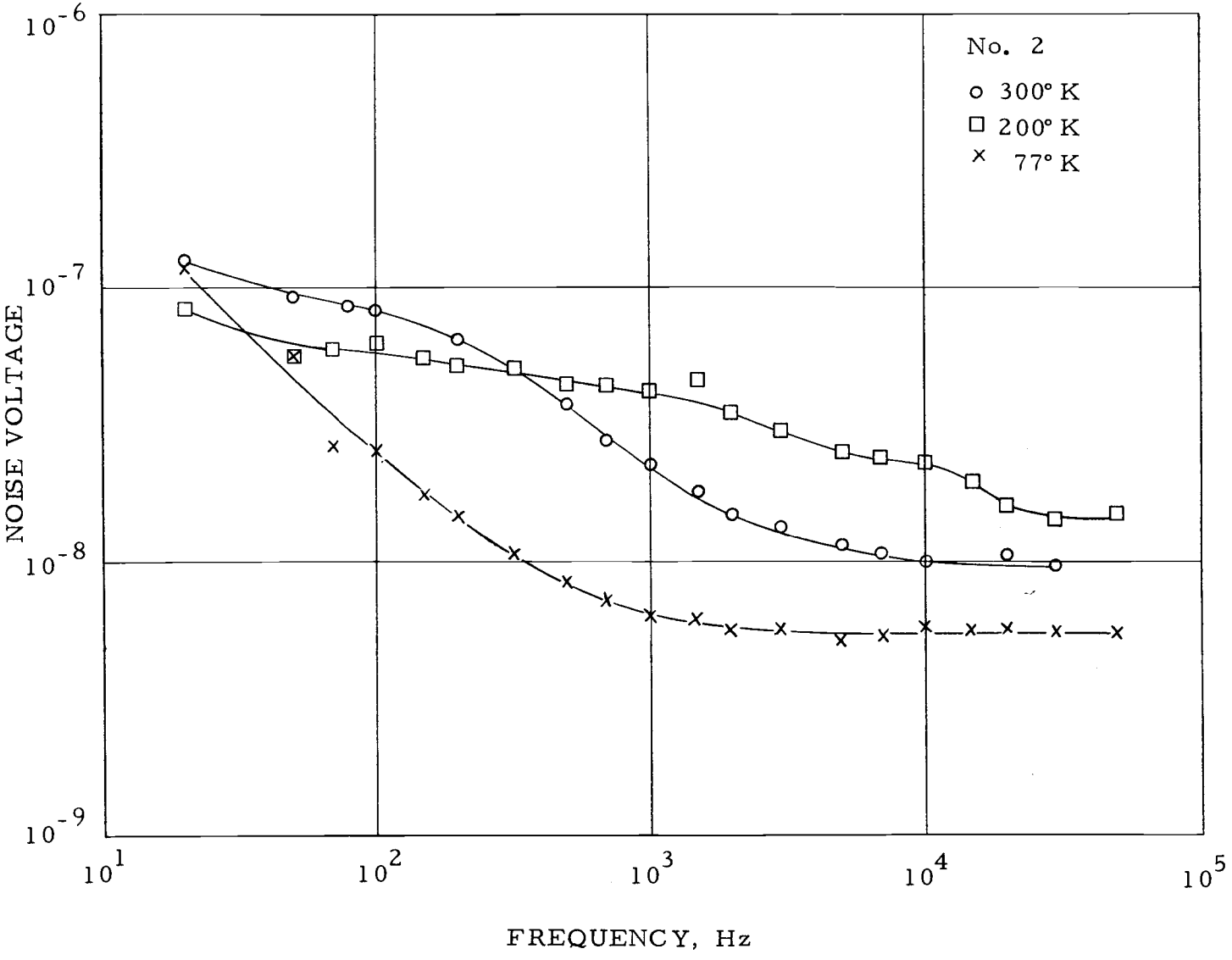
No. 2
o 300° K
□ 200° K
× 77° K
NOISE VOLTAGE
10^{-6}
10^{-7}
10^{-8}
10^{-9}
10^{1}
10^{2}
10^{3}
10^{4}
10^{5}
FREQUENCY, Hz

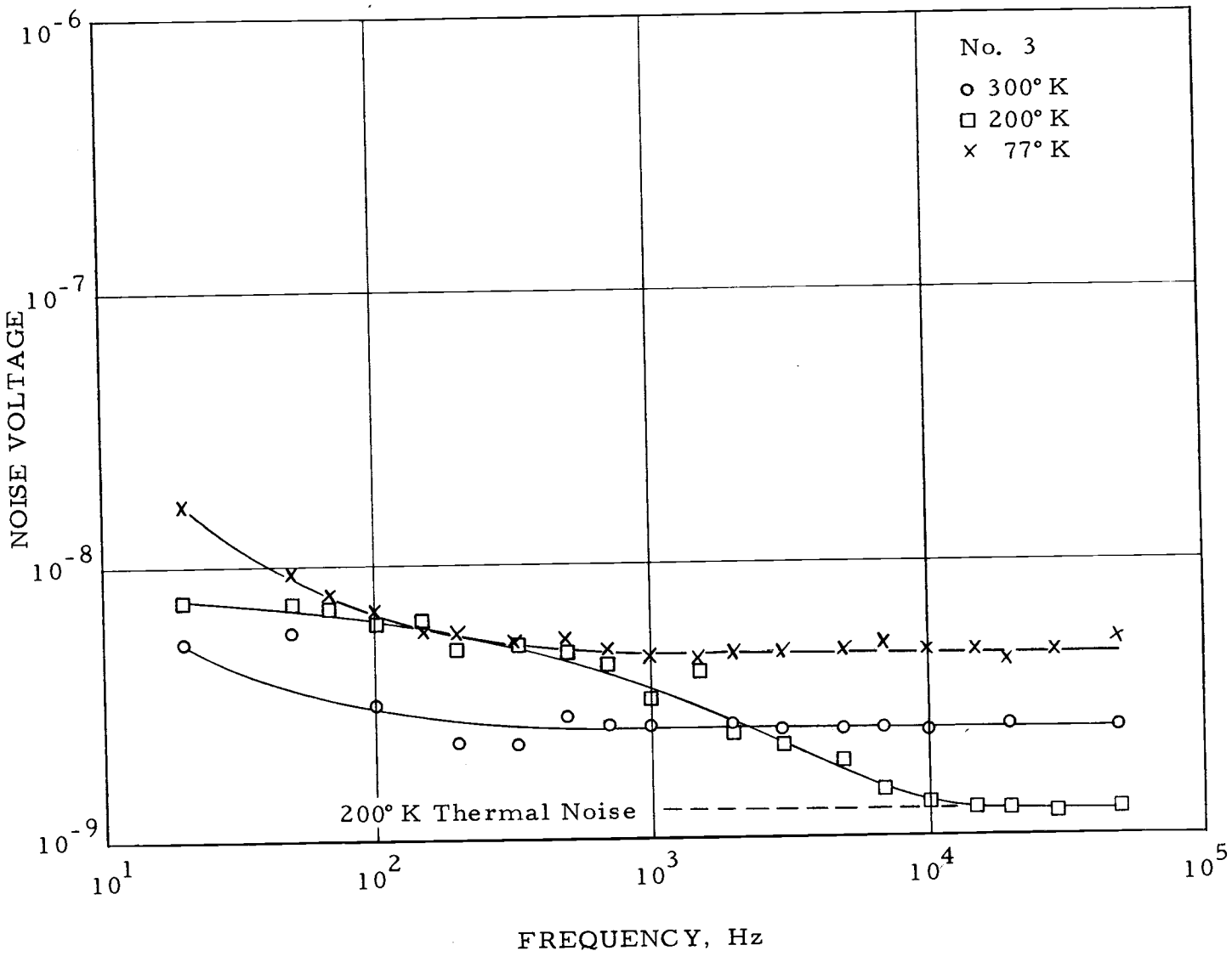
No. 3
o 300° K
□ 200° K
× 77° K
NOISE VOLTAGE
10^{-6}
10^{-7}
10^{-8}
10^{-9}
200° K Thermal Noise
10^{1}
10^{2}
10^{3}
10^{4}
10^{5}
FREQUENCY, Hz

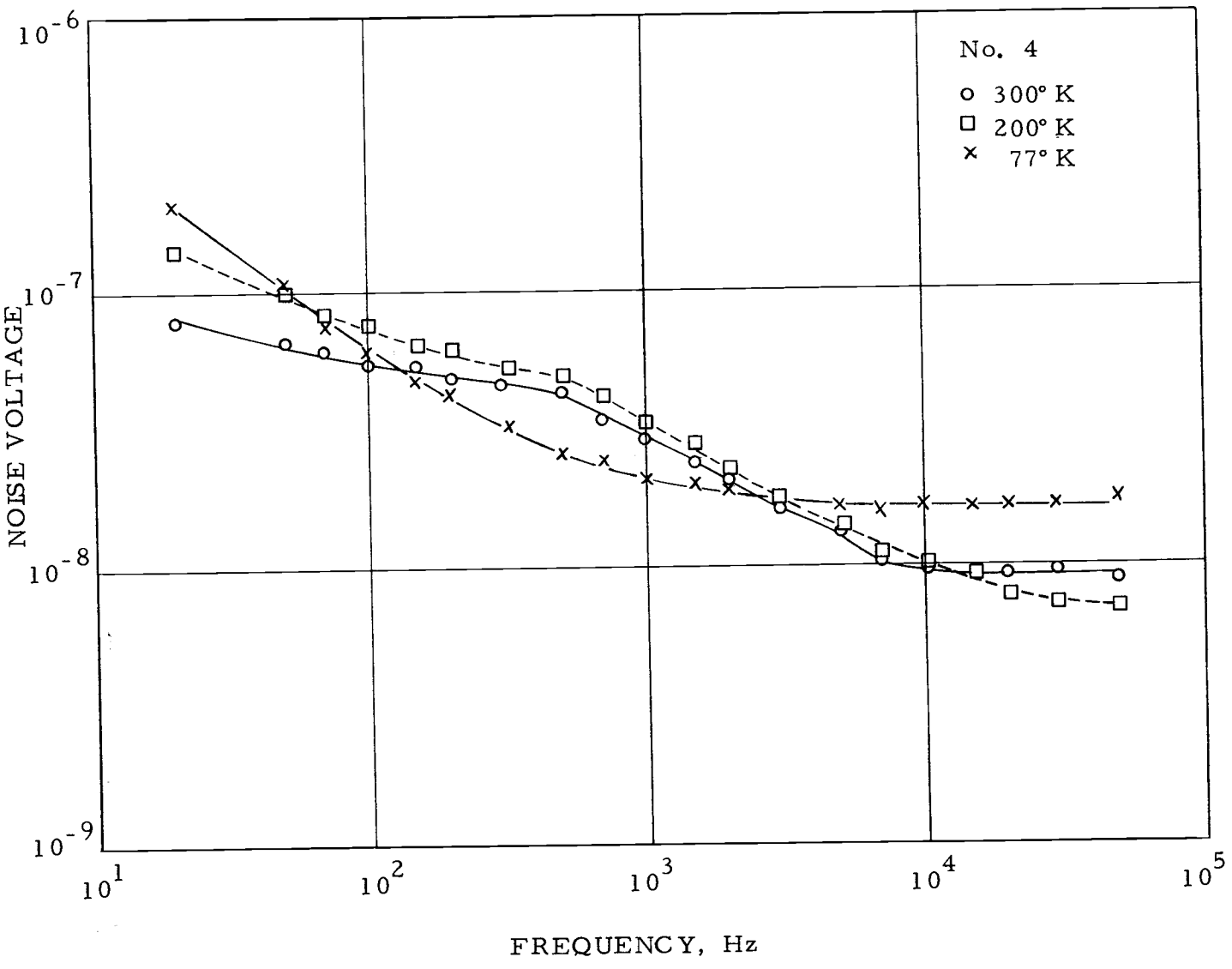
No. 4
300° K
200° K
77° K
NOISE VOLTAGE
10^{-6}
10^{-7}
10^{-8}
10^{-9}
10^{1}
10^{2}
10^{3}
10^{4}
10^{5}
FREQUENCY, Hz

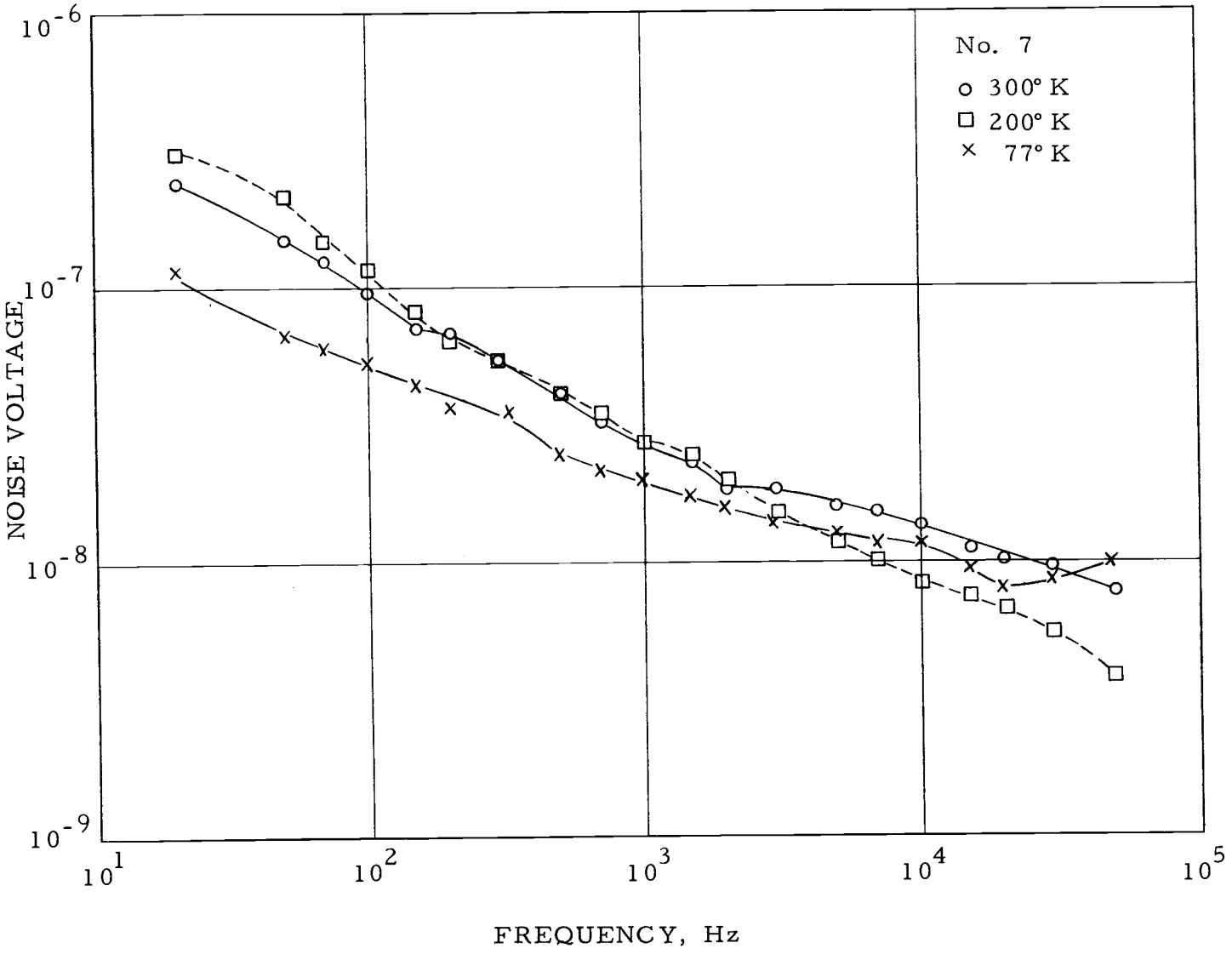
No. 7
o 300° K
□ 200° K
× 77° K
NOISE VOLTAGE
10^{-6}
10^{-7}
10^{-8}
10^{-9}
10^{1}
10^{2}
10^{3}
10^{4}
10^{5}
FREQUENCY, Hz

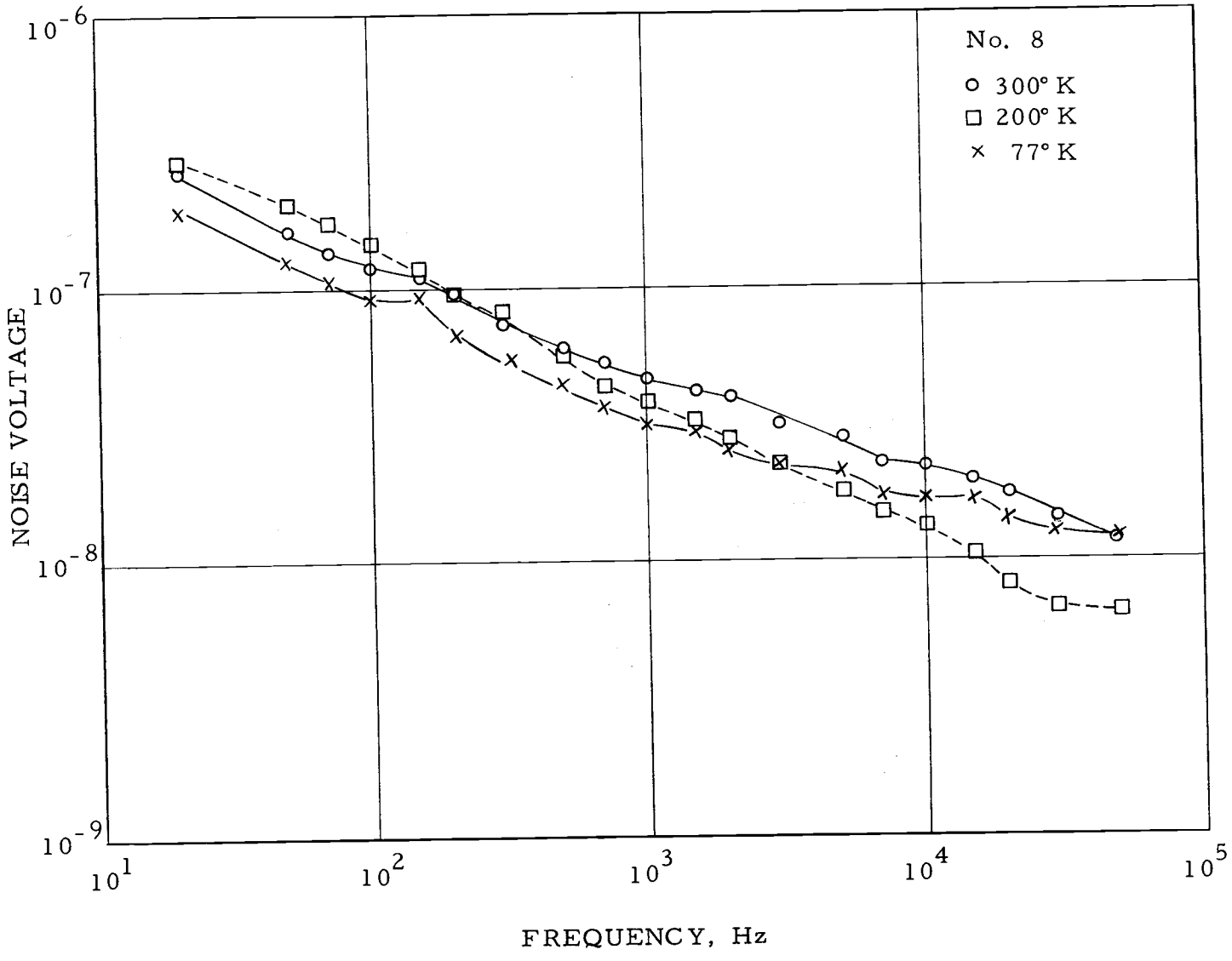
No. 8
o 300° K
□ 200° K
× 77° K
NOISE VOLTAGE
10^-6
10^-7
10^-8
10^-9
10^1
10^2
10^3
10^4
10^5
FREQUENCY, Hz

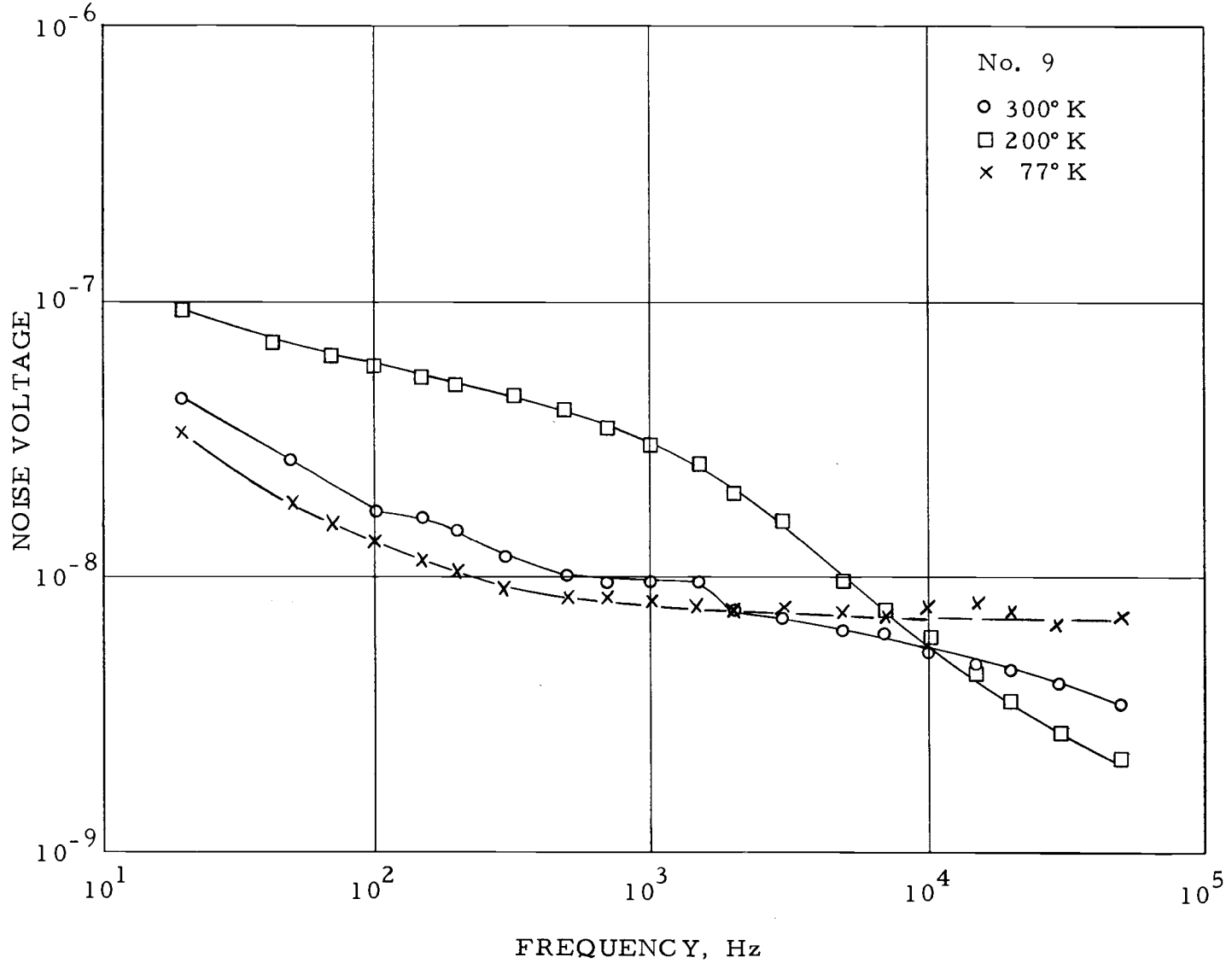
No. 9
300° K
200° K
77° K
NOISE VOLTAGE
10^{-6}
10^{-7}
10^{-8}
10^{-9}
10^{1}
10^{2}
10^{3}
10^{4}
10^{5}
FREQUENCY, Hz

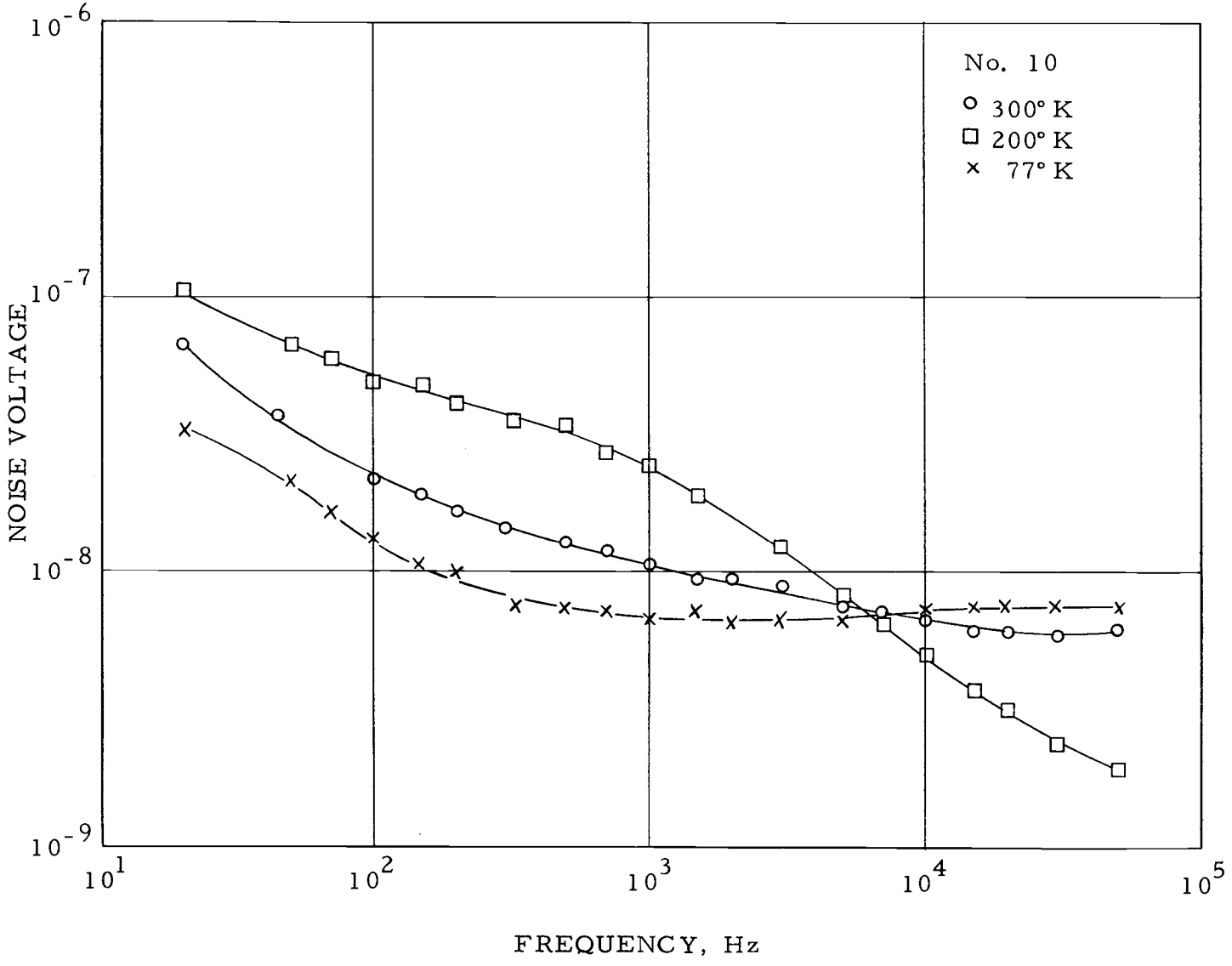
No. 10
300° K
200° K
77° K
NOISE VOLTAGE
10^{-6}
10^{-7}
10^{-8}
10^{-9}
10^{1}
10^{2}
10^{3}
10^{4}
10^{5}
FREQUENCY, Hz

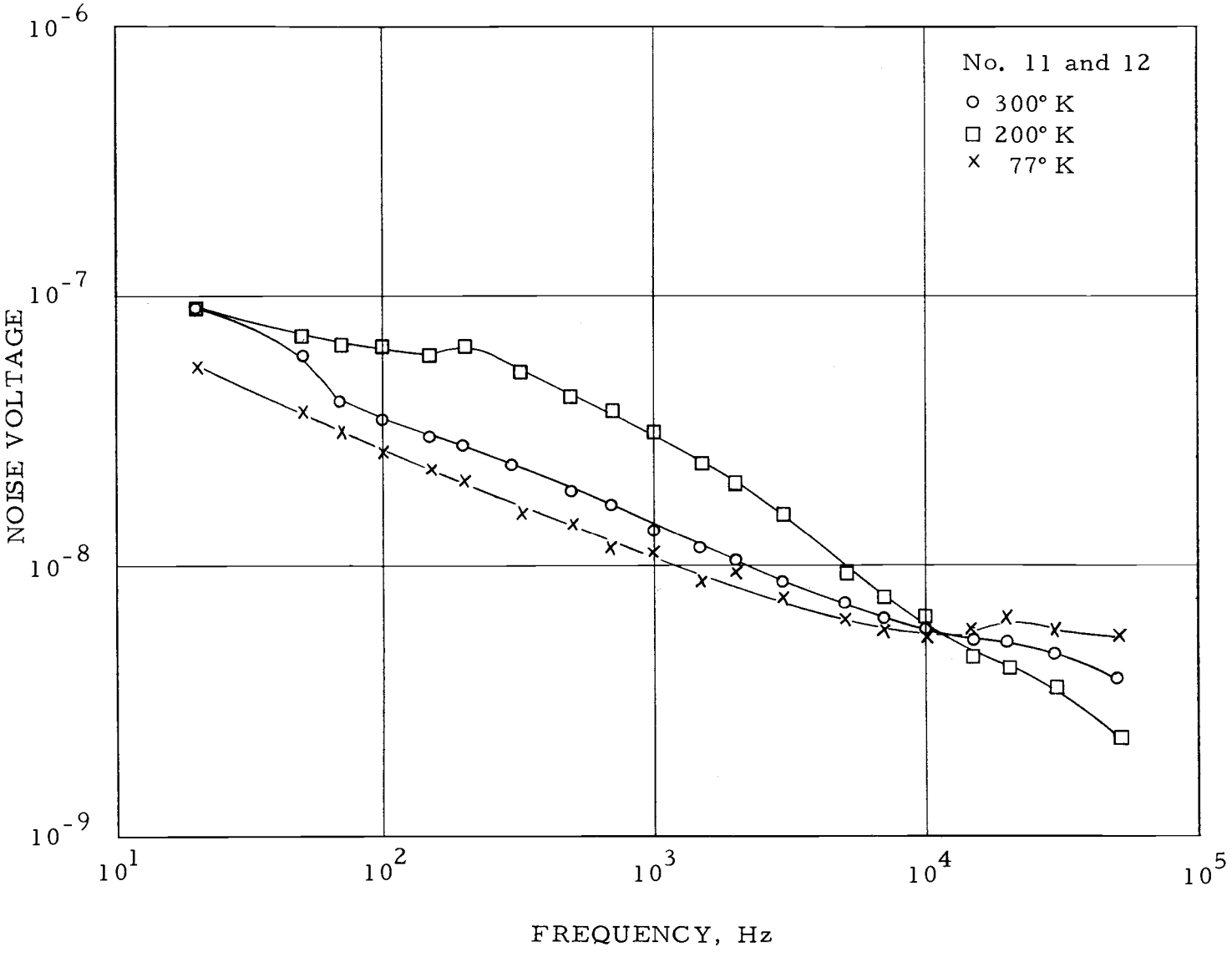
No. 11 and 12
o 300° K
□ 200° K
× 77° K
NOISE VOLTAGE
10^{-6}
10^{-7}
10^{-8}
10^{-9}
10^{1}
10^{2}
10^{3}
10^{4}
10^{5}
FREQUENCY, Hz

APPENDIX II

Determination of Trap Activation Energy

As derived in Section II, the expression for the SRH time constant with only donor traps present is

$$\tau_{t_n} = CT^{-3/2} \exp\left(\frac{E_c - E_t}{kT}\right)$$

where C is a constant with respect to temperature. In deriving this equation it was assumed that the trap Fermi level was equal to the donor trap energy. If we retain this assumption, and let the activation energy E_a be defined as the difference between the Fermi level and the band edge, then the time constant may be expressed as

$$\tau_t = CT^{-3/2} \exp\left(\frac{E_a}{kT}\right).$$

If the quantity $(\tau_t T^{3/2})$ is plotted versus T^{-1} on semi-logarithmic coordinates, the slope of the curve is proportional to E_a:

$$\log\left(\tau_t T^{3/2}\right) - \log C = \frac{\ln\left[\exp\left(\frac{E_a}{kT}\right)\right]}{\ln 10} = \frac{E_a}{kT \ln 10}.$$

The slope of the curve is

$$\frac{d[\log(\tau_t T^{3/2}) - \log C]}{d[T^{-1}]} = \frac{d[\log(\tau_t T^{3/2})]}{d[T^{-1}]} = \frac{E_a}{k \ln 10} .$$

Therefore,

$$E_a = k \ln 10 \text{ (slope)} = (2.3)(8.6 \times 10^{-5} \text{ eV/°K})(\text{slope})$$

$$= 1.98 \times 10^{-4} \text{ (slope)}.$$

APPENDIX III

Error Analysis

Noise Measurement Error

The rms value of a random-noise waveform can be accurately measured only on a "true rms" meter that measures the mean-square value. Most rms voltmeters actually use a linear rectifier instead of a square-law rectifier. The meter indicates the average value of the full-wave-rectified waveform, and is calibrated to read the rms value of a sine wave. When such a meter is used to measure a random-noise waveform, an error results due to the difference in the average values of the rectified noise voltage and the calibrating sine wave. The following analysis is presented to derive the error when a narrow-band wave analyzer, such as the Hewlett-Packard 302A, is used for absolute noise voltage measurements.

Consider the full-wave linear rectifier characteristics shown below:

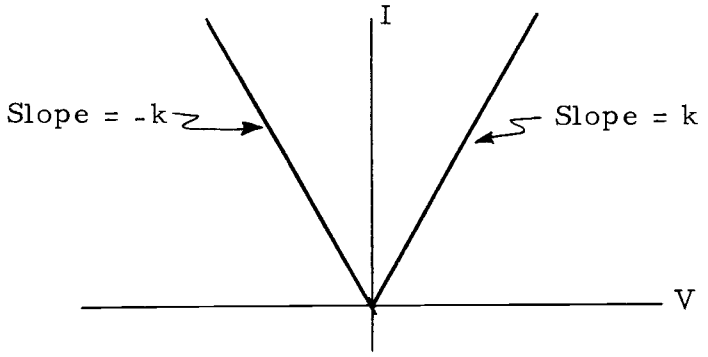

A sine-wave voltage applied to this characteristic results in a full-wave rectified current output. The factor k is the slope of the current voltage characteristic. Thus, for an applied voltage of the form $V(t) = V_o \sin \omega t$, the output current is $I(t) = kV_o \sin \omega t$.

The meter reads the average value of the rectified current waveform. This reading, designated by M, is

$$M = \frac{4k}{2\pi} \int_o^{\pi/2} V_o \sin \omega t \, d(\omega t) = \frac{2kV_o}{\pi} .$$

This is the meter reading when the input voltage is a sine wave with peak value V_o. Since the rms value of this voltage is $V_{rms} = V_o/\sqrt{2}$,

$$M = \frac{2\sqrt{2}k}{\pi} V_{rms} .$$

For a meter calibrated to read 1.0 full-scale with a 1.0 V_{rms} sine-wave input, the value of k is found to be

$$k = \frac{\pi}{2\sqrt{2}} .$$

Now let the input to the same meter be a random-noise voltage $v(t)$. It is assumed that this noise voltage is constant in time so that it is stationary. It is further assumed that an ensemble of noise voltage wave-forms sampled at a given instant in time will give the same distribution in amplitudes as a series of samples of one noise

waveform in time. Thus, the noise voltage is stationary and ergodic, so that its probability distribution is independent of time. We use the symbol $p(v)$ to designate the probability density function of the random variable v.

Once the probability density function of the noise is known, the rectifier response may be calculated. From the central limit theorem of probability theory, it can be shown that for large numbers of random variables, their sum approaches the Gaussian distribution. Thus, any ergodic noise waveform will have the probability density function

$$p(v) = \frac{1}{\sigma\sqrt{2\pi}} \exp\left(-\frac{v^2}{2\sigma^2}\right).$$

The rms value of the noise voltage is the standard deviation σ, defined as the square root of the difference between the mean-square and squared-mean values of the function.

The rectifier output is found by integrating the product of the input voltage and rectifier characteristic over all possible values of v. Thus, the average value of the rectified current is

$$<I> = -k \int_{-\infty}^{0} vp(v)dv + k \int_{0}^{\infty} vp(v)dv$$

$$= 2k \int_{0}^{\infty} vp(v)dv$$

$$= \frac{2k}{\sigma\sqrt{2\pi}} \int_{0}^{\infty} v \exp\left(\frac{-v^2}{2\sigma^2}\right) dv$$

$$= \frac{2\pi}{\sigma\sqrt{2\pi}} \left[-\sigma^2 \exp\left(-\frac{v^2}{2\sigma^2}\right) \right] = \sigma k \sqrt{\frac{2}{\pi}} \ .$$

This average value $<I>$ corresponds to a meter reading M' produced by the input noise. We now substitute the value of k for the rms-calibrated meter, yielding

$$M' = <I> = \sigma k \sqrt{\frac{2}{\pi}} = \frac{\sqrt{\pi}}{2}\sigma \ .$$

Since σ is the actual rms value of the noise voltage,

$$\sigma = \frac{2}{\sqrt{\pi}} M' = 1.128 \text{ times (the indicated meter reading)}.$$

In other words, the indicated meter reading is low by 12.8%.

This result is valid for narrow bandwidths and non-zero frequencies, with the input noise having a Gaussian distribution.

Experimental Errors

The various errors in the measured quantities are estimated from a knowledge of the measurement instrumentation. Experimental errors of the individual equipments are based upon observed deviations (4, p. 34).

Component	Observed deviation	Squared error	rms error
1. Noise Voltage Measurement, $V_n(T)_f$			
Preamplifier	1%	1×10^{-4}	
302A Wave Analyzer	4%	16	
RC Integration	1%	1	
y-axis Recorder Fluctuations	10%	100	
Graphical Averaging	2%	4	
		122×10^{-4}	11.1%
2. Noise Voltage Measurement, $V_n(f)_T$			
Preamplifier	1%	1×10^{-4}	
302A Wave Analyzer	4%	16	
RC Integration	1%	1	
Meter Reading Fluctuation	10%	100	
		118×10^{-4}	10.9%

3. Absolute Temperature Measurement (T)

   x-axis measurement of thermocouple voltage, maximum measured error = ±1.5C°. This yields a worst-case error at 77° K of 2%.

4. Voltage Gain of FET and Preamplifier, A(T)

   The combined accuracy of the 302A and signal source is 4%.

Component	Observed deviation	Squared error	rms error
5. Calculated Value of $e_n(T) = V_n(T)/A(T)(\Delta f)^{1/2}$			
Noise bandwidth Δf	5%	25×10^{-4}	
Noise voltage $V_n(T)$	11.1%	122	
Voltage gain $A(T)$	4%	16	
		163×10^{-4}	12.8%
6. Transconductance, g_m			
Signal source	1.5%	2×10^{-4}	
Drain load resistor	1%	1	
302A	5%	25	
y-axis of recorder	1%	1	
		29×10^{-4}	5.4%
7. Drain Saturation Current, I_{DSS}			
Drain load resistor	1%	1×10^{-4}	
y-axis of recorder	1%	1	
		2×10^{-4}	1.4%
8. Time Constant $\tau(T)$ at Noise Maximum			
The frequency is measured with a digital counter to an accuracy of 5% at 20 Hz. Since $\omega\tau = 1$ at the maximum, the error in τ is 5% or better. The temperature at which τ is measured may be determined to an accuracy of 2.5%.			
9. Activation Energy E_a From Plot of $(\tau T^{3/2})$ Versus T^{-1}			
$\tau(T_1)$	5%	25×10^{-4}	
T_1	2.5%	6	
T (absolute)	2%	4	
		35×10^{-4}	5.9%
10. Activation Energy E_a From Plot of $e_n(T)$ Versus T^{-1}			
$e_n(T)$	12.8%	163×10^{-4}	
T (absolute)	2%	4	
		167×10^{-4}	13%